6-2013

Utilization of Wet Corn Distillers Grain for the Production of Cellulase Enzymes and Value Added Products

Hunter R. Flodman
University of Nebraska-Lincoln, hunter.flodman@unl.edu

UTILIZATION OF WET CORN DISTILLERS GRAIN FOR THE PRODUCTION OF CELLULASE ENZYMES AND VALUE ADDED PRODUCTS

By

Hunter R. Flodman

A DISSERTATION

Presented to the Faculty of

The Graduate College at the University of Nebraska

In Partial Fulfillment of Requirements

For the Degree of Doctor of Philosophy

Major: Chemical and Biomolecular Engineering

Under the Supervision of Professor Hossein Noureddini

Lincoln, Nebraska

June, 2013

UTILIZATION OF WET CORN DISTILLERS GRAIN FOR THE PRODUCTION OF CELLULASE ENZYMES AND VALUE ADDED PRODUCTS

Hunter R. Flodman, Ph.D.

University of Nebraska, 2013

Adviser: Hossein Noureddini

Distillers grain, a byproduct from the dry grind corn ethanol industry, is an industrially available, abundant, preprocessed material comprised primarily of cellulose, hemicellulose, protein, oil, and minerals. This research investigated the utilization of distillers grain as a substrate for solid-state fermentation (SSF). SSF is the growth of microorganisms on a moist, solid substrate in the absence of free water. The substrate acts as both the nutrient source and as a solid support for the microorganisms, typically filamentous fungi. SSF has the unique ability to convert agricultural byproducts into valuable bioproducts such as enzymes and organic acids without hydrolyzing polysaccharides to monomeric sugars prior to fermentation.

This research used the organism *Triochoderma reesei* with the goal of producing cellulase enzymes used in the production of lignocellulosic biofuels. Research investigated the effects of temperature and moisture on fungal activity, cellulase production, and substrate weight loss. The residual distillers grain substrate after SSF was evaluated as an animal feed product. Reductions in cellulose and hemicellulose content of the substrate with an increase in protein content, makes SSF an attractive method for simultaneously producing value added bioproducts while increasing the feed value of byproducts. The effect of mechanical mixing on fungal growth and product

formation was also investigated to determine if bioreactor designs incorporating mechanical agitation were feasible. The results showed mechanical agitation at frequencies of up to 6 d^{-1} resulted in minimal effects on product formation. Data from labscale experiments were used to develop a kinetic model for fungal activity and product formation as a function of temperature, moisture, and fermentation time. The kinetic model was based on easily measurable CO_2 concentration, which can be incorporated into online monitoring of bioreactors. The kinetic model was combined with material and energy balances to evaluate the design and scale-up of SSF bioreactors.

Acid and base catalyzed soluble fiber extraction from distillers grain was also investigated as a method of reducing hemicellulose content while simultaneously producing monomeric sugars.

Acknowledgements

I would like to thank several people who have contributed significantly to the completion of this degree. First and foremost, I would like to thank my wife, Nichole, for supporting me both psychologically and financially for the past four years. We are both excited to celebrate at the end of August with the birth of our first child. I would also like to thank my family for their support and encouragement. I would like to thank my committee members, Dr. Demirel, Dr. Harris, Dr. Timm, and especially my advisor, Dr. Noureddini for patience, support, and advice throughout this project as well as my teaching appointments. I would also like to thank Dr. Timm, who has mentored me while I assisted in the instruction of Process Control and Unit Operation courses over the past several years. I would like to thank all of the undergraduates and UCARE students who worked in the laboratory including Linda Beckwith, Elizabeth Boyer, Arthy Muthu, and Wade Hunt who contributed considerably to the completion of Chapter 6 of this document. Thank you to the Nebraska Ethanol Board for financial support to complete research projects, and the Nebraska Corn Board for financial support to travel to conferences. Thanks to Abengoa Bioenergy in York for samples of WS and WDG. I would like to thank the entire Chemical Engineering department for their unwavering support throughout my higher education. And the last individual I would like to thank, but definitely not least, is Leonard Akert for help designing and building numerous new Unit Operations lab experiments as well as help with countless other side projects.

Table of Contents

Chapter 1

Introduction

1.1. Background

The future sustainability of the dry grind corn ethanol production industry is dependent on the ability to transform existing ethanol plants into biorefineries which use current distillers grain byproducts to produce additional valuable biochemicals. Ethanol production in the U.S. reached 13.9 billion gallons in 2011 [1]. For every bushel of corn processed, approximately 2.8 gallons of ethanol is produced along with 16-18 lbs of distillers grain with solubles (DGS) byproduct. About half of the DG is composed of insoluble solids known as wet distillers grain (WDG) and the other half is soluble in water and referred to as solubles (S). The byproducts are currently dried to various degrees, blended and sold as animal feed. DGS is composed primarily of the remaining corn kernel that was not converted to ethanol which includes protein, oil, cellulose, hemicellulose, and nutrients making an excellent supplement to cattle rations.

An ideal process would utilize the cellulose and hemicellulose portion of the DGS while the remaining components could be marketed as a high protein, low fiber animal feed product for both ruminants and non-ruminants. Recently oil separation from the soluble portion of the distillers grain has gained widespread acceptance and is increasing the profit margins of ethanol producers. The separated oil is typically used as biodiesel production feedstock. WDG is an excellent substrate for solid-state fermentation (SSF). It is a preprocessed nutrient rich material that is readily available at existing corn ethanol plants. SSF utilizes primarily carbohydrates such as cellulose and hemicellulose to

produce valuable bioproducts. An alternative fiber utilization technology is soluble fiber extraction from DGS using acid or base catalyzed hydrolysis.

SSF has been defined as the growth of microorganisms on a moist solid substrate in the absence or near absence of free water. The solid media contains nutrients required for growth and acts as a support for the microorganisms. SSF has the unique ability to use cellulose and hemicellulose substrates directly from agricultural byproducts, residues, and waste products without the need for hydrolyzing saccharides to simple sugars. SSF allows filamentous fungi to grow in conditions that resemble their natural environments [2]. Laboratory scale SSF exhibits many advantages over submerged fermentation. A few of the notable advantages include increased fermentation productivity, end product concentration, and product stability [3]. Numerous researchers have noted a decrease in catabolic repression [3-5]. Another important advantage is improving the feed quality and digestibility of the residual WDG substrate after SSF [6].

Scale-up, product purification, and biomass estimation are major barriers that need to be overcome before SSF can become industrially viable [7]. The reason scale-up is difficult is because transport phenomena limitations within a large reactor cause temperature, nutrient, pH, and oxygen gradients. These gradients cause a significant volume fraction of the reactor to operate at suboptimal conditions that can halt product formation and impede microorganism growth and activity. Scale-up for submerged fermentation is typically dominated by dissolving oxygen into the liquid state. Scale-up for SSF processes depends on the type of reactor used, but the most frequent challenges are temperature and moisture control [8]. Heat buildup in the reactor is caused by metabolic heat produced by the microorganisms. This problem is not typically found in

submerged fermentation due to the thermodynamic properties of water coupled with near ideal mixing of the reactor. Temperature gradients in SSF reactors cause liquid water to evaporate from the surface of the substrate leading to moisture gradients. Excessive heat accumulation and evaporation are not typically found in lab scale reactors due to the large surface area to volume ratios which allows metabolic heat to dissipate through the reactor walls [8]. In order for reliable scale-up to occur, mathematical models describing transport phenomena within the reactor must be developed and validated through testing various size bioreactors.

1.2. Objectives

The goal of this research was to evaluate methods to convert DGS byproducts to valuable biochemicals while preserving the animal feed quality of the residual DGS used. SSF for cellulase enzyme production and soluble fiber extraction were examined as techniques to attain this goal. The objectives required to evaluate SSF are outlined in Figure 1.1. Objectives 1-4 have been completed and are included as chapters in this dissertation. The infrastructure for objective 5, a fully automated pilot scale SSF bioreactor has also been completed but is not included as part of this document.

Soluble fiber extraction was also evaluated as means of removing a portion of the hemicellulose from DGS. Objectives for soluble fiber extraction included: investigation of the effects of sulfuric acid concentration and sodium hydroxide concentration, temperature, and time on the extraction of soluble fiber and the formation of monomeric sugars.

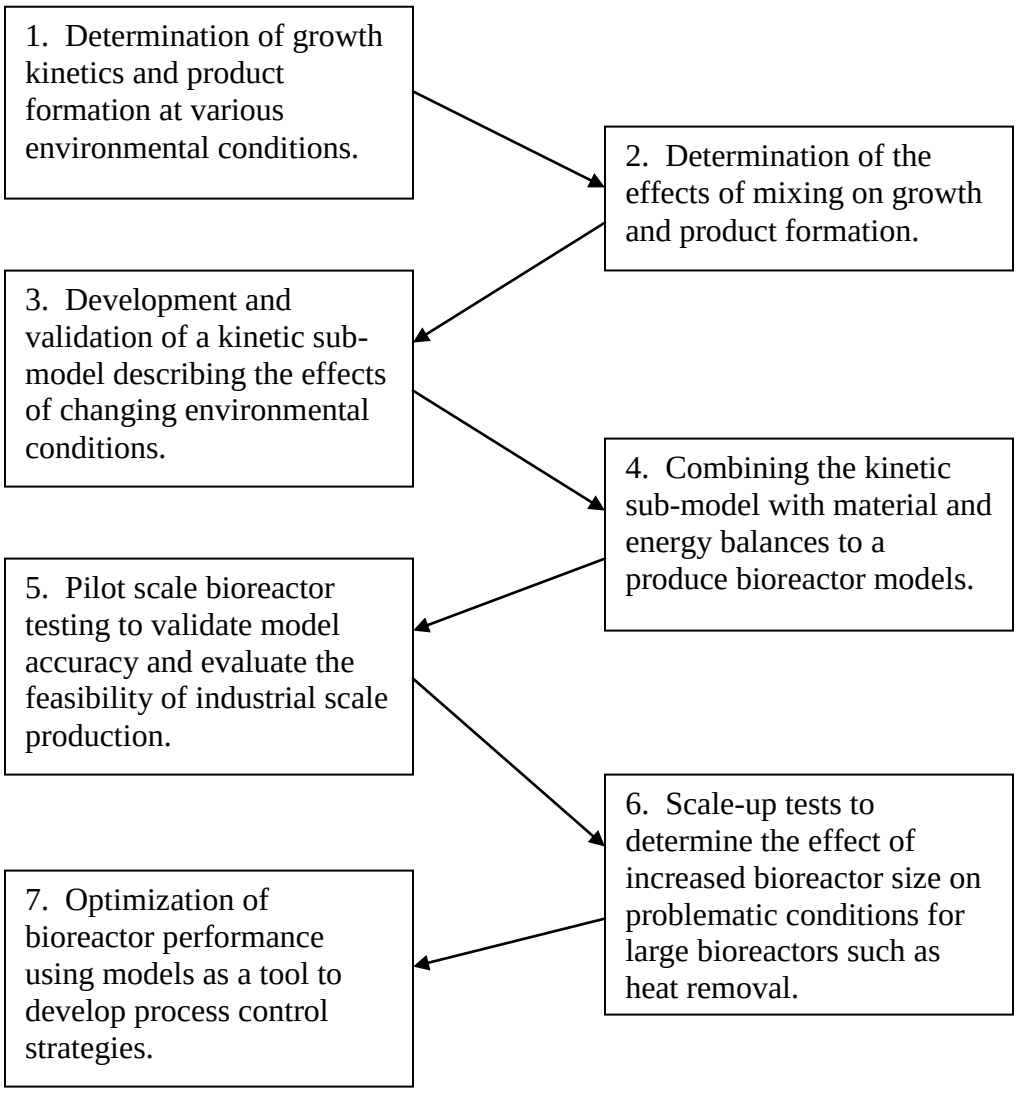

Figure 1.1. Research strategy to investigate solid state fermentation for the production of cellulase using WDG. (Adapted from Mitchell et al [9])

1.3. Organization of Dissertation

Chapters 2-6 are written as standalone documents which include the literature review, materials and methods, results and discussion, conclusions, and references. Chapter 2 investigates the effects of temperature and moisture content on the fungal growth of *T. reesei* NRRL 11460 during solid-state fermentation of wet corn distillers grain. Chapter

3 examines the effects of mechanical mixing on the fermentation. Chapter 4 uses data obtained from previous chapters to develop a kinetic model for fungal growth and cellulase enzyme production. The kinetic model is combined with material and energy balances in Chapter 5 to simulate an intermittently mixed packed bed bioreactor. Acid and base catalyzed extraction of soluble dietary fiber from whole stillage are evaluated in Chapter 6. Chapter 7 contains recommendations for future work. Chapter 8 contains a list of nomenclature and abbreviations used throughout the dissertation.

References

[1] Renewable Fuels Association. 2012 Ethanol Industry Outlook. http://www.ethanolrfa.org/pages/annual-industry-outlook. Accessed 2 August 2012.

[2] P. Cen, L. Xia, Production of cellulase by solid-state fermentation, Adv. Biochem. Eng. Biotechnol. 65 (1999) 69-92.

[3] U. Holker, M. Hofer, J. Lenz, Biotechnological advantages of laboratory-scale solid-state fermentation with fungi, Appl. Microbiol. Biotechnol. 64 (2004) 175-186.

[4] G. Viniegra-Gonzalez, E. Favela-Torres, C.N. Aguilar, S.D.J. Romero-Gomez,G. Diaz-Godinez, C. Augur, Advantages of fungal enzyme production in solid state over liquid fermentation systems, Biochem. Eng. J. 13 (2003) 157-167.

[5] G. Viniegra-Gonzalez, E. Favela-Torres, Why Solid-State Fermentation Seems to be Resistant to Catabolite Repression. Food Technol. Biotechnol. 44 (2006) 397-406.

[6] S. Yang, J.Y. Lio,T. Wang, Evaluation of enzyme activity and fiber content of soybean cotyledon fiber and distiller's dried grains with solubles by solid state fermentation. Appl. Biochem. Biotechnol. 167 (2012) 109-121.

[7] R.R. Singhania, A.K. Patel, C.R. Soccol, A. Pandey, Recent advances in solid-state fermentation, Biochem. Eng. J. 44 (2009) 13-18.

[8] D.A. Mitchell, M. Berovic, N. Krieger, Introduction to Solid-State Fermentation Bioreactors, in: D.A. Mitchell, N. Krieger, M. Berovič (Eds.), Solid-State Fermention Bioreactors Fundamentals of Design and Operation, Springer, Berlin, 2006, pp. 33-44.

[9] D.A. Mitchell, L.F.L. Luz Jr, M. Berovic, N. Krieger, Approaches to Modeling SSF Bioreactors, in: D.A. Mitchell, N. Krieger, M. Berovič (Eds.), Solid-State Fermention Bioreactors Fundamentals of Design and Operation, Springer, Berlin, 2006, pp. 159-178.

Chapter 2

Solid-State Fermentation of Wet Corn Distillers Grain with *Trichoderma reesei*

Abstract

The production of cellulase by solid-state fermentation using wet corn distillers grain, an untreated, non-supplemented substrate available at existing biofuel production facilities, was evaluated at temperatures ranging from 22.5 to 32.5 °C and initial substrate moistures ranging from 45 to 60%. The CO_2 evolution rate was measured to indicate fungal activity of the microorganism used, *T. reesei* NRRL 11460. The substrate weight loss and the moisture content were monitored throughout the fermentation. The filter paper activity of the extracted cellulase was measured as a function of time and fermentation conditions. The highest yield of cellulase was 28.8±0.8 filter paper units (FPU) per gram of initial dry substrate at a fermentation temperature of 22.5 °C with an initial moisture content of 50%. The effectiveness of the extracted crude enzyme cocktail was demonstrated by hydrolyzing distillers grain to monomeric sugars. The residual fermentation substrate was investigated as an animal feed product. Reductions in acid detergent fiber and neutral detergent fiber with an increase in protein content make the residual substrate after solid-state fermentation an attractive feed for ruminants and nonruminants. The data demonstrates that wet corn distillers grain from existing dry grind ethanol production facilities is a potential substrate for cellulase production warranting further investigation. The onsite production of cellulase at biofuel facilities would help the industry transition feedstocks from food crops to biomass by reducing enzyme costs for the conversion of biomass to fermentable sugars.

2.1. Introduction

Dry grind corn ethanol production produces 16-18 lb of distillers grain with solubles (DGS) for every bushel of corn processed. DGS is typically used as an animal feed product. In 2010, approximately 27 million metric tons of DGS were produced in the U.S. [1]. DGS is a readily available, abundant substrate that can be converted to value added products such as cellulase enzymes.

Cellulase enzymes are used in a variety of applications including cotton processing, paper recycling, juice extraction, animal feed additives, and biofuel production. Cellulase is a general term used to describe a system of β-1,4 glycoside hydrolases. Cellulases hydrolyze the glucosidic linkages of cellulose, a linear crystalline polymer comprised of anhydrous glucose molecules, to form glucose, cellobiose, and cello-oligosaccharides. The conversion of cellulose into sugars is a major economical hurdle in the production of fuels and other commodity products derived from biomass [2].

The majority of cellulase is produced with submerged fermentation (SmF) techniques [3]. An alternative to SmF is solid-state fermentation (SSF). Solid-state fermentation is the growth of microorganisms on a moist solid substrate. The solid media contains nutrients required for growth and acts as a support for the microorganisms, conditions that resemble the natural environment of filamentous fungi [4]. As the substrate is consumed, CO_2, water, metabolites, and microbial biomass are produced during fermentation.

A variety of microorganisms are involved in cellulase production; some of the most common industrially utilized producers are filamentous fungi including *Trichoderma Reesei*. *T. reesei*, which was used in this study, produces a wide variety of cellulases that

are active between pH values of 4-6 with optimum activities near a pH of 5. Activities at this pH are desirable when dilute acid hydrolysis is used as pretreatment for biomass to be converted into biofuels. Ethanol fermentations also typically occur within the active pH range of the cellulase produced.

For the production of enzymes using filamentous fungi, laboratory research has indicated that SSF has several advantages over SmF. A few of the notable advantages include increased fermentation productivity and end product concentration[5]. Viniegra-Gonzalez et al [6] compared SSF to SmF for the production of three different fungal enzymes. Enzyme production using SSF was higher in each case. The authors concluded that SSF naturally behaves similar to a fed batch culture commonly used for SmF. Low water activities inhibit many competing organisms, effectively limiting contamination risks and reducing sterility requirements [5]. SSF can be used to produce cellulase on a variety of low cost agricultural residues such as sugar cane bagasse, wheat bran, and orange peel as demonstrated by da Silva Delabona et al [7]. Other advantages include reduced water usage and wastewater quantities due to the absence of free water.

Although advantages exist when using SSF on a laboratory scale, industrial scale production is relatively uncommon when compared to SmF. The online monitoring of SSF processes is one critical aspect that is required for SSF to be successful on a commercial scale. Direct measurement of cells in SSF is difficult because the microbes are fixed to substrate particles. Nevertheless, indirect online monitoring may be achieved by measuring oxygen consumption and CO_2 evolution. Indirect cell monitoring techniques may be integrated in to process models to provide predictions of online process behavior. Desgranges et al [8] showed that CO_2 evolution was a satisfactory

indicator of fungal biomass. The measurement of CO_2 showed specific improvements in sensitivity at the beginning and at the end of the fermentations when physiological activity was low. CO_2 evolution measurements have the advantage of measuring only the physiologically active cell biomass. Cooney et al [9] correlated metabolic heat evolution to oxygen consumption and also to CO_2 evolution.

In this study, *T. Reesei* NRLL 11460 was used to produce cellulase enzymes using wet corn distillers grain (WDG) as a substrate. Cellulase enzyme production was examined for multiple temperatures and initial moisture contents as a function of incubation time. Enzyme assays were used to quantify the cellulase activity of the extracted product. The CO_2 evolution was measured as means of monitoring active fungal biomass. The nutritional value of the residual fermented substrate was evaluated as an animal feed product. Hydrolysis experiments using WDG and dilute acid pretreated WDG as substrates were carried out to determine the effectiveness of the crude enzyme product on hydrolyzing lignocellulosic material.

2.2. Materials and Methods

2.2.1. Inoculum Preparation

T. Reesei NRRL 11460 was obtained from USDA Northern Regional Research Laboratories. The microorganism was grown on potato dextrose agar slants at 30 ºC for 5 days. Slants were then used immediately or stored at 4 ºC for future use. The inoculum was prepared by adding approximately 5 mL of deionized water to the slant and dislodging spores by gentle pipetting. The solution was then diluted to 10^7 spores per mL

using a hemacytometer and 0.5 mL of the spore suspension was used to inoculate 2 g of substrate.

2.2.2. Substrate Preparation

WDG was provided by Abengoa Bioenergy, a dry grind corn ethanol facility in York, Nebraska. The WDG was stored at –4 ºC. The substrate was dried in an oven at 75ºC before the moisture content was adjusted to the desired value using deionized water and the prepared inoculum.

2.2.3. Solid-State Fermentations

Fermentations were carried out in 50 mL Erlenmeyer flasks and Kontes Flex Column glass chromatography columns (VWR International, Batavia, IL) with a 1.0 cm diameter and 20 cm in length. Each flask or column contained 2 g of inoculated WDG adjusted to the desired moisture content. Fermentations using the flasks were completed in a Precision temperature controlled water bath (Thermo Scientific, Pittsburgh, PA). Fermentations in the columns used the apparatus developed by Raimbault and Alazard [10] to quantify the effects of fermentation time, moisture, and temperature on fungal growth as shown in Figure 2.1. Humidified air was used to aerate the column and prevent moisture loss. The columns were submerged in a temperature controlled water bath. An aeration rate of 50 mL/min was maintained using mass flow controllers (Brooks, Hatfield, PA) or rotameters (Cole Parmer, Vernon Hills, IL). The CO_2 content of the effluent air was monitored by a K-33 ICB infrared CO_2 sensor (CO2meter, Ormond Beach, FL). Moisture was removed from the effluent air sample with 4-20 mesh calcium chloride desiccant (Fisher Scientific, Pittsburgh, PA) to protect the meter from condensation while avoiding measurement errors due to CO_2 adsorption [11].

The dry matter weight loss and moisture content of the fermented material were analyzed for each sample. The dry matter weight loss was determined by weighing the vessel and contents before and after fermentation. The moisture content of the substrate was combined with gravimetric measurements to determine the dry matter weight loss. The moisture fraction of the fermented substrate was determined by removing a portion of the fermented substrate, approximately 0.3 g, and monitoring weight loss after oven drying for 24 h at 100 ºC.

The effects of temperature on the fermentation process were completed at 22.5, 25.0, 27.5, 30.0, 32.5 ºC with an initial moisture content of 50%. An additional two stage temperature experiment was completed by keeping the fermentation temperature at 27.5 ºC for the first 66 h of fermentation and then reducing the temperature to 22.5 ºC for the remainder of the fermentation. Fermentation experiments were also completed with initial moisture contents of 45, 50, 55, and 60% at a temperature of 30 ºC to establish the effects of moisture. Samples were analyzed approximately every 24 h for enzyme activity, moisture content, and dry matter weight loss starting after ~65 h by sacrificing the contents of an entire flask or column. Fermentation samples were analyzed in triplicate consisting of two flask samples and one column sample per sampling period. The fermentation experiments for a set of conditions were terminated when the CO_2 evolution rate reached zero or at a maximum time of 8 days.

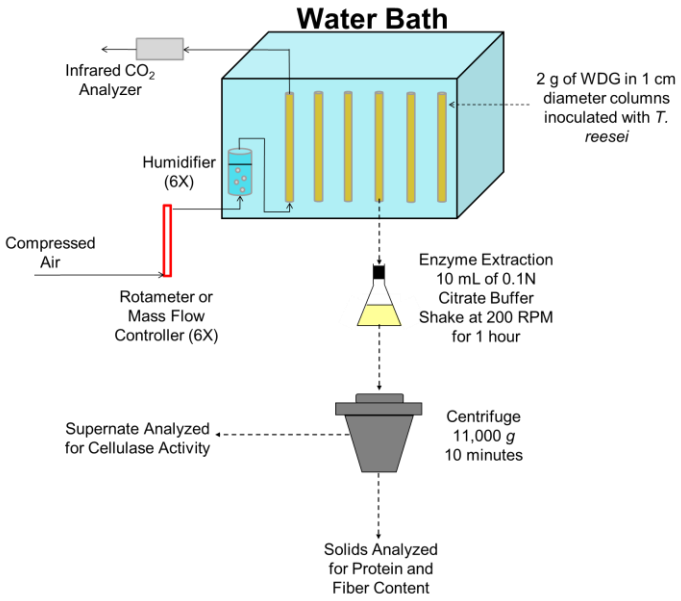

Figure 2.1. Experimental apparatus used to determine the effects of temperature, moisture, and fermentation time on fungal activity and product formation.

2.2.4. Enzyme Extraction

Cellulase was extracted from the fermented substrate by adding 10 mL of 0.05M sodium citrate buffer solution with a pH of 4.8. Samples were agitated at 200 rpm for 1 h on a platform shaker at room temperature. The liquid phase was separated from residual solids by centrifugation at 11,000 *g* for 10 min. Enzyme assays were used to determine standard cellulase activities.

2.2.5. Enzyme Assays

Standard IUPAC assays were used to analyze cellulase activity in the extracted enzyme solution as outlined by Ghose [12]. FPU was measured by adding 0.5 mL of diluted sample to 1.0 mL of 0.05 M sodium citrate buffer with a pH of 4.8. The sample was diluted to release slightly more and diluted to release slightly less than 2 mg of reducing sugars from a 1.0 X 6.0 cm strip of Whatman No. 1 filter paper when incubated

at 50 ºC for 1 h. Cellobiase activity (CBU) was measured by adding 1 mL of diluted enzyme to 1 mL of 15 mM cellobiose at 50 ºC for 30 minutes. The sample was diluted to release slightly more and diluted to release slightly less than 1 mg of glucose. Glucose concentrations were determined using HPLC analysis.

2.2.6. WDG Composition Analysis

The WDG substrate and post fermentation residual solids were analyzed for acid detergent fiber (ADF) [13], neutral detergent fiber (NDF) and fat [14], and crude protein [15] by the University of Nebraska Animal Science Ruminant Nutrition Laboratory. The nitrogen content used for crude protein determination was quantified by combustion analysis using a LECO TruSpec N-Nitrogen/Protein Analyzer (Leco, St. Joseph, MI). ADF is a measure of the combined cellulose and lignin content, and NDF measures the hemicellulose content in addition to the cellulose and lignin.

2.2.7. Pretreatment and Enzymatic Hydrolysis

Hydrolysis experiments were performed with the extracted enzyme following procedures outlined by Noureddini et al [16]. WDG and dilute acid pretreated WDG were used as substrates. Dilute acid pretreatment of WDG utilized a 15 wt% solids loading with 1 vol% H_2SO_4 at 120 ºC for 30 min. A 450 mL Parr 4562 reactor (Parr Instrument Company, Moline, IL) was loaded with 30 g of WDG ground in a Mr. Coffee grinder (Mr. Coffee, Cleveland, OH) and 194 mL of deionized water. The reactor was stirred at 500 rpm and heated to 120 ºC. When the contents reached 120 ºC, 6 mL of 33.3 vol% sulfuric acid was added via a catalyst basket which was opened using air pressure. After 30 min, the reaction vessel was cooled in an ice bath and the contents of the reactor were adjusted to a pH of 5.0 by the addition of a 10N NaOH solution. The contents were

vacuum filtered using Whatman #1 filter paper. Filtrate samples were taken for HPLC sugar analysis. The remaining solids were oven dried at 70 ºC and reground for enzymatic hydrolysis. Experiments were conducted in triplicate.

Enzymatic hydrolysis experiments were performed at 50 ºC in a Precision shaking water bath at 150 rpm. A solids loading of 15 wt% was used by mixing 7.5 g of dried ground WDG or pretreated WDG with 50 mL of 0.05 M sodium citrate buffer solution containing the enzyme cocktail at a pH of 4.8. The enzyme activities for hydrolysis were 12.7 FPU and 30.7 CBU per g substrate. Cellulase produced from *T. reesei* characteristically lacks sufficient quantities of cellobiase. Cellobiase from *Aspergillus Niger* was purchased from Sigma Aldrich (St. Louis, MO). Due to the synergistic nature of cellulase, cellobiase was added to the extracted enzyme solution to meet the specified CBU enzyme loading. Samples were taken at 0, 1, 3, 6, 12, 24, 48, and 72 h by withdrawing ~5 mL aliquots for HPLC analysis. Samples were stoppered and added to a boiling water bath for 2 min to terminate the hydrolysis reaction. Samples were then cooled in an ice water bath and centrifuged. The supernatant was filtered with a 0.2 μm cellulose acetate syringe filter for HPLC analysis. Experiments were completed in triplicate.

2.2.8. Sugar Analysis

Monomeric sugar and cellobiose concentrations were measured using a HPLC with the method developed by NREL [17]. A Waters 2695 separations module (Waters Corporation, Milford, MA) equipped with a Bio Rad HPX-87P column (Bio-Rad Laboratories, Hercules, CA) and a Waters 2414 refractive index detector were used to

determine the concentrations of glucose, xylose, arabinose, galactose, and cellobiose. Calibration curves were developed using standard solutions.

2.3. Results and Discussion

2.3.1. Substrate Selection

Agro-industrial residues have been considered the choice substrates for SSF. Substrate availability and cost are imperative factors for consideration. The substrate acts as both a nutrient source and the solid support for fungal growth; therefore substrate composition as well as particle size are important substrate qualities. Many substrates require mechanical and/or chemical pretreatment to obtain desired particle sizes and to increase the availability of substrate nutrients. DGS from dry grind corn ethanol producing facilities is an abundant and readily available material originating from existing biofuel production facilities. DGS has already undergone chemical, thermal, and mechanical pretreatment during the corn ethanol production process. A wide variety of trace minerals, nutrients, carbohydrates, and protein are present in DGS [18], averting the need for supplementation. WDG, which does not contain condensed distillers solubles (CDS), was chosen as the substrate for this study. Wet distillers grain with solubles (WDGS) was not used in this study because of undesirable particle clumping and increased bulk density when compared to WDG [19].

2.3.2. Temperature Effects

Fermentation temperature has been shown to be a critical factor affecting both microbial growth and cellulase production in SSF [20]. Xin and Geng [20] also concluded that optimum conditions for microbial growth are not necessarily the optimum

conditions for cellulase production. The effect of temperature on cellulase production, dry matter weight loss, CO_2 evolution rate, and moisture content were investigated at temperatures of 22.5, 25.0, 27.5, 30.0, and 32.5 ºC by fermenting WDG with an initial moisture content of 50%. An additional two stage temperature experiment was completed in which the temperature for the first 66 h was 27.5 ºC and then was dropped to 22.5 ºC for the remainder of the fermentation. Results showing the effects of temperature are presented in Figure 2.2. Cellulase produced in FPU per g of the initial dry WDG is shown in Figure 2.2(a). Dry matter weight loss during fermentation in g of dry matter weight lost per g of initial dry WDG substrate is presented in Figure 2.2(b). The CO_2 evolution rate in μmol of CO_2 released per min per g of the initial dry WDG is displayed in Figure 2.2(c). The moisture content of the fermentation solids are shown in Figure 2.2(d). Error bars in the figure represent variability calculated by standard error.

As is shown in Figure 2.2(a), the lowest cellulase yield (8.1±1.2 FPU/g) occurred at the highest temperature tested, 32.5 ºC. As the temperature of the fermentation decreased, the cellulase yield consistently increased. The highest yield (26.8±1.9 FPU/g) occurred at the lowest temperature tested, 22.5 ºC, while the fermentation was still active after 8 days since the CO_2 evolution rate had not yet begun to decline (Figure 2.2(c)). Therefore the two stage temperature fermentation was tested which resulted in the highest yield of 28.8±0.8 FPU/g after 162 h of fermentation. Cellulase production did not correlate with fungal activity which is apparent when comparing Figure 2.2(a) with Figure 2.2(c). In fact the highest CO_2 evolution rate occurred at 32.5 ºC which produced the lowest quantity of cellulase. This observation complements the conclusions drawn by Xin and Geng [20]. Fermentations at low temperatures resulting in relatively low CO_2 evolution

rates for an extended period of time were the most favorable for cellulase production but had longer lag phases and longer active fermentation times from the end of the lag phase to the end of the decay phase. The two stage temperature fermentation decreased the lag phase and shortened the overall time of fermentation while increasing the cellulase yield. Conditions which led to high CO_2 evolution, shown in Figure 2.2(c), led to high weight losses shown in Figure 2.2(b). The greatest weight loss occurred at 30.0 ºC resulting in 24.0% of the initial substrate mass being lost. A 15.9% weight loss was observed for the two stage temperature fermentation.

Fermentation experiments began with an initial moisture content of 50.0%. The final moisture contents, graphed in Figure 2.2(d), ranged from 56.7 to 61.1% upon termination. Fermentation temperature significantly impacted cellulase production with maximum cellulase yields ranging from 8.1 to 28.8 FPU/g. The effects of the initial substrate moisture were also investigated.

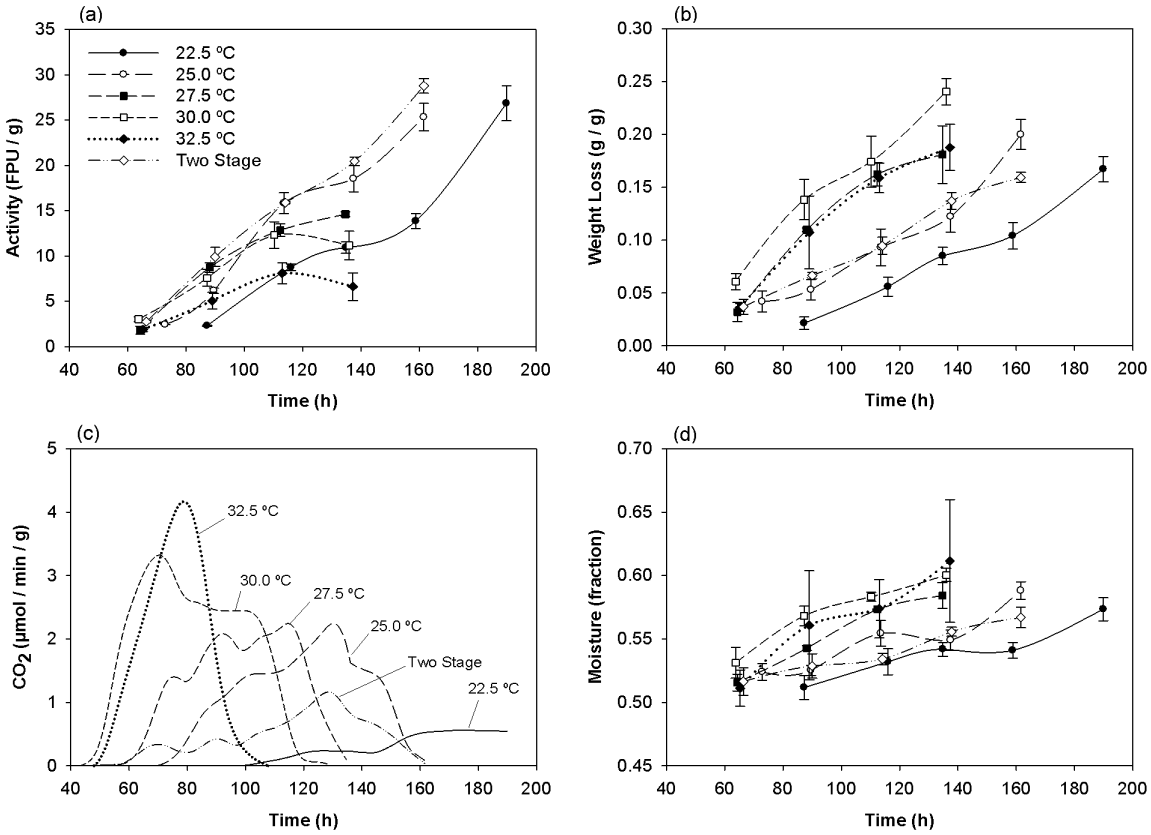

Figure 2.2. Effects of fermentation temperature with an initial substrate moisture of 50% on (a) cellulase production, (b) substrate weight loss, (c) CO_2 evolution rate, and (d) substrate moisture.

2.3.3. Initial Substrate Moisture Content Effects

The water content of the substrate influences the mass transfer of water and solutes across the cell membrane and can be used to adjust the metabolic production and excretion of enzymes [21]. Excess water is undesirable due to decreased porosity in the substrate bed and increased risk of bacterial contamination [10]. The effect of substrate moisture was investigated by adjusting the initial substrate moisture content to 45, 50, 55, and 60%. The temperature of the fermentations was held at 30.0 ºC. The effects of moisture on (a) cellulase production, (b) substrate weight loss, (c) CO_2 evolution, and (d) moisture content throughout the fermentation experiments are shown in Figure 2.3.

Data presented in Figure 2.3(a) indicates cellulase production ranged from 9.5 – 13.7 FPU/g for all of the initial substrate moistures tested. Significant cellulase production resulting from all of the initial moisture contents examined is conducive to large scale operations which often demonstrate moisture gradients due to evaporation [22]. The large moisture content operating range is also advantageous for temperature control using evaporative cooling over an extended time period, avoiding the need for frequent moisture additions. As shown in Figure 2.3(b), the weight loss after 140 h was similar for 45, 55, and 60% initial moistures and slightly higher for an initial moisture content of 50%. Results displayed in Figure 2.3(c) indicate the lag phase for microbial growth was approximately 45 h for the initial moisture contents of 50, 55, and 60%. The lag phase for 45% moisture content was about 55 h but microbial activity lasted an additional 10 h indicating the active fermentation time was approximately the same as other initial moisture conditions examined. The moisture fractions throughout fermentations are displayed in Figure 2.3(d). Each condition tested showed a 5 - 8% increase in moisture over the 140 h fermentation.

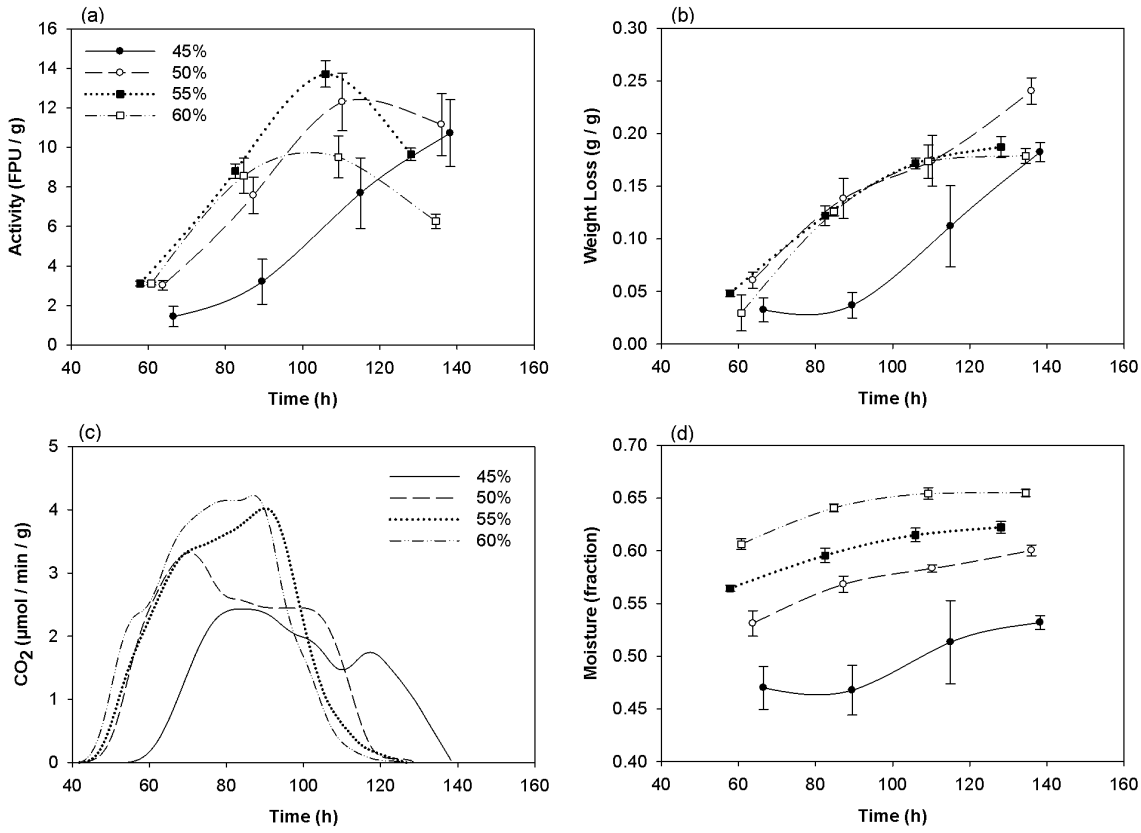

Figure 2.3. Effects of initial substrate moisture at 30 ºC on (a) cellulase production, (b) substrate weight loss, (c) CO_2 evolution rate, and (d) substrate moisture.

2.3.4. CO_2 Evolution and Weight Loss Correlation

The correlation between CO_2 evolution and substrate dry matter weight loss for the growth of *T. reesei* on wheat bran has been documented by Smits et al [23]. A similar correlation for the growth of *T. reesei* on WDG for all of the temperature and moisture conditions tested is shown in Figure 2.4. The best fit linear regression line does not pass through the origin as expected; this is likely due to the lack of CO_2 meter sensitivity at low concentrations. As indicated by the figure, a linear relationship exists between dry matter weight loss and CO_2 evolution exceeding 99% confidence level independent of

temperature and moisture content with a correlation coefficient of 0.83. This relationship indicates that CO_2 evolution could be used to estimate weight loss for online monitoring.

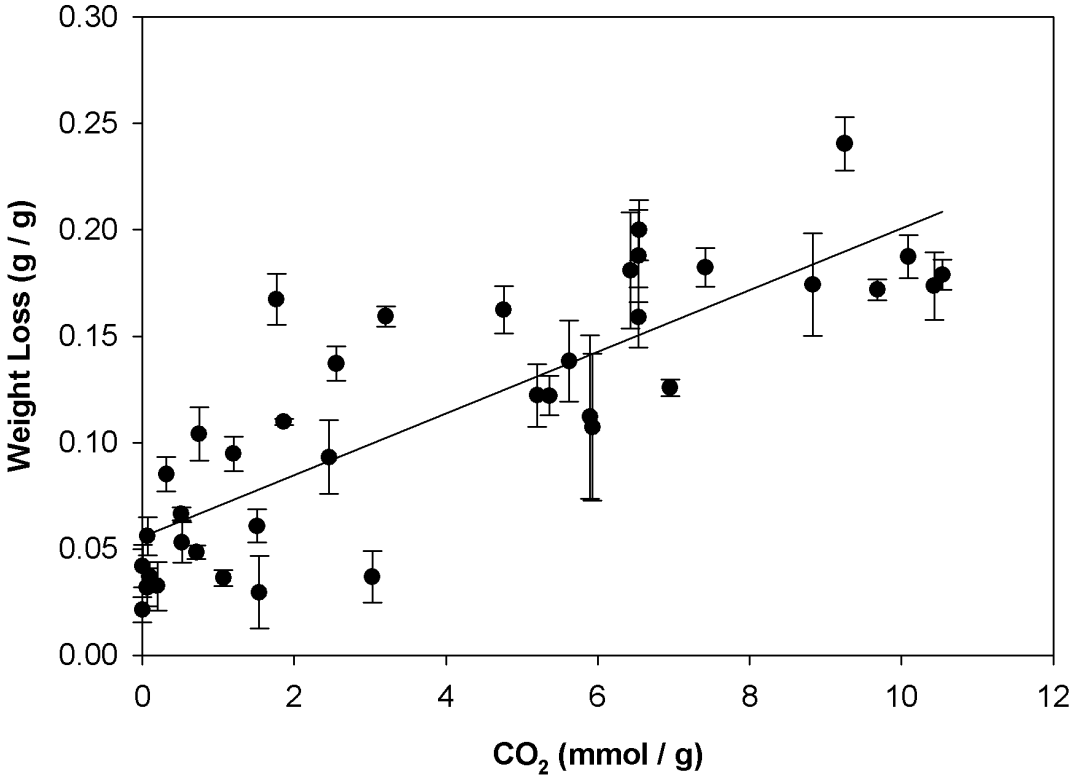

Figure 2.4. Experimental correlation between substrate weight loss and cumulative CO_2 evolution.

2.3.5. Compositional Changes

DGS coproducts have become an important economic component of the fuel ethanol industry. Any research utilizing distillers grain must consider the potential impact of the process on the feed value of the resulting DGS. Yang et al [24] showed reductions in the total content of ADF and NDF during the SSF process when a mixture of DDGS and soybean cotyledon fiber was used as the fermentation substrate. The authors concluded that the value of the resulting substrate when evaluated as a monogastric animal feed was enhanced. In this study the substrate and the solids after fermentation and enzyme

extraction were analyzed for fat, ADF, NDF, and protein. The remaining components not analyzed include ash, starch, sugar, and cell biomass components. Results for the fermentation experiments which included 50% initial moisture at 25.0 ºC, 30.0 ºC, and the two stage temperature experiments are shown in Table 2.1. As shown in this table, the fat content of the WDG was reduced in all cases; however, CDS contains high quantities of fat [18] which can be blended with the fermented solids to increase the fat content of the feed product if desirable. The ADF and NDF were reduced in all cases; a desirable alteration when WDG is used as a nonruminant feed. Experiments at 30.0 ºC showed the highest fungal activity of the three conditions tested, see Figure 2.2(c), and resulted in the largest reduction in ADF and NDF. The two stage temperature and the 25.0 ºC experiments had lower fungal activities but higher cellulase productions and resulted in a lower reduction in total carbohydrates. The lack of correlation between cellulase production and the reduction in total carbohydrates in these experiments indicate that lower fermentation temperatures promote higher cellulase production while higher temperatures promote higher fungal biomass production and metabolism. The crude protein content showed a slight increase after the fermentation was complete for all of the conditions examined. The increase in protein content is likely due to the reduced overall mass of the substrate caused by carbohydrate consumption during fungal metabolism.

Table 2.1. Compositional changes on a dry basis of the substrate and solids after fermentation and enzyme extraction.

Conditions		% Fat	% ADF	% NDF	% Protein
25 °C	Substrate	9.7	29.8	50.5	33.2
	Fermented Solids	4.4	16.9	39.5	36.1
30 °C	Substrate	8.7	34.7	59.5	31.9
	Fermented Solids	2.7	17.8	40.3	36.7
Two Stage	Substrate	8.7	29.3	49.6	32.7
	Fermented Solids	5.3	24.5	44.9	34.1

ADF Acid Detergent Fiber, *NDF* Neutral Detergent Fiber

The NDF, ADF, and fat losses as a function of the substrate weight loss per g of the initial fermented solids are presented in Figure 2.5. As is shown in this figure, there was a direct correlation between the substrate weight loss and losses for the three compositional components. As the substrate weight loss was increased, the ADF, NDF, and fat losses were also increased, suggesting weight loss to be an indicator of substrate consumption. This is a useful relationship which could be incorporated into online monitoring and kinetic modeling by combining the relationships shown in Figure 2.4 and 2.5. The reduction in NDF and fat exceeded the total weight loss as indicated in Figure 2.5, which is expected since carbohydrates and fat are being converted into fungal biomass, enzymes, and CO_2.

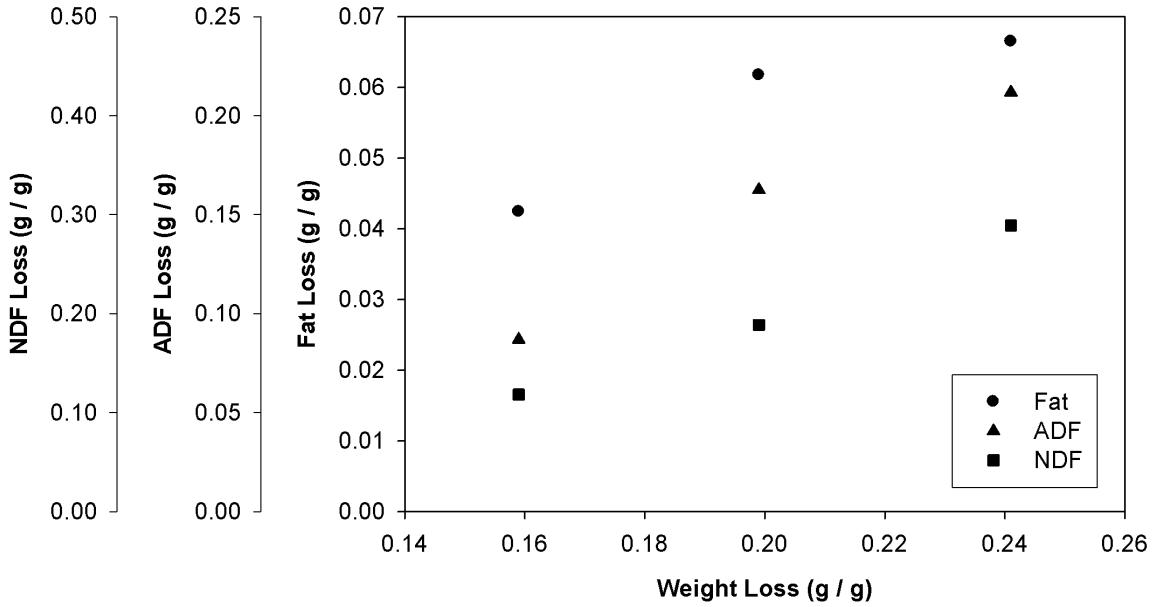

Figure 2.5. Compositional losses of NDF, ADF, and fat vs. weight loss per g initial substrate for the fermented substrate.

2.3.6. Pretreatment and Enzymatic Hydrolysis of WDG

Hydrolysis experiments were performed to determine the effectiveness of the enzymes prepared by SSF on substrates that could be used to produce cellulosic biofuels. Previous studies have shown poor correlations between measured enzyme activities and their effectiveness during hydrolysis of agro-industrial residues [25]. WDG was chosen as a substrate because of its availability, and because it originates at existing biofuel production facilities which eliminates additional agriculture, transportation, and pre-processing costs. Dilute acid pretreated WDG and non-pretreated WDG were tested.

Dilute acid hydrolysis was performed on WDG using 15% solids loading and 1 vol% sulfuric acid at 120 ºC for 30 min. Results of the dilute acid pretreatment are presented in Table 2.2. The monomeric sugar concentration of the hydrolysate was 29.91±0.83 g/L (0.199±.006 g per g substrate), which is within the margin of variability when compared with results obtained by Noureddini et al [16] using DDG as a substrate. The monomeric

sugar yield was comprised mostly of xylose and arabinose, the primary sugars found in hemicellulose. The pretreated material was adjusted to a pH of 5.0 using NaOH and the solids were then recovered for enzymatic hydrolysis.

Table 2.2. Dilute acid pretreated WDG sugar hydrolysate concentrations and yield (15 wt% solids loading, 1 vol% H_2SO_4).

	Concentration (g / L)	**Yield (g / g WDG)**
Glucose	5.10 ± 0.28	0.034 ± 0.002
Xylose	12.98 ± 0.44	0.087 ± 0.003
Galactose	2.21 ± 0.05	0.015 ± 0.000
Arabinose	9.63 ± 0.09	0.064 ± 0.001
Cellobiose	1.00 ± 0.00	0.007 ± 0.000
Monomeric Sugars	29.91 ± 0.83	0.199 ± 0.006

Enzymatic hydrolysis utilized the extracted enzyme solution from two stage temperature fermentations previously described. Additional cellobiase from *A. niger* was added to adjust enzyme activities to 12.7 FPU and 30.7 CBU per g substrate. A 15% solids loading was used at a temperature of 50 ºC for 72 h. The concentration profiles for monomeric sugars and glucose are shown in Figure 2.6(a) and (b), respectively. The concentration of monomeric sugars was 33.7±0.3 g/L (0.225±0.002 g per g substrate) for pretreated WDG and 25.5±0.2 g/L (0.170±0.001 g per g substrate) for WDG. The initial concentration of monomeric sugars in the non-pretreated WDG may be attributed to the sugars in the extracted enzyme solution and to the residual sugars left after the ethanol fermentation process. In addition, the pretreated WDG contains residual sugar from the dilute acid pretreatment process since the solids were not washed. During the enzymatic hydrolysis the sugar concentration increased by 24.6 g/L for pretreated WDG and 21.8 g/L for non-pretreated WDG; however, the pretreated WDG had the advantage of approaching its maximum yield at a faster rate compared to the non-pretreated WDG.

Noureddini et al [16] used commercially available enzymes at a hydrolysis temperature of 45 ºC under otherwise identical experimental conditions for the hydrolysis of DDG and obtained a total monomeric sugar concentration of 24.3±1.1 g/L, within the range of variability compared to the result of this study, confirming the effectiveness of the enzyme cocktail prepared from the fermentation experiments.

The glucose concentration profiles for the hydrolysis of WDG are presented in Figure 2.6(b). The initial glucose concentration for both substrates was nearly the same. The pretreated WDG had a 20.9 g/L increase while the non-pretreated WDG increased by 13.0 g/L during the hydrolysis experiments. The significant difference in liberated glucose is likely due to the increased accessibility of the cellulose due to the hydrolysis of hemicellulose in the pretreated WDG. Comparing Figure 2.6(b) to Figure 2.6(a), an additional 5.1 g/L of non-glucose sugars were liberated from non-pretreated WDG compared to pretreated WDG, indicating that hemicellulase activity was likely present in the enzyme cocktail.

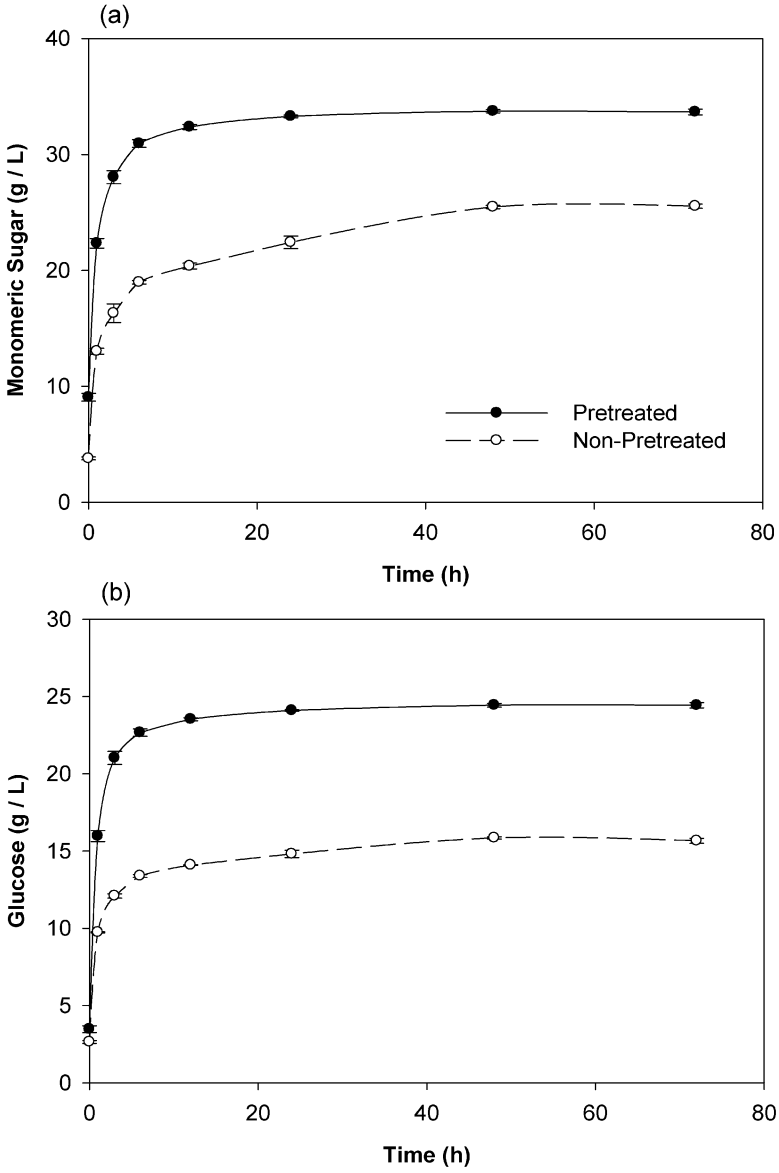

Figure 2.6. Concentration profiles for the enzymatic hydrolysis of WDG for (a) monomeric sugars and (b) glucose.

Based on the yield of cellulase production by SSF in this study (28.8 FPU/g), 0.44 g of WDG would be required to produce enough enzymes to hydrolyze 1 g of WDG at the enzyme loading tested. If dilute acid pretreatment is utilized then 0.388 g of sugar would be liberated for every 1 g of WDG hydrolyzed. Without pretreatment, 0.170 g of sugar would be available for every 1 g of WDG hydrolyzed. Assuming an average yield of

0.510 g ethanol per g sugar, 0.087 g ethanol per g non-pretreated WDG and 0.198 g ethanol per g pretreated WDG could be produced. On a dry basis, approximately half of the coproducts from a modern dry grind corn ethanol plant are WDG and the other half are CDS [26]. Therefore, a plant could increase ethanol production by up to 6.4% if a portion of the WDG was used to produce cellulase to hydrolyze the remaining pretreated WDG. The residual fermented solids could be blended with CDS and sold as a reduced fiber, high value animal feed product. Residual cellulase enzymes in the fermented substrate could potentially increase the feed value [27].

2.4. Conclusions

The production of cellulase by SSF using WDG as a substrate was demonstrated without supplementation of nutrients. The highest yield of cellulase, 28.8±0.8 FPU/g, occurred at 50% moisture when the temperature for the first 66 h was 27.5 ºC and was then lowered to 22.5 ºC. Significant cellulase production was observed for a wide range of initial substrate moisture contents indicating that large scale fermentations which often exhibit moisture gradients are feasible. The fermented WDG showed reductions in ADF and NDF content and an increase in protein content making it an attractive animal feed product. The extracted enzyme cocktail was shown to effectively hydrolyze WDG, producing additional sugars which could be used to increase ethanol production at the existing dry grind facilities. The enzymes produced could also be used to hydrolyze biomass such as corn stover. The conversion of cellulosic biomass to fermentable sugars is largest economic and technological barrier for the production of cellulosic biofuels [2]. The onsite production of cellulase enzymes at existing biofuel facilities using a readily

available substrate produced at the same facilities is expected to greatly reduce the cost of converting biomass to fermentable sugars. The residual fermented distillers grain substrate after enzyme extraction is expected to retain or even increase in feed value. These findings indicate that the production of cellulase enzymes from WDG should be investigated further.

Acknowledgements

We would like to thank the Nebraska Ethanol Board for their support of this work. We also thank the Abengoa Bioenergy facility in York, NE for providing the WDG used in this study and the University of Nebraska Animal Science Ruminant Nutrition Laboratory for completing composition analyses.

References

[1] Renewable Fuels Association. 2012 Ethanol Industry Outlook. http://www.ethanolrfa.org/pages/annual-industry-outlook. Accessed 2 August 2012.

[2] Viikari I, Vehmaanpera J, Koivula A. Lignocellulosic ethanol: From science to industry. Biomass Bioenerg 2012; 46: 13-24.

[3] Singhania RR, Sukumaran RK, Patel AK, Larroche C, Pandey A. Advancement and comparative profiles in the production technologies using solid-state and submerged fermentation for microbial cellulases. Enzyme Microb Technol 2010; 46: 541-549.

[4] Cen P, Xia L. Production of Cellulase by solid-state fermentation. Advances in Biochem Eng Biotechnol 1999; 65: 69-92.

[5] Holker U, Hofer M, Lenz J. Biotechnological advantages of laboratory-scale solid-state fermentation with fungi. Appl Microbiol Biotechnol 2004; 64: 175-186.

[6] Viniegra-Gonzalez G, Favela-Torres E, Aguilar CN, Romero-Gomez SDJ, Diaz-Godinez G, Augur C. Advantages of fungal enzyme production in solid state over liquid fermentation systems. Biochem Eng J 2003; 13: 157-167.

[7] da Silva Delabona P, Buzon Pirota RDP, Codima CA, Tremacodi CR, Rodrigues A, Farinas CS. Using Amazon forest fungi and agricultural residues as a strategy to produce cellulolytic enzymes. Biomass and Bioenerg 2012; 37: 243-250.

[8] Desgranges C, Georges C, Vergoignan C, Durand A. Biomass estimation in solid state fermentation II. On-line measurements. Appl Microbiol Biotechnol 1991; 35: 206-209.

[9] Cooney CL, Wang DIC, Mateles RI. Measurement of heat evolution and correlation with oxygen consumption during microbial growth. Biotechnol Bioeng 1968; 11: 269-281.

[10] Raimbault M, Alazard D. Culture method to study fungal growth in solid fermentation. European J Appl Microbiol Biotechnol 1980; 9: 199-209.

[11] Elia M, McDonad T, Crisp A. Errors in measurements of CO2 with the use of drying agents. Clin Chim Acta 1986; 158: 237-244.

[12] Ghose, TK. Measurement of cellulase activities. Pure Appl Chem 1987; 59: 257-268.

[13] Van Soest PJ. Use of Detergents in the Analysis of Fibrous Feeds. II. A Rapid Method for the Determination of Fiber and Lignin. J AOAC Int 1963; 46: 830.

[14] Bremer VR, Buckner CD, Brown AW, Carr TP, Diedrichsen RM, Erickson GE, Klopfenstein TJ. Lipid and NDF Analysis of Ethanol Byproduct Feedstuffs. Nebraska Beef Cattle Reports 2010; Paper 552.

[15] Hames B, Scarlata C, Sluiter A. In NREL laboratory analytical procedure. Determination of protein content in biomass. 2008; http://www.nrel.gov/biomass/pdfs/42625.pdf. Accessed 15 January 2011.

[16] Noureddini H, Byun J, Yu T J. Stagewise dilute-acid pretreatment and enzyme hydrolysis of distillers' grains and corn fiber. Appl Biochem Biotechnol 2009; 159: 553–567.

[17] Ruiz R, Ehrman T. In NREL laboratory analytical procedure. HPLC analysis of liquid fractions of process samples for monomeric sugars and cellobiose.1996; http://www.nrel.gov/ biomass/pdfs/4696.pdf. Accessed 27 December 2007.

[18] Liu K. Chemical composition of distillers grains, a review. J Agric Food Chem 2011; 59: 1508-1526.

[19] Kingsly ARP, Ileleji KI, Clementson CL, Garcia A, Maier DE, Stroshine RL, Radcliff S. The effect of process variables during drying on the physical and chemical

characteristics of corn dried distillers grains with solubles (DDGS) – plant scale experiments. Bioresour Technol 2010; 101: 193-199.

[20] Xin F, Geng A. Horticultural Waste as the Substrate for Cellulase and Hemicellulase Production by *Trichoderma reesei* Under Solid-State Fermentation. Appl Biochem Biotechnol 2010; 162: 295-306.

[21] Pandey A. Solid-state fermentation. Biochem Eng J 2003; 13: 81-84.

[22] Mitchell DA, von Meien OF, Luz Jr LFL, Berovič M. The scale-up challenge for SSF bioreactors. In: Mitchell DA, Krieger N, Berovič M, editors. Solid-State Fermention Bioreactors Fundamentals of Design and Operation, Berlin: Springer; 2006, p. 57-64.

[23] Smits JP, Rinzema A, Tramper J, Van Sonsbeek HM, Knol W. Solid-state fermentation of wheat bran by *Trichoderma Reesei* QM9414: substrate composition changes, C balance, enzyme production, growth and kinetics. Appl Microbiol Biotechnol 1996; 46: 489-496.

[24] Yang S, Lio JY, Wang T. Evaluation of enzyme activity and fiber content of soybean cotyledon fiber and distiller's dried grains with solubles by solid state fermentation. Appl Biochem Biotechnol 2012, 167: 109-121.

[25] Kabel MA, van der Maarel MJEC, Klip G, Voragen AGJ, Schols HA. Standard assays do not predict the efficiency of commercial cellulase preparations towards plant materials. Biotechnol Bioeng 2006; 93: 56-63.

[26] Monceaux DA, Kuehner D. Dryhouse technologies and DDGS production. In: Ingledew WM, Austin G, Kelsall D, Kluhspies C, editors. The Alcohol Textbook fifth ed., Nottingham: Nottingham University Press; 2009, p. 303-322.

[27] Bedford MR. Exogenous enzymes in monogastric nutrition – their current value and future benefits. Anim. Feed Sci. Technol. 2000; 86: 1-13.

Chapter 3

Effects of Intermittent Mechanical Mixing on Solid-State Fermentation of Wet Corn Distillers Grain with *Trichoderma reesei*

Abstract

The influence of mixing on microorganism integrity and product formation is a critical design parameter for solid-state fermentation bioreactors. The effects of intermittent mechanical mixing on the solid-state fermentation of wet corn distillers grain with *T. reesei* NRRL 11460 for the production of cellulase were investigated. Experiments were conducted at mixing frequencies of 0, 1, 2, 3, and 6 d^{-1} at 27.5°C with an initial moisture content of 50%. The results indicate that mixing caused a one order of magnitude increase in spore production compared to fermentations at static conditions. The cellulase enzyme activity produced was minimally affected by mixing with only a 5-10% decrease in filter paper activity for mechanically mixed fermentations compared to static fermentations. Mixing at lower frequencies of 1, 2, and 3 d^{-1} caused an increase in CO_2 evolution compared to static conditions and higher mixing frequencies of 6 d^{-1}. A correlation between substrate weight loss and cumulative CO_2 evolution was established. The ability to intermittently mix a solid-state fermentation bioreactor with minimal detrimental effects increases the feasibility of onsite production of enzymes at biofuel facilities to lower the overall production costs of cellulosic biofuels.

3.1. Introduction

Solid-state fermentation (SSF) is the growth of microorganisms on a moist, solid substrate. SSF primarily uses filamentous fungi capable of producing a variety of

different products including enzymes, organic acids, conidia, and fungal biomass. SSF has the potential to become an economically competitive method of producing cellulase enzymes if biofuel produced from cellulosic biomass becomes an important part of the transportation fuel supply [1]. Cellulase enzymes are used to deconstruct cellulose, a crystalline glucose polymer. Cellulase enzymes are commonly produced from filamentous fungi such as *Trichoderma*, which has been shown to be an effective organism when used in SSF systems [2,3].

The removal of heat generated by microbes to control temperature while maintaining the moisture content of the substrate is a major barrier for SSF bioreactors [4]. In forcefully-aerated bioreactors, the air stream serves as the oxygen source and is the primary heat removal mechanism. Increases in bed temperature due to heat production often lead to excessive evaporation, even if the air stream is humidified to saturation. When heat is transferred from the bed to the air stream, the air becomes unsaturated and moisture is absorbed from the bed. Evaporative cooling can be used intentionally to regulate temperature with the consequence of lowering the moisture content. Research has shown that the presence of moisture is critical in maintaining microorganism activity and product formation [2]. Substrate particle aggregation is another concern that can lead to poor bioreactor yield in SSF systems. Weber et al [5] concluded that substrate shrinkage combined with strong hyphal networks caused channeling, overheating, and non-homogenous fungal growth in a packed bed reactor when growing *A. oryzae* on wheat and hemp. Schutyser et al [6] found that breaking mycelia was required to prevent process failure due to channeling before moisture addition was needed when growing *A. oryzae* on wheat. Mixing can be used to mitigate channeling caused by mycelial growth

and allows for the uniform distribution of water to make up for evaporative moisture loss. Fungal morphology, substrate characteristics, fermentor design, and mixing regime all play a role in the effect of mixing on SSF processes, indicating the need for further experimental investigation [6].

One of the most important factors when designing a SSF bioreactor is the effect of mixing on microorganism growth and product formation [4,7]. Nava et al [8] showed that there were no significant differences in CO_2 evolution, oxygen uptake, or sporulation when mixing was used to reduce particle aggregation for *A. tamarii* growth on coffee pulp. Casas-Flores et al [9] observed mycelial injury induced conidiation in *Trichoderma* which may impact cellulase production, particularly after mixing. Silva and Yang [10] used a bench scale spouted bed reactor to determine the effect of mixing via spouting to produce amylases by fermenting rice with *A. oryzae*. The results showed that the unmixed packed bed and intermittent spouting every 4 h resulted in similar protein production rates of 3.1 mg/g. Spouting frequencies of 1 h and 2 h resulted in lower protein productions of 2.5 and 2.2 mg/g, respectively. Continual spouting resulted in a protein production of 0.7 mg/g. The authors concluded that spouting likely caused shear damage to the fungus which resulted in lower enzyme production at high spouting frequencies. Continuous agitation has the advantage of improving heat and oxygen transport, but is often unfavorable due to hyphal damage. Rotating drum bioreactors are often used for continuous or intermittent mixing but have limited capacities and are not typically considered forcefully aerated since air primarily flows over top of the substrate bed [4]. As a result, oxygen supply may be the limiting factor influencing mixing instead of temperature, moisture, or particle agglomeration.

Static forcefully-aerated bioreactors typically experience large temperature and moisture gradients. In order to minimize heterogeneity, complex internal airflow distributors are used as demonstrated by Brijwani et al [11]. However, internal airflow distributors may lead to maintenance, sanitation, and product transfer complexities as well as increased capital cost. If microorganisms can tolerate mixing, an alternative to bioreactors with internal airflow distributors are forcefully-aerated bioreactors with intermittent mechanical mixing. Intermittent mechanical mixing on a large scale process is feasible because a portion of the bed can be static while another portion is being mechanically mixed. Reactor capacities for non-sterile processes are in the order of magnitude of several tons [4]. Intermittent mixing also allows the competing interactions of mixing and static growth to be weighted and optimized. The mixing frequency that will yield optimum product formation can then be determined.

In this study, the effects of intermittent mixing on *T. reesei* NRRL 11460 were investigated by monitoring the conidia formed, cellulase activity produced, CO_2 evolution, substrate moisture content, and substrate weight loss when grown on wet distillers grain (WDG) byproducts from dry grind corn ethanol production. Mixing frequencies of 0, 1, 2, 3, and 6 d^{-1} were examined.

3.2. Materials and Methods

3.2.1. Inoculum Preparation

T. Reesei NRRL 11460 was obtained from USDA Northern Regional Research Laboratories. The microorganism was grown on potato dextrose agar slants at 30 ºC for 7 days. The inoculum was prepared by adding approximately 5 mL of deionized water to

the slant and dislodging spores by gentle pipetting. The solution was then diluted to 10^7 spores per mL using a hemacytometer (Cole-Parmer, Vernon Hills, IL) and 0.5 mL of the spore suspension was used to inoculate 2 g of substrate.

3.2.2. Substrate Preparation

WDG was provided by Abengoa Bioenergy in York, Nebraska. The WDG substrate was initially dried in an oven at 75°C and stored at -4°C. Each fermentation vessel contained 2 g of WDG on a dry basis. The substrate was inoculated with 0.5 mL of the solution as previously described. An additional 1.5 mL of deionized water was added to produce an initial substrate moisture content of 50%.

3.2.3. Solid-State Fermentations

Fermentations experiments were performed in 50 mL Erlenmeyer flasks and 1 cm diameter Kontes Flex Column glass chromatography columns (VWR International, Batavia, IL). The columns were aerated at 50 mL/min with humidified air; the flasks were aerated by natural convection. Experiments occurred at a constant temperature of 27.5 ºC maintained by a water bath. The 50 mL Erlenmeyer flasks were mixed using a VWR Mini Vortexer (VWR International, Batavia, IL) with a 3" rubber head for 30 s at 2000 RPM. The contents of the glass columns were first emptied into 100 mL beakers, mixed with the VWR Mini Vortexer, and then transferred back to the columns. The examined mixing frequencies were 0, 1, 2, 3, and 6 d^{-1}. A buffered fermentation was examined using a 0.05 M sodium citrate buffer at a pH of 4.8 to hydrate the substrate with a mixing frequency of 1 d^{-1}. The first mixing event for all frequencies occurred at approximately 66 h, after the initial lag phase ended and fungal growth had begun.

3.2.4. Fermentation Analysis

The effects of mixing on conidia formed, cellulase activity produced, CO_2 evolution, substrate weight loss, and substrate moisture content were determined. Conidia were measured after 136 h of fermentation by adding 25 mL of 0.01% Tween 80 and agitating on platform mixer at 200 rpm for 1 h. The samples were then appropriately diluted using 0.01% Tween 80 and spores were counted using a hemacytometer. Cellulase was extracted by adding 10 mL of 0.05 M sodium citrate buffer at a pH of 4.8 by agitating on a platform mixer at 200 rpm for 1 h. The contents were then centrifuged at 11,000 *g* for 10 min. The filter paper activity (FPU) of the extracted enzyme solution was determined by the method outlined by Ghose [12]. The effluent air from the forcefully aerated glass columns was dried with $CaCl_2$ desiccant and the CO_2 content was determined by a K-33 ICB infrared CO_2 sensor (CO2meter, Ormond Beach, FL). The dry matter weight loss and the moisture content of the samples were measured when a sample was sacrificed to determine its cellulase activity. Sample data was analyzed in triplicate which included one forcefully-aerated column and two Erlenmeyer flasks aerated by natural convection. Deviations in data are displayed using the standard error of the mean.

3.3. Results and Discussion

3.3.1. Conidiation

Asexual reproduction in *Trichoderma* can be triggered by light exposure and mechanical injury but is influenced by key environmental parameters such as the carbon to nitrogen ratio, ambient pH, and calcium ion concentration [13]. Experiments were performed to determine the influence of mixing on spore production and to determine the

effects of adding a buffering agent to the WDG media. Spores were counted after 136 h at the end of the fermentation experiments. The influence of mixing frequency on the quantity of conidia formed per g of initial dry WDG substrate is shown in Table 3.1. As is shown in this table, static fermentations produced the least amount of conidia, $(0.37 \pm 0.06) \times 10^8$. Mixing frequencies of 1 d^{-1} for buffered and unbuffered WDG resulted in a one order of magnitude increase in conidia when compared to static fermentation. Casas-Flores et al [9] observed conidiation caused by mechanical injury to mycelia for *T. atroviride*. Injury induced conidiation was likely the primary contributing factor to the increased spore production for mechanically mixed fermentations. The buffered media at a pH of 4.8 did reduce the quantity of spores produced compared to the unbuffered WDG. Steyaert et al [14] observed similar results using *T. atroviride* to determine the influence of pH on mycelia injury induced conidiation. They observed conidiation at all tested pH values using unbuffered PDA media, however, conidiation had a low pH dependency on buffered PDA media. The researchers found that conidiation was not triggered when the buffered media was above a pH value of 4.0, whereas the results from this study showed that the quantity of conidia declined under similar conditions.

A strong hyphal network was observed under static conditions. When mechanical mixing was introduced, the hyphal network was disrupted. Visual observations indicated that the network reformed between mixing events for mixing frequencies of 1 d^{-1} and 2 d^{-1}, particularly between 66 – 100 h of the fermentation. However, when the mixing frequency was increased to 3 d^{-1} and 6 d^{-1} the reformation of the hyphal network between substrate particles was not visually observable and mixing occurred the instant mechanical agitation was applied. The reforming and breaking of the hyphal network

between particles may have caused an increase in injury induced conidiation, resulting in higher spore production for mixing frequencies of 1 and 2 d^{-1} compared to 3 and 6 d^{-1}. This data indicates that high mixing frequencies may not be desirable when spore production is the primary objective, such as in the production of biocontrol agents.

Table 3.1. Conidia production at various mixing frequencies after 136 h.

Mixing Frequency (d^{-1})	**Conidia Production** (Spores × 10^8/g)
0	0.37 ± 0.06
1	5.71 ± 0.41
1 Buffered	3.00 ± 0.32
2	7.50 ± 0.05
3	4.50 ± 0.18
6	5.53 ± 0.35

A difference in spore color and hydrophobicity was observed when comparing spores produced during the static fermentation compared with the spores from mechanically mixed fermentations. Conidia produced from the static fermentation were colorless. Conidia from experiments that had been mechanically mixed exhibited green and brown color with increased hydrophobicity. The added color and hydrophobicity are signs of spore maturity, indicating that sporulation occurred earlier in fermentations with mechanical mixing.

3.3.2. Cellulase Production

The effect of mechanical mixing on cellulase production during SSF has significant implications on future biofuel enzyme production methods and costs. Fermentations experiments were performed as described earlier in section 3.2.3. Samples were collected every 24 h after the lag phase, and activities were measured as FPU per g of initial WDG

substrate on a dry basis. Cellulase activity production is plotted as a function of time in Figure 3.1 for different mixing frequencies. Results shown in Figure 3.1 indicate that mixing reduced cellulase production between 5-10% depending on the mixing frequency. The reduction in cellulase yield was significantly lower than results previously reported. Deschamps et al [15] observed a reduction in yield from 18 to 11 FPU per g of substrate due to mechanical mixing during SSF using *T. harzianum*. Ahamed and Vermette [16] found that mechanical agitation decreased cellulase yield from 17 to 13 FPU/mL during the growth of *T. reesei* in a submerged environment.

The static fermentation resulted in the highest cellulase yield of 12.5 ± 0.1 FPU/g at 138 h of fermentation as shown in Figure 3.1. The static fermentation was the only condition tested that yielded a significant increase in cellulase production after 113 h. The fermentations with mechanical mixing yielded cellulase activities ranging from 11.2 to 11.8 FPU/g with maximum values typically occurring at 113 h indicating that fermentations incorporating mixing could shorten the overall fermentation time. The buffered WDG media, mixed at a frequency of 1 d^{-1}, resulted in the lowest cellulase production (8.8 ± 0.9 FPU/g), but exhibited this yield at 88 h of fermentation which was higher than the static and mixing fermentation at this time.

The results of mixing on cellulase production indicate that mixing can be used at frequencies of up to 6 d^{-1} without significantly decreasing the cellulase production. These findings indicate that scale-up of SSF bioreactors for cellulase production is feasible due to the minimal effects of mixing on cellulase production while mitigating channeling and overheating problems that are typically encountered for unmixed systems. The ability to mix also permits engineers to evaluate additional options when choosing or

designing a bioreactor. For example a rotating drum bioreactor could be used which incorporates mixing but is not forcefully aerated since air primarily travels through the headspace and not the substrate itself. Forcefully aerated bioreactors which are intermittently mixed such as the reactor described by Sato and Sudo [17] would also be an attractive option due to their large capacities.

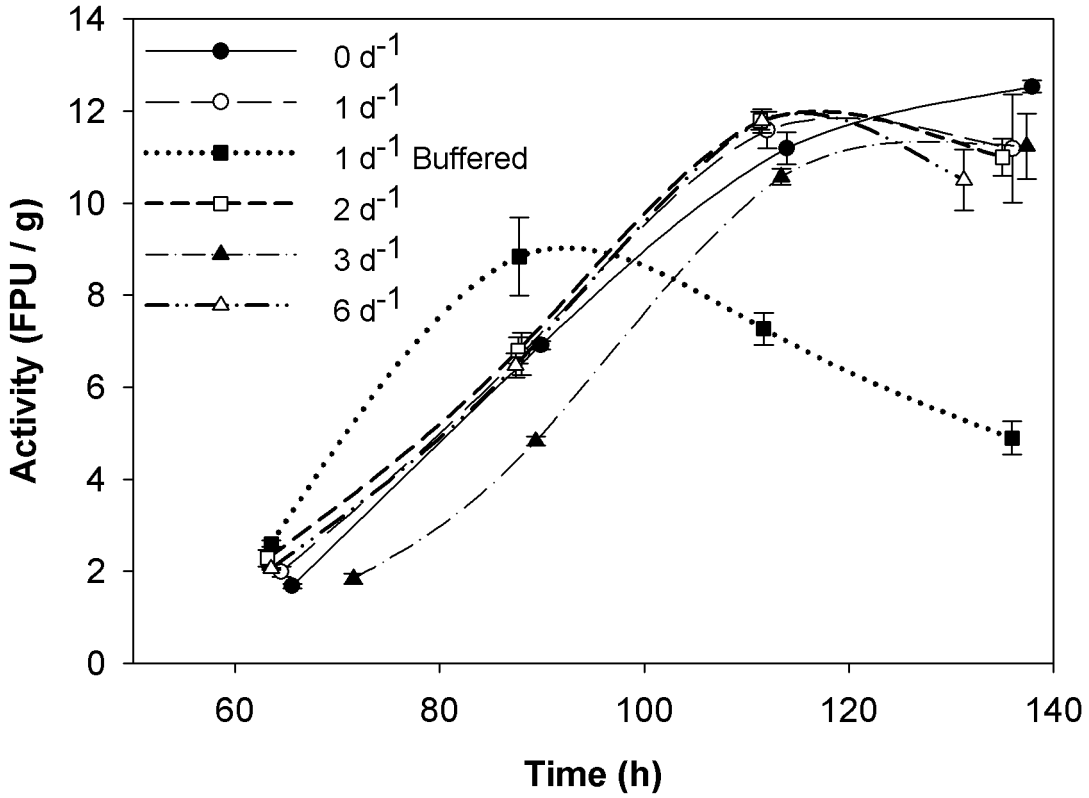

Figure 3.1. Cellulase activities per g of initial dry substrate at different mixing frequencies.

3.3.3. CO_2 Evolution

The direct quantification of fungal biomass in SSF processes is difficult because the microorganisms are fixed to the substrate particles. CO_2 evolution is an indirect measurement of fungal activity and can be used as an online indicator of fermentation conditions [18]. CO_2 production has also been correlated to metabolic heat evolution

[19,20]. The rate of CO_2 production as a function of time is shown in Figure 3.2. Comparing the different mixing frequencies indicates that there was not a significant difference in the length of active fermentation time for all unbuffered substrates. The active fermentation time for the unbuffered substrates was about 75 h from the end of the lag phase to the end of the decay phase. However, the buffered substrate resulted in a lower active fermentation time of about 60 h. The maximum CO_2 evolution rate was slightly higher for mixing frequencies of 1, 2, and 3 d^{-1} compared to 0 and 6 d^{-1}. The lag phase for the mixing frequency of 3 d^{-1} was about 7 h longer than the other conditions tested as indicated in Figure 3.2, but the active fermentation time was similar to other fermentations as the decay phase ended about 7 h later. The extended lag phase may have been caused by a lack of spore maturity or a lower quantity of viable spores in the inoculum. The extended lag phase explains why the cellulase activity for the mixing frequency of 3 d^{-1} appears to be shifted in time in Figure 3.1.

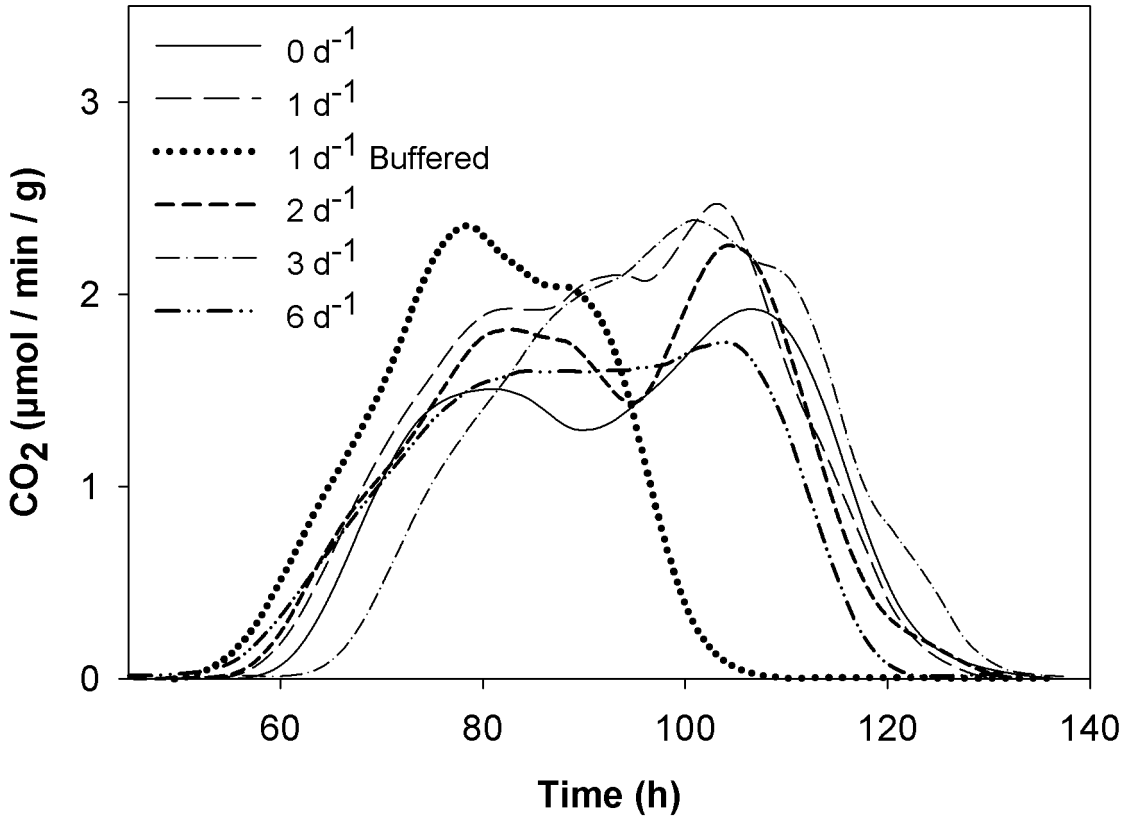

Figure 3.2. CO_2 evolution rate per g of initial dry substrate as a function of time for different mixing frequencies.

The cumulative CO_2 evolution per g of initial dry WDG for each experimental condition is displayed in Figure 3.3. It is clear that the final cumulative CO_2 evolution was also higher for mixing frequencies of 1, 2, and 3 d^{-1} compared to frequencies of 0 and 6 d^{-1}. The overall CO_2 evolution for the total fermentation time was less than 20% higher for the mixed fermentations at 1, 2, and 3 d^{-1} compared with the static fermentation. The buffered media had the lowest cumulative CO_2 evolution which was expected due the truncated active fermentation time.

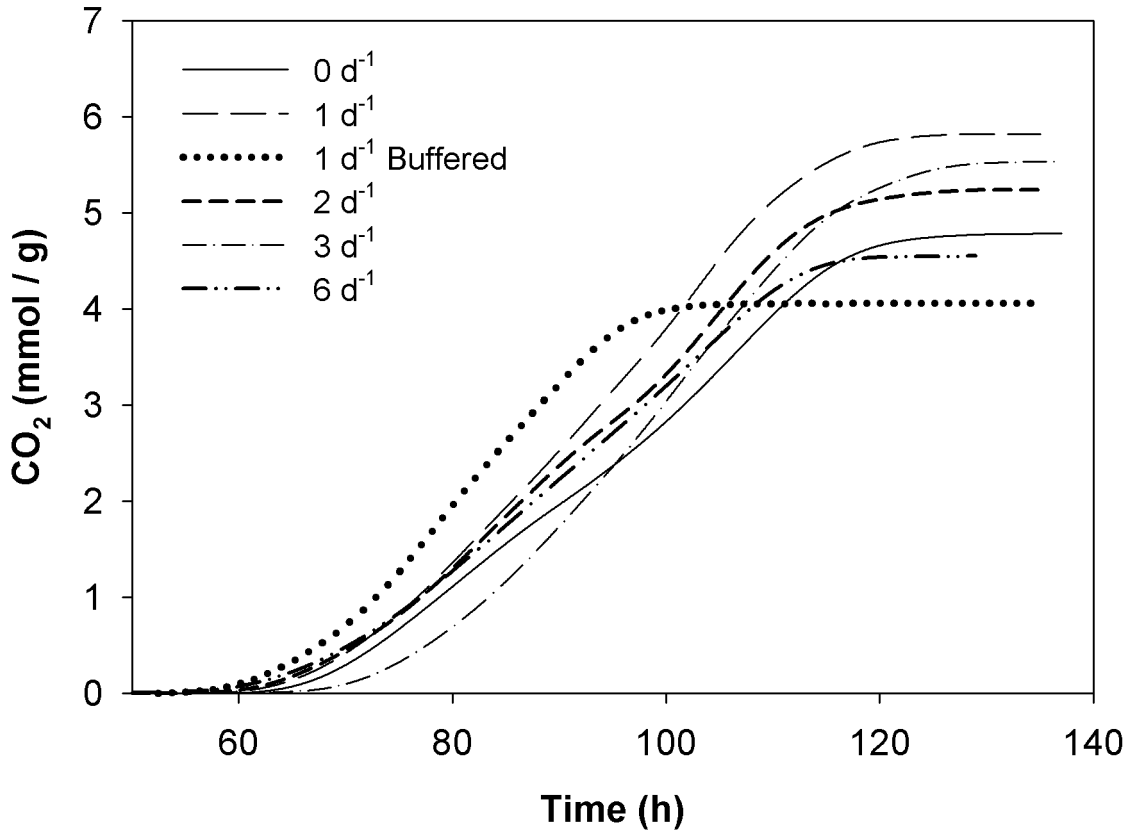

Figure 3.3. Cumulative CO_2 evolution per g of initial dry substrate for different mixing frequencies.

3.3.4. Substrate Weight Loss and Moisture Content

The substrate weight loss and moisture content were monitored during fermentations to determine the effects of mixing. The substrate weight loss in g of dry matter lost per g of initial substrate at the end of the fermentation for each mixing frequency is shown in Table 3.2. The data indicates the differences in substrate weight losses at different mixing frequencies were not significant except for the experiment utilizing the buffered media. The final moisture fraction of the fermented substrate is also displayed in Table 3.2. Once again mixing did not have a significant impact on the final moisture content of the substrate except for the buffered media which did have a significantly lower final

moisture content compared to the unbuffered substrates. Factors affecting moisture content include metabolic water production, evaporation, and condensation. The reduced cumulative CO_2 evolution of the microorganisms on the buffered substrate (Figure 3.3) indicates lower metabolic activity which may have contributed to the lower final moisture content.

Table 3.2. Substrate weight loss in g of dry weight lost per g of initial dry substrate and fermented substrate moisture fraction after 136 h of fermentation for different mixing frequencies.

Mixing Frequency (d^{-1})	Substrate Weight Loss (g/g)	Moisture Content (moisture fraction)
0	0.154 ± 0.020	0.557 ± 0.010
1	0.150 ± 0.006	0.557 ± 0.008
1 Buffered	0.112 ± 0.019	0.534 ± 0.007
2	0.144 ± 0.042	0.550 ± 0.023
3	0.177 ± 0.026	0.558 ± 0.006
6	0.155 ± 0.003	0.552 ± 0.001

Increased spore production caused by mechanical mixing did not have a significant impact on the dry matter weight loss or moisture content of the substrate. However, a correlation existed between the dry matter weight loss and the cumulative CO_2 evolution for various mixing frequencies as illustrated in Figure 3.4. Smits et al [21] showed a similar trend for *T. reesei* grown on wheat bran at various temperatures without mixing. The correlation shown in Figure 3.4 indicates that online monitoring of CO_2 evolution during fermentation yields an estimation of substrate weight loss with mechanically mixed fermentations. The linear regression best fit line does not pass through the origin of the plot indicating the sensors lack of sensitivity at low concentrations of CO_2. The correlation coefficient of determination (R^2) for the fit was 0.873.

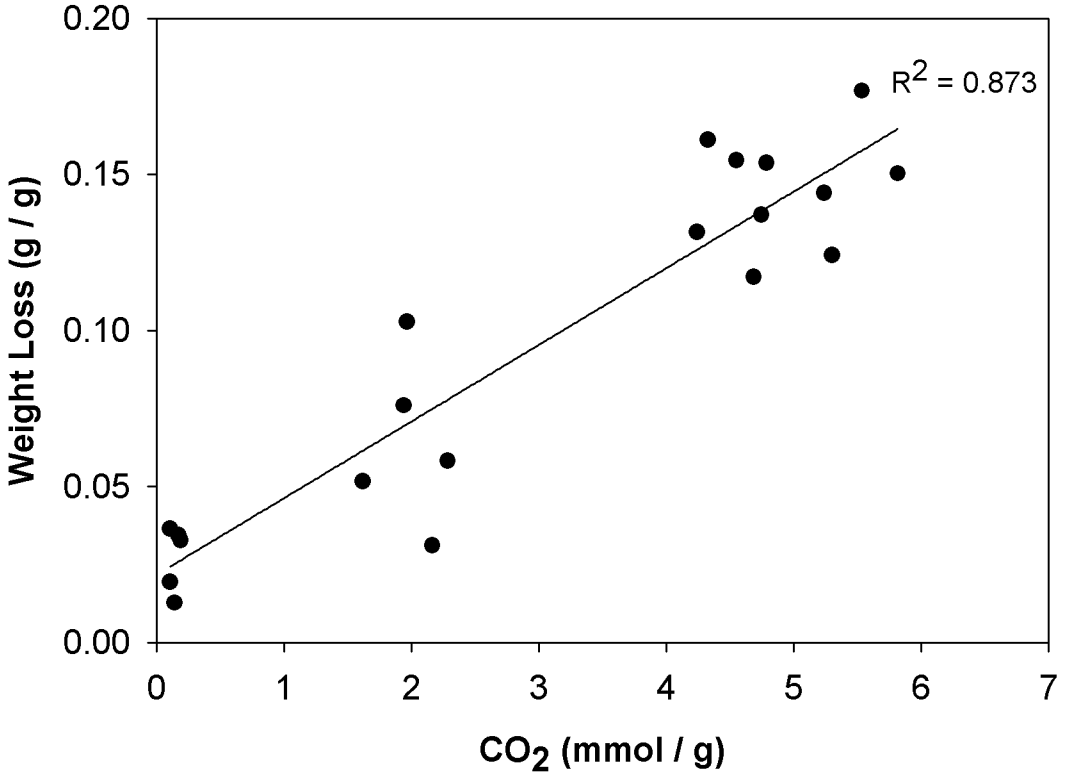

Figure 3.4. Correlation between substrate dry matter weight loss per g of initial dry substrate vs. cumulative CO_2 evolution per g of initial dry substrate for various mixing frequencies.

3.4. Conclusions

Mixing is required in large scale SSF processes to mitigate channeling, overheating, and non-uniform moisture problems; however, mixing is often associated with mycelial damage and reduced product formation. Results of this study show that conidia production can be increased significantly for *T. reesei* using mechanical mixing at frequencies of 1 and 2 d^{-1}, higher mixing frequencies reduced conidia production. Mixing did not have significant effects on substrate weight loss or moisture content throughout fermentations. The effect of mixing on the formation of cellulase activity was minimal, reducing activity by 5-10% for all mixing frequencies examined compared to

static conditions. A correlation was found between dry matter weight loss and cumulative CO_2 evolution at various mixing frequencies.

These results indicate that mixing can be incorporated into bioreactor design and operation when *T. reesei* is grown on WDG. The ability to mix a SSF bioreactor with minimal detrimental effects increases the feasibility of onsite production of enzymes at biofuel facilities, lowering the overall production costs of cellulosic biofuels. Mixing regime and mixing method, for example mechanical versus gas-fluidized based agitation, are expected to play a role in the effects of mixing on fermentation behavior; therefore, pilot scale bioreactor studies are required.

Acknowledgements

We would like to thank the Nebraska Ethanol Board for their support of this work. We also thank the Abengoa Bioenergy facility in York, NE for providing the WDG used in this study.

References

[1] R.P. Tengerdy RP, G. Szakacs, Bioconversion of lignocellulose in solid substrate fermentation, Biochem. Eng. J. 13 (2003) 169-179.

[2] F. Xin, A. Geng, Horticultural Waste as the Substrate for Cellulase and Hemicellulase Production by *Trichoderma reesei* Under Solid-State Fermentation, Appl. Biochem. Biotechnol. 62 (2010) 295-306.

[3] S. Yang, J.Y. Lio, T. Wang, Evaluation of enzyme activity and fiber content of soybean cotyledon fiber and distiller's dried grains with solubles by solid state fermentation, Appl. Biochem. Biotechnol. 167 (2012) 109-121.

[4] A. Durand, Bioreactor designs for solid state fermentation, Biochem. Eng. J. 13 (2003) 113-125.

[5] F.J. Weber, J. Oostra, J. Tramper, A. Rinzema, Validation of a model for process development and scale-up of packed-bed solid-state bioreactors, Biotechnol. Bioeng. 77 (2002) 381-393.

[6] M.A.I. Schutyser, P. de Pagter, F.J. Weber, W.J. Briels, R.M. Boom, A. Rinzema, Substrate aggregation due to aerial hyphae during discontinuously mixed solid-state fermentation with *Aspergillus oryzae*: Experiments and modeling, Biotechnol. Bioeng. 83 (2003) 503-513.

[7] D.A. Mitchell, M. Berovič, N. Krieger, Introduction to Solid-State Fermentation Bioreactors, in: D.A. Mitchell, N. Krieger, M. Berovič (Eds.), Solid-State Fermention Bioreactors Fundamentals of Design and Operation, Springer, Berlin, 2006, pp. 33-44.

[8] I. Nava, E. Favela-Torres, G. Saucedo-Castaneda, Effect of mixing on solid-state fermentation of coffee pulp with *Aspergillus tamari*, Food Technol. Biotechnol. 49 (2011) 391-395.

[9] S. Casas-Flores, M. Rios-Momberg, M. Bibbins, P. Ponce-Noyola, A. Herrera-Estrella, BLR-1 and BLR-2, key regulatory elements of photoconidiation and mycelial growth in *Trichoderma atroviride*, Microbiol. 150 (2004) 3561-3569.

[10] E.M. Silva, S.T. Yang, Production of amylases from rice by solid-state fermentation in a gas-solid spouted-bed bioreactor, Biotechnol. Prog. 14 (1998) 580-587.

[11] K. Brijwani, P.V. Vadlani, K.L. Hohn, D.E. Maier, Experimental and theoretical analysis of a novel deep-bed solid-state bioreactor for cellulolytic enzymes production, Biochem. Eng. J. 58-59 (2011) 110-123.

[12] T.K. Ghose, Measurement of cellulase activities, Pure Appl. Chem. 59 (1987) 257-268.

[13] J.M. Steyaert, R.J. Weld, A. Mendoza-Mendoza, A. Stewart. Reproduction without sex: conidiation in the filamentous fungus *Trichoderma*, Microbiol. 156 (2010) 2887-2900.

[14] J.M. Steyaert, R.J. Weld, A. Stewart, Ambient pH intrinsically influences *Trichoderma* conidiation and colony morphology, Fungal Biol. 114 (2010) 198-208.

[15] F. Deschamps, C. Giuliano, M. Asther, M.C. Huet, S. Roussos, Cellulase production by *Trichoderma harzianum* in static and mixed solid-state fermentation reactors under nonaseptic conditions, Biotechnol. Bioeng. 27 (1985) 1385-1388.

[16] A. Ahamed, P. Vermette, Effect of mechanical agitation on the production of cellulases by *Trichoderma reesei* RUT-C30 in a draft-tube airlift bioreactor, Biochem. Eng. J. 49 (2010) 379-387.

[17] K. Sato, S. Sudo, Small-scale solid-state fermentations, in: A.L. Demain, J.E. Davies (Eds.), Manual of industrial microbiology and biotechnology 2nd Ed., ASM Press, Washington DC, 1999, pp. 61-79.

[18] C. Desgranges, C. Georges, C. Vergoignan, A. Durand, Biomass estimation in solid state fermentation II. On-line measurements, Appl. Microbiol. Biotechnol. 35 (1991) 206-209.

[19] C.L. Cooney, D.I.C. Wang, R.I. Mateles, Measurement of heat evolution and correlation with oxygen consumption during microbial growth, Biotechnol. Bioeng. 11 (1968) 269-281.

[20] J.S. Lekanda, J.R. Perez-Correa, Energy and water balances using kinetic modeling in a pilot-scale SSF bioreactor, Process Biochem. 39 (2004) 1793-1802.

[21] J.P. Smits, A. Rinzema, J. Tramper, H.M. Van Sonsbeek, J.C. Hage, A. Kaynak, W. Knol, The influence of temperature on kinetics in solid-state fermentation, Enzyme Microb. Technol. 22 (1998) 50-57.

Chapter 4

Development of a Solid-State Fermentation Kinetic Model Based on CO_2 Production for the Growth of *T. reesei* on Wet Corn Distillers Grain

Abstract

A kinetic model was developed based on CO_2 production for the growth of *T. reesei* on wet corn distillers grain during solid-state fermentation. The model used the integrated Gompertz equation to fit experimental data using regression analysis. The model parameters were found to be a function of fermentation temperature and initial moisture content. The rate of cellulase production, substrate weight loss, and water production were assumed to be proportional to the rate of CO_2 production. Fermentations with step changes in temperature were then performed to simulate a bioreactor with time dependent changes due to heterogeneity. The rate based model was then integrated numerically and compared to the experimental data. Results show that CO_2 production and substrate weight loss can be predicted using the proposed kinetic model. Cellulase production and water production exhibited larger errors using the rate based model, especially at the end of the fermentation when the rate of CO_2 production was significantly declining. Overall the kinetic model based on CO_2 production instead of difficult to measure biomass concentration, showed advantages due to its simplicity and capability of being incorporated into online monitoring and control of bioreactors. The developed kinetic model can be combined with material and energy balances to predict heterogeneous bioreactor behavior, a useful tool for the design and scale-up of bioreactors.

4.1. Introduction

Kinetic models are integral to the development of solid-state fermentation (SSF) processes. Kinetic models are combined with material and energy balances to design and scale-up bioreactors, develop process control schemes, and optimize product formation and profit. Heterogeneous reactor conditions including temperature and moisture gradients, which are common in SSF bioreactors, affect both microbial growth and product formation increasing the importance of having an accurate kinetic model.

The characteristics of SSF inherently complicate modeling, for example microorganism biomass concentration is difficult to measure since microorganisms are fixed to the substrate and typically exhibit mycelial growth. Synthetic membrane systems have been used under controlled experimental conditions in order to determine indirect biomass concentration indicators. Indirect measurements include microorganism cell constituents such as glucosamine or ergosterol, but the length of time to complete analytical procedures for measurement of these components is a weakness [1]. Infrared methods were also shown to be a valid method of estimating cell constituents and therefore biomass concentration [2,3], but this technique is cost prohibitive and not feasible for online determination of samples with heterogeneous distribution or for large surface areas [4]. The concentration of cell constituents such as glucosamine can also change throughout the fermentation, leading to inaccurate biomass estimations [1,5]. Yingyi et al [4] suggest digital image analysis as another alternative to quantify biomass growth by analyzing high resolution images of the mycelia-substrate matrix.

The continuous on-line measurement of CO_2 production allows biomass concentration to be estimated in real time without analytical lab procedures. Desgranges

et al [2] observed a strong correlation between CO_2 evolution and biomass for a solid state culture of *Beauveria bassiana*. One disadvantage of estimating cell biomass from the quantity of CO_2 produced is that CO_2 production per unit weight of biomass was found to be dependent on conditions such as the substrate media composition.

Many kinetic models have been proposed for the growth of microorganisms during SSF. Due to the complexity of the process, empirical models are typically used. Proposed models include linear, exponential, logistic, and two phase time dependent models [6]. The effect of environmental variables on kinetics is typically modeled through the specific growth rate, μ. For example in the logistic growth equation:

$$\frac{dX}{dt} = \mu X\left(1 - \frac{X}{X_m}\right) \tag{4.1}$$

where X is the microbial biomass concentration, t is time, μ is the specific growth rate, and X_m is the maximum microbial biomass concentration. The specific growth rate and maximum microbial biomass concentration would then be evaluated at different fermentation conditions and could be written as a function of temperature and/or moisture. Typically, the kinetic parameters are evaluated using fermentations with a constant temperature throughout the fermentation time and fit to Eq. 4.1 after integration. After multiple temperatures are tested, then the fitted kinetic parameters are plotted vs. the varied environmental variable and a correlation is determined. A rate based modeling approach that describes the rate of microbial growth at any instant at any environmental condition is desirable since SSF reactors typically exhibit temperature and moisture gradients, however kinetic determinations are typically based on constant conditions as demonstrated by Smits et al [7]. The constant conditions are then fit to rate based model

by making the growth rate and maximum biomass concentration a function of temperature and/or moisture. Saucedo-Castaneda et al [8] fit the specific growth rate, μ, to a double Arrhenius equation and the maximum biomass concentration to a fourth order polynomial as a function of temperature. However, as Mitchell et al [9] hypothesized, the value for the maximum biomass concentration likely depends on the temperature history of the fermentation. The effects of moisture content have also been used to adjust the specific growth rate. Von Mein and Mitchell [10] fit the specific growth rate to data from Glenn and Rogers [11] as a function of the water activity. Sargantanis et al [12] suggested that both the effects of temperature and moisture could be incorporated into the specific growth parameter by the relationship:

$$\mu = \sqrt{\mu_T(T)\mu_W(\phi)} \tag{4.2}$$

where μ_T is the specific growth rate as a function of temperature, μ_W is the specific growth rate as a function of moisture content, and Φ is the moisture content in mass of water per mass of dry solids.

Modeling product formation, especially for enzymes or secondary metabolites, can be difficult since production is often dependent on a variety of conditions including the metabolic state of the cell [13]. Ooijkaas et al [14] modeled the rate of spore formation by the relationship:

$$\frac{dP}{dt} = Y_{PX}\frac{dX}{dt} + m_P X \tag{4.3}$$

where P is the product concentration, Y_{PX} is the yield of product from microbial growth, and m_P is the coefficient for product formation related to maintenance metabolism. Because of the difficulty associated with modeling fungal biomass growth, modeling

product formation has not been emphasized in literature even though it is often the objective of SSF processes. Similar to product formation, the same form of Eq. 4.3 can be used to predict substrate consumption, metabolic heat evolution, and metabolic water production as demonstrated by Lekanda and Perez-Correa [15].

An alternative approach to modeling was used by Christen et al [16] to model fruity aroma and CO_2 production during SSF. A sigmoidal Gompertz model was used:

$$G = G_{\max} \exp(-b * \exp(-kt)) \tag{4.4}$$

where G is the quantity of CO_2 produced per unit weight of substrate as a function of time, G_{max} is the maximum quantity of CO_2 produced, k is the production rate constant, and b is a dimensionless factor. The value of k determines the time it takes for the value of G to reach G_{max}; larger values of k will cause G to reach G_{max} in a shorter amount of time. The value of b determines the shape of the sigmoidal curve; larger values of b will cause the initial exponential growth phase to be slower and the deceleration phase to reach the asymptote faster whereas smaller values of b will cause a rapid exponential growth phase and slower deceleration before the asymptote of G_{max} is reached.

A version of the Gompertz model was used by Laird [17] to model the growth of tumors for various types of cancer. Similar to microorganisms growing in SSF bioreactors, tumors typically grow in a confined space with cancerous cells competing for a limited quantity of nutrients. Therefore growth may initially exhibit exponential behavior, but as nutrients and space become limited, growth deceleration is observed until an asymptote is reached. Growth and deceleration characteristics are inherently found in the Gompertz model. The Gompertz model has also been used to model product formation when producing lactic acid on cassava [18,19].

In this study, a kinetic model for data reported in the previous chapters for the production of CO_2, cellulase, and water during SSF of wet corn distillers grain (WDG) with *Trichoderma reesei* NRRL 11460 was developed based on the Gompertz equation, Eq. 4.4. The kinetic model was based on easily measurable CO_2 production instead of biomass concentration. Additional experiments were conducted to determine if a rate based Gompertz model could adequately predict non-constant fermentation conditions by varying the temperature of the fermentation with time. A rate based model for changing fermentation conditions can be used for predicting large scale bioreactor behavior when combined with mass and energy balances.

4.2. Materials and Methods

4.2.1. Solid-State Fermentations

Solid state fermentation of wet corn distillers grain (WDG) with *Trichoderma reesei* NRRL 11460 at different temperature and moisture conditions were previously completed as reported in Chapter 2. Experimental conditions included a temperature range of 22.5 to 32.5°C at an initial moisture content of 1.00 kg water per kg of initial dry substrate. Moisture contents ranging from 0.82 to 1.50 kg of water per kg of initial dry substrate at a constant temperature of 30.0°C were also examined. The cellulase activity, CO_2 production, dry matter weight loss, and moisture content were monitored throughout the fermentation. The experimental procedure outlined in Chapter 2 was used to complete additional experiments at non-uniform fermentation conditions by making step changes in temperature.

4.2.2. Modeling Equations

The integrated Gompertz model (Eq. 4.4) was used to model the experimental data for cumulative CO_2 production. The rate based Gompertz model is found by taking the derivative of Eq. 4.4 with respect to time:

$$\frac{dG}{dt} = G_{\max} bk \exp(-kt) \exp(-b * \exp(-kt)). \quad (4.5)$$

The rate based model can be used to estimate CO_2 production as fermentation conditions change, therefore the values of G_{max}, b, and k in Eq. 4.5 can change as a function of time due to temperature and moisture changes during fermentation. The integrated rate based model with changing fermentation conditions would not result in Eq. 4.4 since parameters would not be considered constants. CO_2 production is an indirect indicator of fungal biomass quantity, but was assumed to be dependent on temperature and moisture content.

Cellulase formation was modeled with the assumption that product formation is proportional to fungal activity and therefore to the rate of CO_2 production. The formation of cellulase during fermentation is:

$$\frac{dP}{dt} = Y_P \frac{dG}{dt} \quad (4.6)$$

where P is the cellulase activity produced in FPU per g of initial dry substrate and Y_P is the cellulase yield coefficient with units of FPU per mmol CO_2 produced which is dependent on fermentation conditions such as temperature and moisture content. Substrate weight loss was also modeled using the same form of Eq.4.6:

$$\frac{dS}{dt} = Y_S \frac{dG}{dt} \quad (4.7)$$

where S is the substrate weight loss in g per g of initial dry substrate and Y_S is the substrate weight loss yield coefficient with units of g of weight lost per mmol CO_2 produced. Similarly, the production of water was modeled:

$$\frac{dW}{dt} = Y_W \frac{dG}{dt} \tag{4.8}$$

where W is the g of water produced per g of initial dry substrate and Y_W is the water yield coefficient in g of water produced per mmol CO_2 produced.

4.2.3. Data Analysis

Mathcad software was used to fit the model parameters to experimental data using a Levenburg-Marquardt nonlinear regression analysis. Time zero was defined as the first measurable quantity of CO_2 produced; therefore the lag phase occurred before time zero. The parameters G_{max}, b, and k for cumulative CO_2 production were fit to the fermentations occurring at uniform temperature conditions using the integrated Gompertz model (Eq. 4.4). The CO_2 modeling parameters were used with experimental data for cellulase production, substrate weight loss, and water production for the nonlinear regression of yield coefficients in Eqs. 4.6, 4.7, and 4.8.

4.3. Results and Discussion

4.3.1. CO_2 Production

The cumulative CO_2 production from the SSF of WDG with *T. reesei* was modeled using a Gompertz model (Eq. 4.4). The model parameters G_{max}, b, and k were found by nonlinear regression analysis using the Levenberg-Marquardt method. An example of the fit from experimental data at 32.5 ºC with an initial moisture content of 1.00 kg water per kg of initial dry substrate is shown in Figure 4.1(a). The figure shows that the

experimental values for cumulative CO_2 production first exhibit an exponential increase followed by a linear increase before deceleration tapers CO_2 production to an asymptote. The Gompertz model exhibits similar characteristics, adequately fitting the data. This procedure was repeated for all of the conditions examined in Chapter 2, finding values for G_{max}, b, and k using regression analysis.

Figure 4.1(b) demonstrates the goodness of fit for all the experimental conditions tested by plotting the fitted CO_2 production model vs. the measured CO_2 production. The experimental data is distinguished by conditions that investigated the effects of temperature with an initial moisture content of 1.00 kg water per kg dry solids and conditions that investigated the effects of initial moisture content at a constant temperature of 30ºC. Ideally all of the data points would lie on the 45° line.

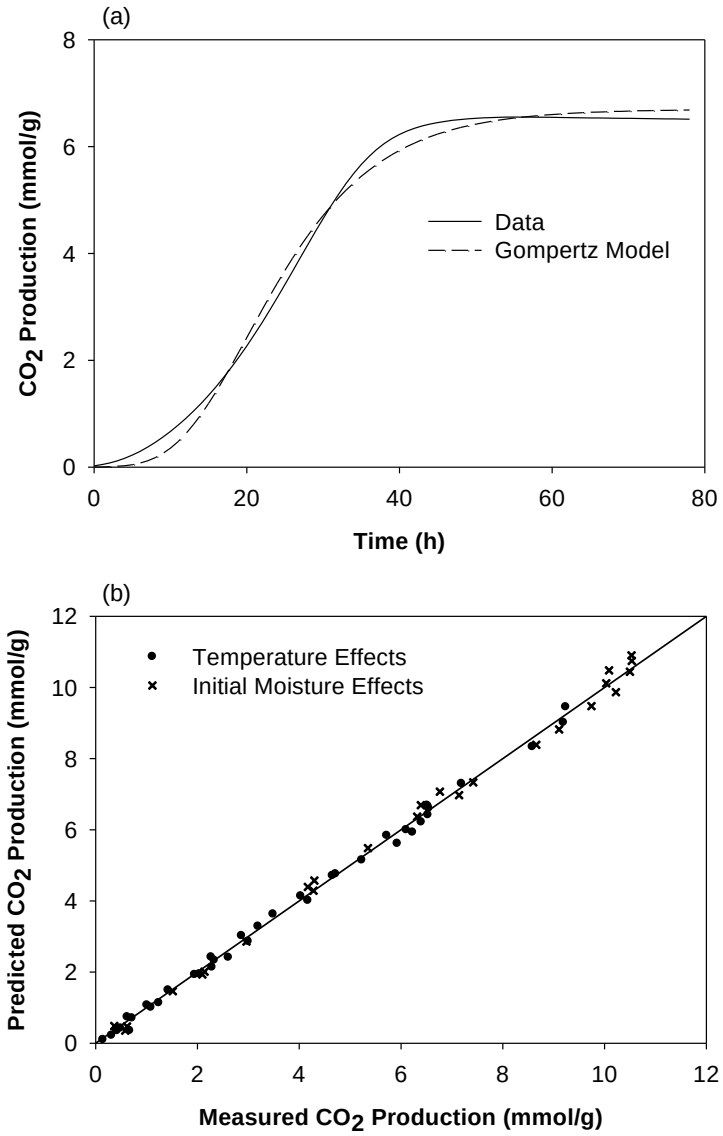

Figure 4.1. Example of the Gompertz model fit for (a) CO_2 production in mmol CO_2 per g of initial dry substrate at 32.5 ºC with an initial moisture content of 1.00 kg water per kg dry solids, and (b) predicted vs. measured CO_2 production in mmol of CO_2 per g of substrate demonstrating the goodness of fit for the Gompertz model over the range of conditions tested.

The values of the Gompertz fitted parameters as a function of temperature and moisture are shown in Figure 4.2. Trends in parameter values were fitted to polynomials as functions of fermentation temperature and initial substrate moisture content which are also presented in Figure 4.2. Figure 4.2(a) shows how the value of G_{max} changed as the

fermentation temperature changed when the initial moisture content was 1.00 kg water per kg of dry substrate. The data shows that the maximum quantity of CO_2 produced increased with temperature from 22.5 to 25.0°C. The value of G_{max} showed some variability between 25.0 and 32.5°C with values ranging from 7-10 mmol CO_2 per g of substrate. Figure 4.2(b) shows how the value of G_{max} changed with the initial moisture content of the substrate. As the moisture content increased from 0.82 to 1.50 kg water per kg of initial dry substrate the value of G_{max} increased in linear manner from 8 to 11 mmol CO_2 per g substrate.

The value of b determines the shape of the sigmoidal curve. Figure 4.2(c) and (d) show how the value of b changed as a function of temperature and moisture, respectively. Figure 4.2(c) shows that the value of b decreased when temperature was increased from 22.5 to 25.0°C, had an approximately constant value with temperature values from 25.0 to 30.0°C, and then increased when the temperature was increased from 30.0°C to 32.5°C. These results indicate that at 22.5 and 32.5°C, CO_2 production had a longer, slower exponential growth phase and a shorter, faster deceleration phase compared to temperatures ranging from 25.0 to 30.0°C. The initial exponential cell growth and subsequent CO_2 production may have been inhibited at the lower and higher temperature ranges for cell growth which is normally expected.

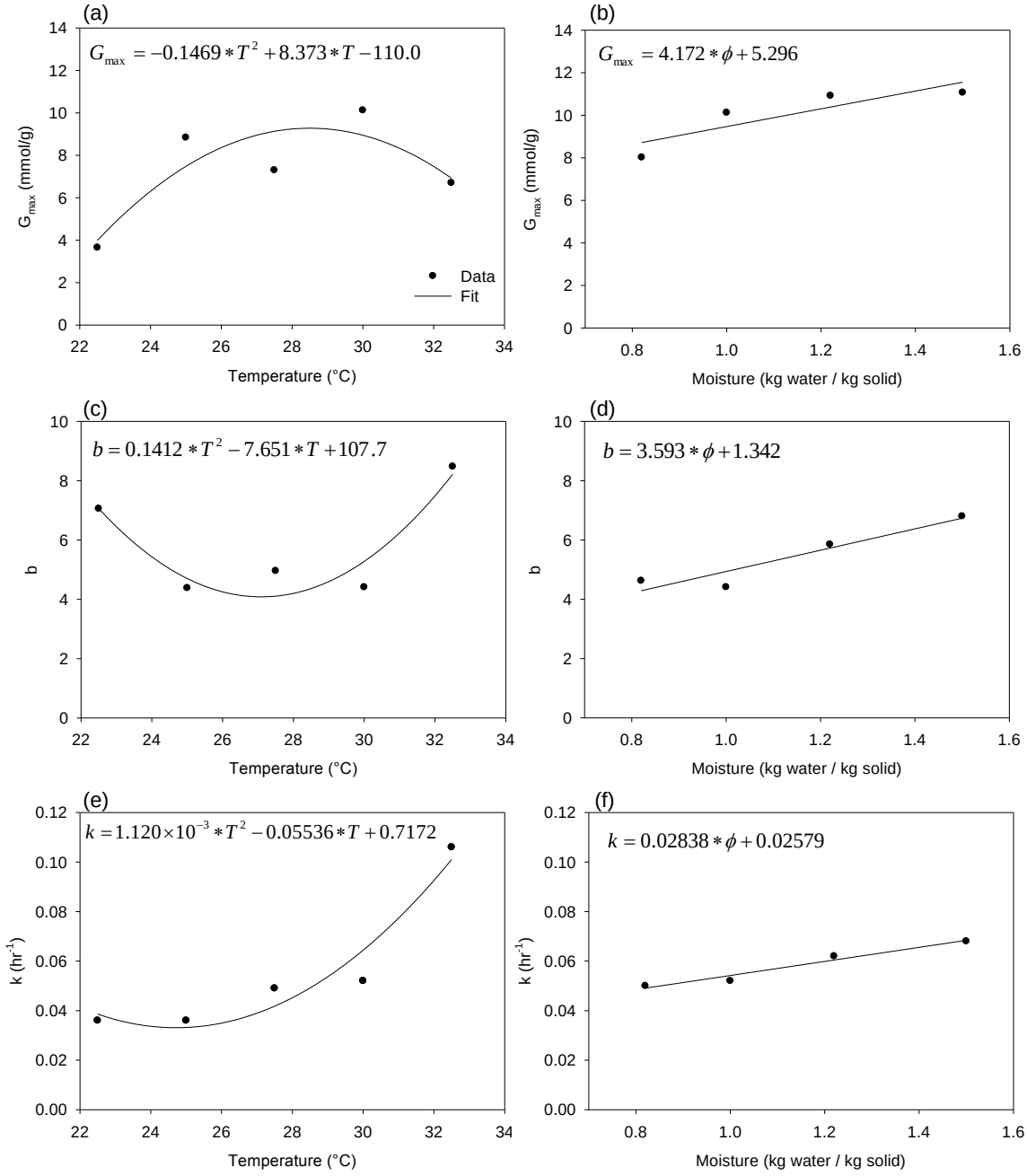

Figure 4.2. Gompertz parameters fitted to curves as a function of temperature and moisture content for modeling CO_2 production: (a) and (b) maximum CO_2 production, G_{max}; (c) and (d) dimensionless parameter, b; and (e) and (f) rate constant, k.

Figures 4.2(e) and (f) show how the value of the rate constant k changed with temperature and initial moisture content. The value of k increased as both the

temperature and moisture content were increased as indicated in the figure. An increasing rate constant indicates that the total active fermentation time was shorter. Therefore, by maintaining the temperature and moisture content at the higher range of the temperature and moisture tested, the total length of the fermentation will decrease. But shorter fermentation times are not always advantageous as product formation must also be considered.

Overall, the fitted parameters varied significantly more with temperature compared to initial moisture content over the range of conditions examined. The values also appeared to vary nonlinearly with temperature and linearly with initial moisture content. These results indicate that temperature plays an important role in fungal metabolism for this system whereas moisture is less critical when growing *T. reesei* on the WDG substrate. These factors are important to consider when designing a SSF bioreactor. The extrapolation of the data and fitted equations presented in Figure 4.2 are not expected to be reliable.

4.3.2. Cellulase Production

The cellulase activity produced during the fermentation is considered a product of fungal metabolism. It was assumed that the rate of cellulase production was proportional to the rate of CO_2 production according to Eq. 4.6. The value of the cellulase yield coefficient, Y_P, was allowed to vary with temperature and moisture since the quantity of product formed was dependent on the environmental conditions. An example of the cumulative cellulase activity production is shown in Figure 4.3(a) for the fermentation condition of 32.5°C at an initial moisture content of 1.00 kg water per kg of initial dry substrate. The model fails to predict the decline of activity toward the end of the

fermentation when the rate of CO_2 production was approaching zero. The decline in activity was likely caused by the degradation of cellulase by proteases produced by the fungi. The proteases degrade proteins such as cellulase causing a decline in cellulase activity [20]. As a result, the regression analysis for the model averaged the peak quantity of cellulase activity produced at 60 h and the lower activity at 85 h since a decline in cellulase activity was not built into the model. However, not all fermentation conditions tested included a data point after the maximum cumulative CO_2 production was reached. Therefore, not all of the data for other conditions examined exhibited a decline in cellulase even though the decline would have likely become apparent if additional data would have been taken at later times. As a result, the product formation model may be inaccurate at the end of the fermentation when the rate of CO_2 production is significantly declining and the degradation of cellulase by proteases is greater than cellulase production.

The fitted vs. the measured cellulase activity production is shown in Figure 4.3(b) for all of the fermentation conditions. The results show that the model both under predicts and over predicts the measured cellulase production at times, but overall fits the general trend of the data as demonstrated in Figure 4.3(a).

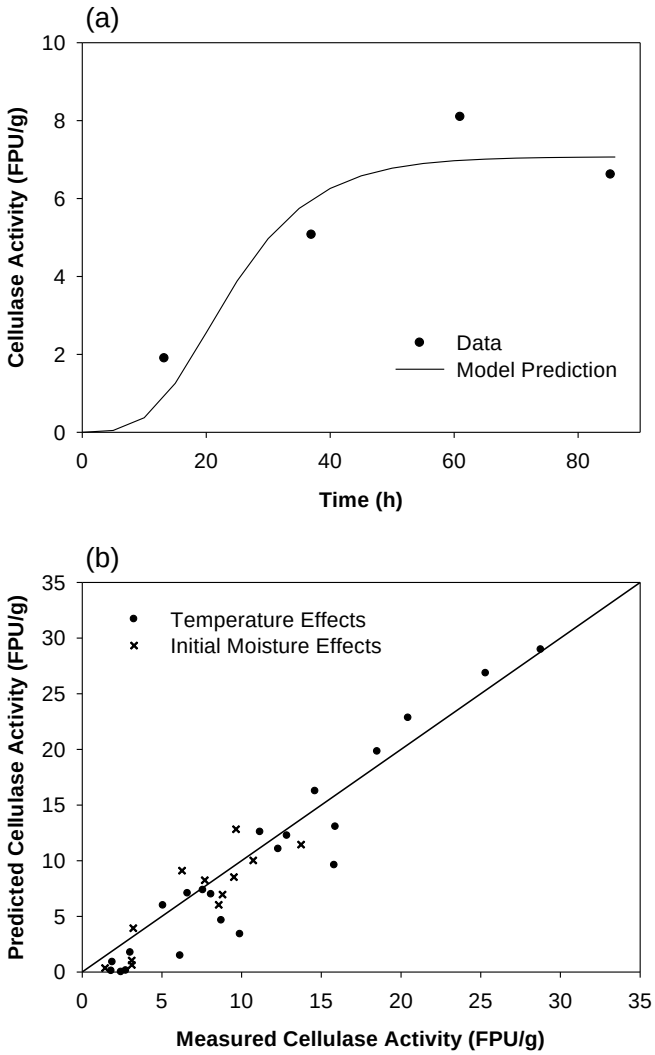

Figure 4.3. Example of cellulase activity produced for (a) the fermentation condition of 32.5°C and 1.00 kg water per kg of substrate, and (b) predicted vs. measured cellulase activity in FPU per g of initial substrate demonstrating the goodness of fit for product formation over the range of conditions tested.

The value of the cellulase yield coefficient, Y_P, was considered to be a function of the environmental conditions. Figures 4.4(a) and (b) show how the value of Y_P changed with temperature and initial moisture content respectively. Second order polynomials displayed in the figure show the overall trends and can be used to interpolate between temperatures and initial moisture contents. Low fermentation temperatures resulted in the lowest CO_2 production but had the highest cellulase activity, therefore the value of Y_P

was the greatest. As temperatures increased, CO_2 production increased, and cellulase activity decreased causing the value of Y_P to decline. As the moisture content increased, the cellulase activity production declined causing the value of Y_P to decrease. The relationships in Figure 4.4 can be used to predict cellulase activity when combined with Gompertz model to predict CO_2 production.

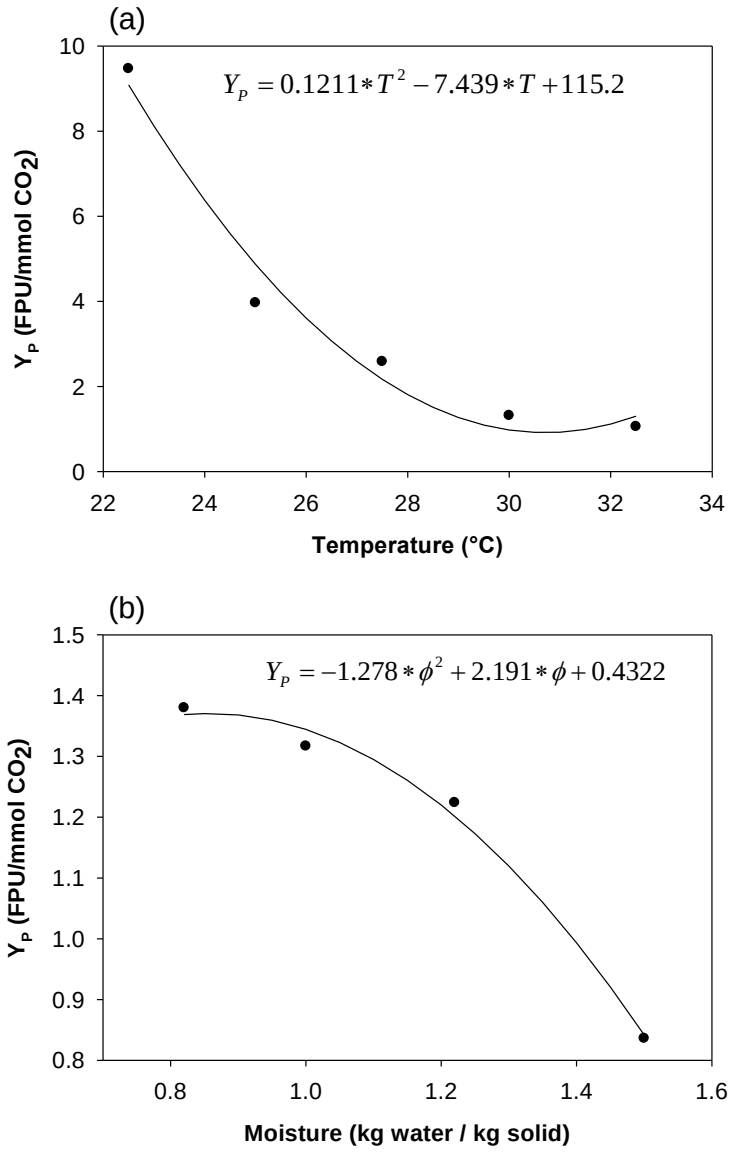

Figure 4.4. Cellulase production yield coefficient, Y_P, fitted to polynomial curves as a function of (a) temperature and (b) initial moisture content.

4.3.3. Substrate Weight Loss

Substrate weight loss is an important parameter in SSF processes and has been correlated to biomass estimation by Terebiznik and Pilosof [21]. Substrate weight loss is also important when modeling the change in moisture content due to the reduction in solids weight. The rate of substrate weight loss was assumed to be proportional to the rate of CO_2 production (Eq. 4.7). The substrate weight loss yield coefficient, Y_S, was assumed to be independent of fermentation conditions such as temperature and moisture. Experimental findings by Smits et al [7] have shown correlations between CO_2 production and substrate weight loss to be independent of fermentation temperature. An example of the experimental data fit to Eq. 4.7 is shown in Figure 4.5(a). The data from all of the experimental conditions were used simultaneously in a regression analysis to find the value of Y_S that best described substrate weight loss yielding a value of 0.022 g of weight lost per mmol CO_2. Therefore, some error is expected when examining individual data sets.

Figure 4.5(b) shows the overall goodness of the fit for substrate weight loss graphing the predicted values vs. the measured experimental data. The figure shows that the model tends to under predict the weight loss when different fermentation temperatures were examined and over predict weight loss when different initial substrate moistures were examined. These results indicate that the correlation between weight loss and CO_2 production may be dependent on fermentation conditions, but in order to keep the model sufficiently simple with the goal of being combined with material and energy and balances, the value of Y_S was considered to be a constant.

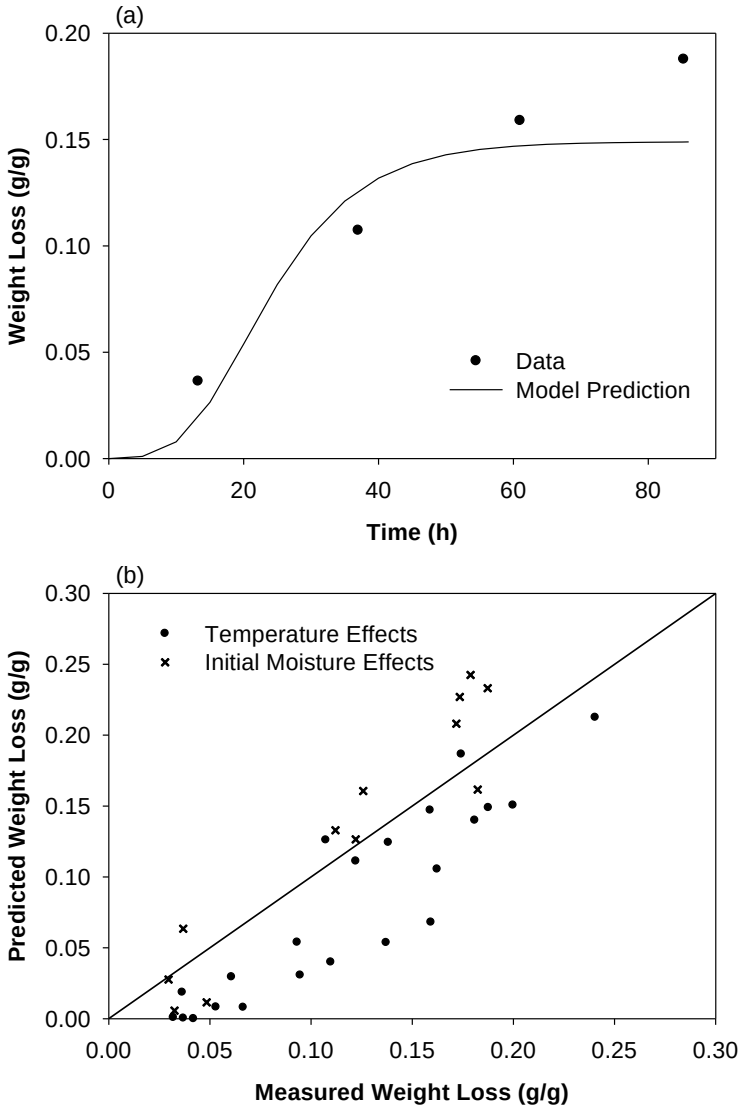

Figure 4.5. Example of substrate weight loss prediction for (a) 32.5°C and 1.00 kg water per kg of initial dry substrate, and (b) predicted vs. measured substrate weight loss per g of initial substrate demonstrating the goodness of fit for the model over the range of conditions tested.

4.3.4. Water Production

Metabolic water production can be considered a fermentation product similar to cellulase production. The correlation between CO_2 production and water production is most likely dependent on fermentation conditions similar to cellulase. However, the rate of water production was considered to be independent of fermentation conditions and

directly proportional to the CO_2 production with the goal of straightforwardly incorporating the approximation into bioreactor models.

A material balance was performed in order to calculate the quantity of water produced in kg of water per kg of initial dry substrate while taking into account the substrate weight loss. The material balance yields:

$$W = \phi(1 - S) - \phi_0 \tag{4.9}$$

where the variable Φ_0 is the initial moisture content of the substrate in kg water per kg of initial dry solids. A regression analysis utilizing Eq. 4.8 was then used to find the water production yield coefficient, Y_W, using all of the data sets simultaneously. It was assumed that under the controlled experimental conditions used to obtain the data, negligible changes in moisture occurred due to evaporation or condensation. The value of Y_W was determined to be 0.0149 g water per mmol of CO_2 produced. Figure 4.6(a) shows the results of the model and the experimental data at 32.5°C with an initial moisture content of 1.00 kg water per kg initial substrate. The figure shows that the quantity of water produced is under predicted by the model for this data set. This large error is likely due to the dependence of metabolic water production on fermentation conditions which is not accounted for due to model simplification. Figure 4.6(b) shows the predicted vs. the measured water production for all of the data sets. The figure shows that the model tends to under predict water production for fermentations at different temperatures and over predict water production for fermentations at different initial moisture contents.

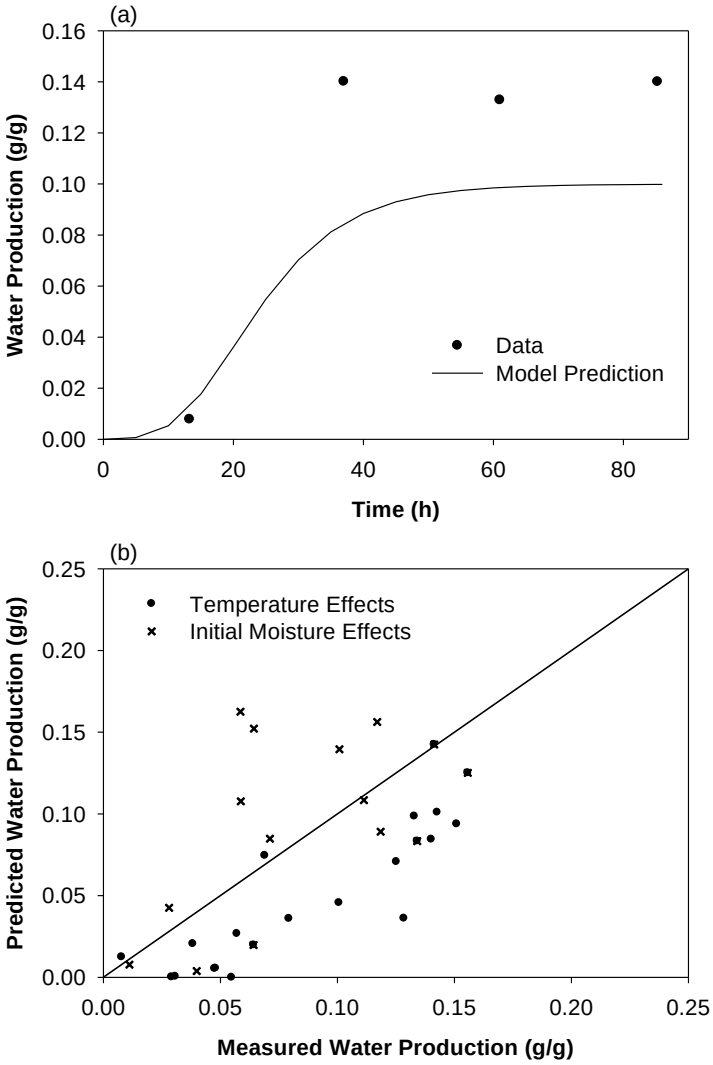

Figure 4.6. Example of predicted water production for (a) 32.5°C and 1.00 kg water per kg of initial dry substrate, and (b) predicted vs. measured water production per g of initial substrate demonstrating the goodness of fit for the model over the range of conditions tested.

4.3.5. Time Dependent Fermentation Conditions

It is not feasible to carry out industrial scale fermentations at constant conditions, therefore fermentation conditions are expected to change with time and position within bioreactors. In order to test the accuracy of the proposed model for changing temperature conditions, several additional experiments were completed. The experiments involved making various step changes in temperature during the active fermentation time. The rate

based Gompertz models were then integrated numerically using the Mathcad ordinary differential equation solver.

Fermentation with an initial temperature of 27.5°C and an initial moisture content of 1.00 kg water per kg of initial dry substrate was changed to 30.0°C at 31 h and then back to 27.5°C at 45 h and finally 25.0°C at 55 h where it remained until the fermentation was terminated. Figure 4.7(a) indicates the CO_2 production model over predicts the quantity of cumulative CO_2 produced initially but follows the trend of the experimental data throughout the remaining fermentation time. Figure 4.7(b) plots the rate of CO_2 production vs. the unfiltered and unsmoothed CO_2 production rate data. The figure clearly shows definite changes in CO_2 production when temperatures were changed in both the model prediction and the experimental data. The immediate changes in CO_2 production occurring after a step change in temperature indicate the validity of the inherent initial assumption of CO_2 production being dependent on environmental conditions as well as the quantity of biomass present in the system.

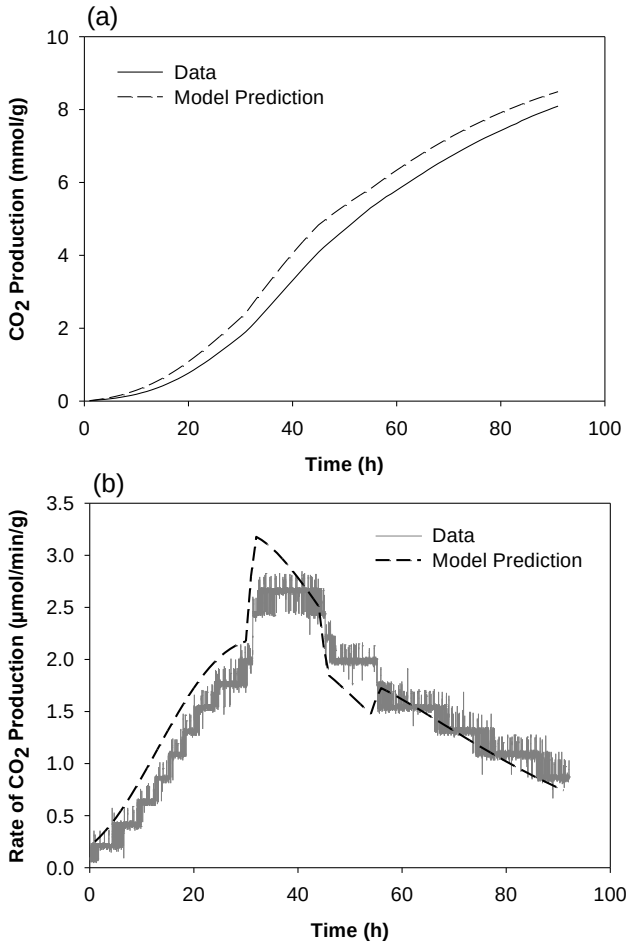

Figure 4.7. Predicted and experimental (a) cumulative CO_2 production and (b) rate of CO_2 production for step changes in fermentation temperature at an initial moisture content of 1.00 kg water per kg of initial substrate.

Figure 4.8(a) shows the predicted and experimental data for cellulase production. The figure indicates that the quantity of cellulase produced is overestimated, especially at the end of the fermentation time. This data indicates that cellulase production is likely dependent on the temperature history of the fermentation as well as current conditions; the proposed model only takes into account the current fermentation conditions at any given time. The expected error would be greatly magnified if the conditions were outside of the experimental range where cell death or inactivation may occur. As previously discussed, another large source of error is likely the production of proteases which

degrade the cellulase. The degradation of cellulase seems to be prominent at the end of the active fermentation time when the rate of CO_2 production is approaching zero. Based on this data, it is recommended that caution should be used when predicting cellulase production using Eq. 4.6, especially when the rate of CO_2 is rapidly decaying at the end of fermentation.

The predicted and experimental substrate weight loss is graphed in Figure 4.8(b). Because substrate weight loss has been directly correlated to CO_2 production, the proposed model was expected to accurately predict the experimental results since the predicted CO_2 production rate closely fit the experimental data in Figure 4.7. The metabolic water production is shown in Figure 4.8(c). Similar to cellulase activity, the model did a reasonable job of predicting water production up to approximately 60 h of fermentation time until the rate of CO_2 declines rapidly as it approaches zero. Although the rate based models did not closely fit the experimental data throughout the entire length of the active fermentation, it appears that the rate based models can predict general trends in data, especially for the time period before the rate of CO_2 production begins to decline.

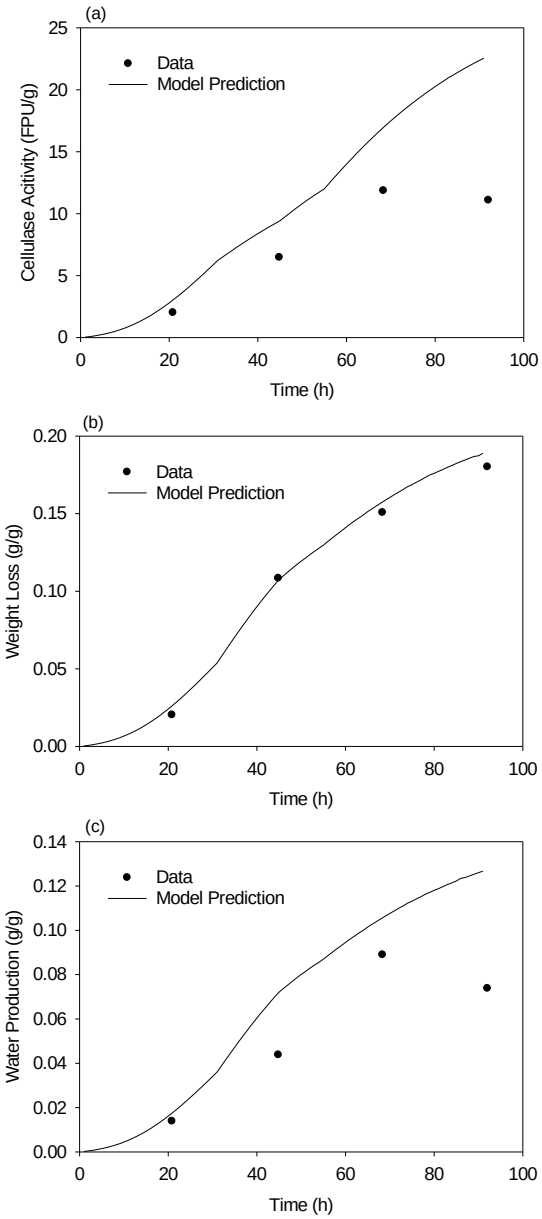

Figure 4.8. Predicted and experimental (a) cellulase activity production, (b) substrate weight loss, and (c) water production for changing fermentation temperature at an initial moisture content of 1.00 kg water per kg of initial substrate.

A second experimental trial was completed which involved changing the fermentation temperatures when the initial substrate moisture content was 1.22 kg of water per kg of initial dry substrate. The initial temperature of the fermentation was 27.5°C which was changed to 25.0°C at 44.5 h and then to 30.0°C at 68 h. Because the experimental

fermentation conditions used to develop the kinetic model did not include the investigation of multiple temperatures at a moisture content of 1.22 kg/kg, model parameters for temperature and moisture effects were estimated by:

$$G_{\max}(T,\phi) = G_{\max}(T,1.00)\frac{G_{\max}(30°C,\phi)}{G_{\max}(30°C,1.00)}. \quad (4.10)$$

The value of G_{max} as a function of temperature and moisture content is represented by the left hand side of Eq. 4.10. The equation assumes that the interacting effects of temperature and moisture are proportional to the data sets examined in Chapter 2. The values of G_{max} on the right hand side of the equation can be calculated using the fitted equations expressed in Figure 4.2. The same form of Eq. 4.10 was also used to adjust the values of b, k, and Y_P which were considered to be dependent on temperature and initial moisture content.

Figure 4.9 compares the experimental and predicted CO_2 production. The figure shows that between 20 and 60 h the predicted CO_2 production is slightly higher than the experimental data. The model fails to predict the sudden increase in the rate of CO_2 production at 68 h when the temperature is changed from 25.0°C to 30.0°C; but the sudden increase in CO_2 production was followed by rapid decline as predicted by the model.

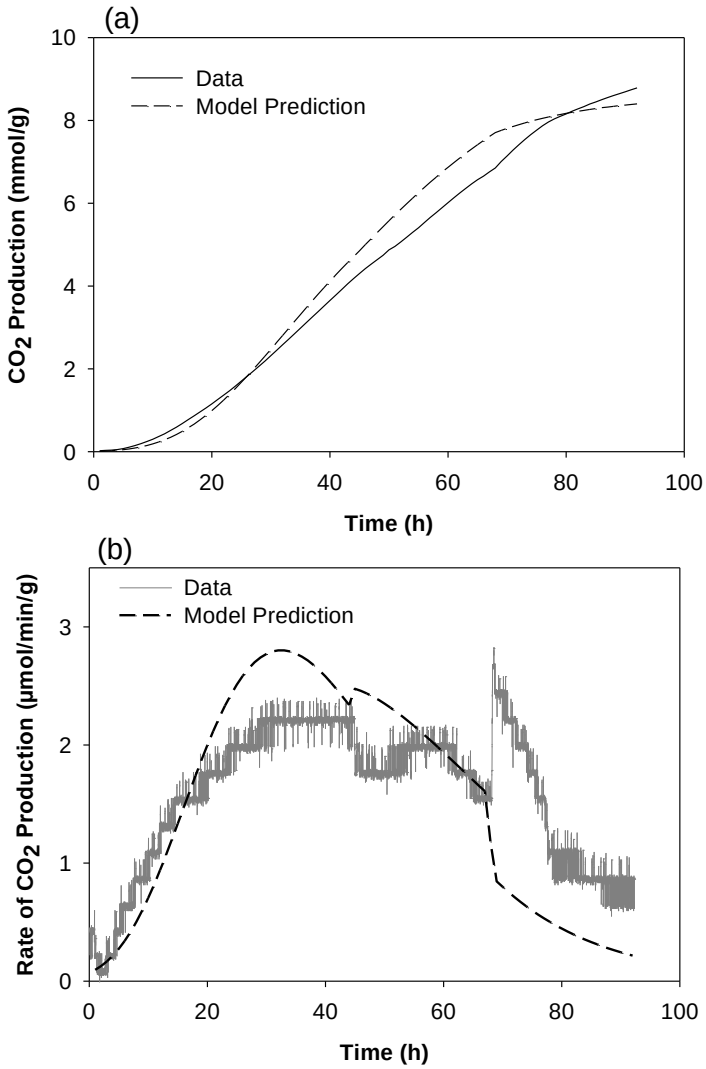

Figure 4.9. Predicted and experimental (a) cumulative CO_2 production and (b) rate of CO_2 production for changing fermentation temperature at initial moisture content of 1.22 kg water per kg of initial substrate.

The predicted cellulase production is plotted with the experimental data in Figure 4.10(a). Similar to the previous experimental conditions shown in Figure 4.8(a), the model over predicted the cellulase production with the error increasing with fermentation time. Based on the results shown in Figures 4.8(a) and 4.10(a), caution should be used when attempting to apply Eq.4.6 to fermentations with changing conditions. Similar to Figure 4.8(b), the substrate weight loss, as shown in Figure 4.10(b), was predicted well

by the model. The prediction for the water production rate was high as demonstrated in Figure 4.10(c). Some errors are expected since the value of Y_W in Eq. 4.8 was considered to be a constant. Overall the experimental conditions were qualitatively predicted by the model using Eq. 4.10 to adjust parameters for changing fermentation conditions. A kinetic model capable of predicting parameters during changing fermentation conditions is a powerful tool required for simulating large scale bioreactor behavior.

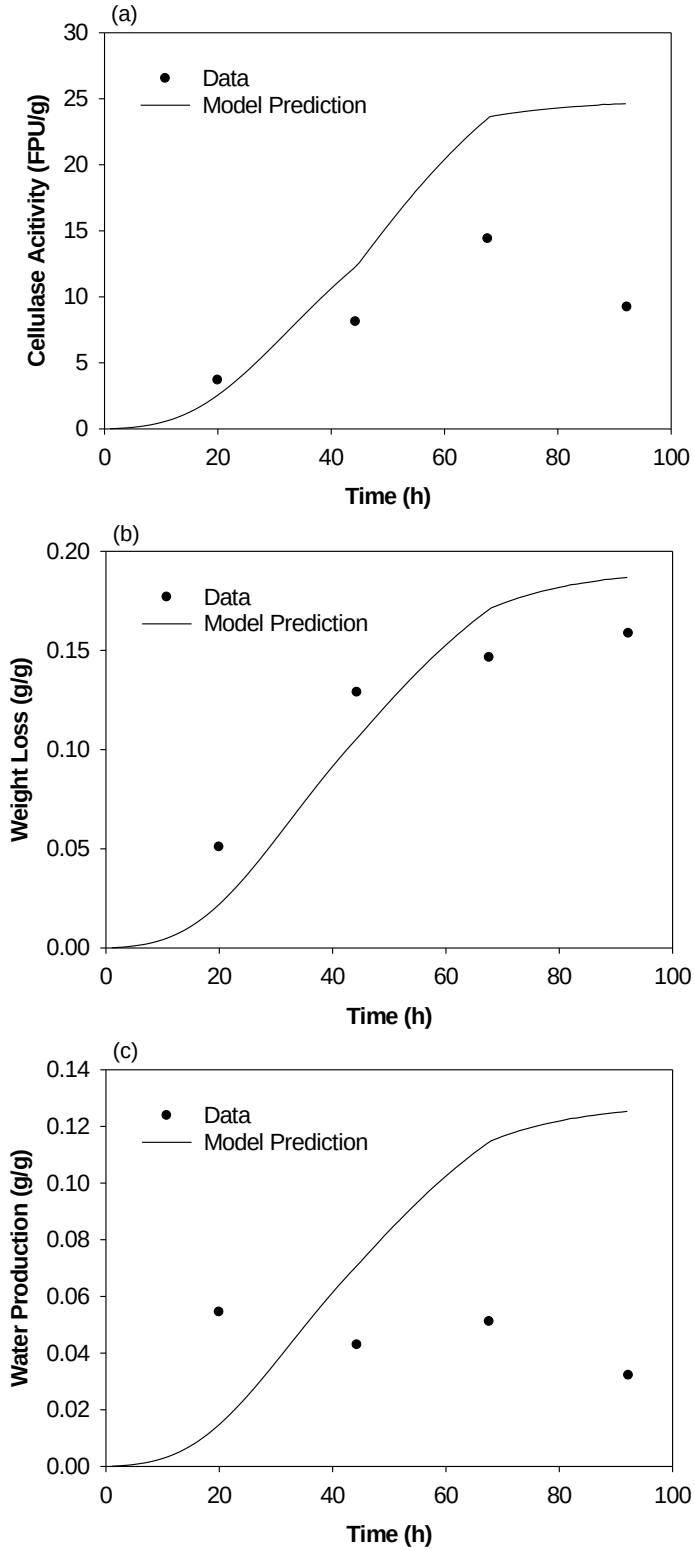

Figure 4.10. Predicted and experimental (a) cellulase activity production, (b) substrate weight loss, and (c) water production for changing fermentation temperature at an initial moisture content of 1.22 kg water per kg of initial substrate.

4.4. Conclusions

A kinetic model based on CO_2 production instead of biomass concentration was examined in order to simplify required experiments for kinetic model development. The kinetic model based on CO_2 production has the advantage of being suitable for incorporation into online bioreactor monitoring and control schemes. A Gompertz model was used to fit the experimental data and to predict the quantity of CO_2 produced in experiments with changing temperatures. The Gompertz model inherently simulates both growth and death kinetics simultaneously because of its sigmoidal form. The model also takes into account maintenance metabolism since only the active cells are undergoing respiration. Low model complexity combined with easily measurable CO_2 production is an advantage.

The rate of cellulase production, substrate consumption, and water production were considered to be proportional to the rate of CO_2 production. The model parameters were initially fit to experimental data at constant temperature conditions using the integrated Gompertz model. The rate based model was then tested for changing fermentation conditions using numerical integration. Results showed that CO_2 production and substrate weight loss can be accurately predicted by the rate based models. The model predictions for cellulase and water production were not as accurate but showed a qualitative trend in fermentation behavior. Fermentation conditions outside the range of conditions used to develop the empirical kinetic model should not be used to predict fermentation behavior. The model can be combined with material and energy balances to predict heterogeneous bioreactor behavior, a useful tool for the design and scale-up of bioreactors.

References

[1] C. Desgranges, C. Vergoignan, C. Georges, A. Durand, Biomass estimation in solid state fermentation I. Manual biochemical methods, Appl. Microbiol. Biotechnol. 35 (1991) 200-205.

[2] C. Desgranges, C. Georges, C. Vergoignan, A. Durand, Biomass estimation in solid state fermentation II. On-line measurements, Appl. Microbiol. Biotechnol. 35 (1991) 206-209.

[3] H.Q. Li, H.Z. Chen, Near-infrared spectroscopy with a fiber-optic probe for state variables determination in solid-state fermentation, Process Biochem. 43 (2008) 511-516.

[4] D. Yingyi, W. Lan, C. Hongzhang, Digital image analysis and fractal-based kinetic modeling ofr fungal biomass determination in solid-state fermentation., Biochem. Eng. J. 67 (2012) 60-67.

[5] F.J. Nagel, J. Tramper, M.S.N. Bakker, A. Rinzema, Model for on-line moisture-content control during solid-state fermentation, Biotechnol. Bioeng. 72 (2001) 231-243.

[6] D.A. Mitchell, O.F. von Meien, N. Krieger, F.D.H. Dalsenter, A review of recent developments in modeling of microbial growth kinetics and intraparticle phenomena in solid-state fermentation, Biochem. Eng. J. (2004) 15-26.

[7] J.P. Smits, A. Rinzema, J. Tramper, H.M. Van Sonsbeek, J.C. Hage, A. Kaynak, W. Knol, The influence of temperature on kinetics in solid-state fermentation, Enzyme Microb. Technol. 22 (1998) 50-57.

[8] G. Saucedo-Castaneda, M. Gutierrez-Rojas, G. Bacquet, M. Raimbault, G. Viniegra-Gonzalez. Heat transfer simulation in solid substrate fermentation, Biotechnol. Bioeng. 35 (1990) 802-808.

[9] D.A. Mitchell, G. Viccini, L. Ikasari, N. Krieger, Basic Features of the Kinetic Sub-model, in: D.A. Mitchell, N. Krieger, M. Berovič (Eds.), Solid-State Fermention Bioreactors Fundamentals of Design and Operation, Springer, Berlin, 2006, pp. 219-234.

[10] O.F. von Meien, D.A. Mitchell, A two-phase model for water and heat transfer within an intermittently-mixed solid-state fermentation bioreactor with forced aeration, Biotechnol. Bioeng. 79 (2002) 416-428.

[11] D.R. Glenn, P.L. Rogers, A solid substrate fermentation process for an animal feed product: Studies on fungal strain improvement, Australian J. Biotechnol. 2 (1988) 50-57.

[12] J. Sargantanis, M.N. Karim, V.G. Murphy, D. Ryoo, R.P. Tengerdy, Effect of operating conditions on solid substrate fermentation, Biotechnol. Bioeng. 42 (1993) 149-158.

[13] D.A. Mitchell, N. Krieger, Modeling the Effects of Growth on the Local Environment, in: D.A. Mitchell, N. Krieger, M. Berovič (Eds.), Solid-State Fermention Bioreactors Fundamentals of Design and Operation, Springer, Berlin, 2006, pp. 235-248.

[14] L.P. Ooijkaas, R.M. Buitelaar, J. Tramper, A. Rinzema, Growth and sporulation stoichiometry and kinetics of *Coniothyrium minitans* on agar media, Biotechnol. Bioeng. 69 (2000) 292-300.

[15] J.S. Lekanda, J.R. Perez-Correa, Energy and water balances using kinetic modeling in a pilot-scale SSF bioreactor, Process Biochem. 39 (2004) 1793-1802.

[16] P. Christen, J.C. Meza, S. Revah, Fruity aroma production in solid state fermentation by *Ceratocystis fimbriata*: influence of the substrate type and the presence of precursors, Mycol. Res. 101 (1997) 911-919.

[17] A.K. Laird, Dynamics of tumor growth, Br. J. Cancer 18 (1964) 490-502.

[18] G.C. Saucedo, P.B. Gonzalez, S.M. Revah, G.G. Viniegra, M. Raimbault, Effect of Lactobacilli inoculation on cassava (*Manihot esculenta*) silage: Fermentation pattern and kinetic analysis, J. Sci. Food Agric. 50 (1990) 467-477.

[19] M. Meraz, K. Shirai, P. Larralde, and S. Revah, Studies on the bacterial acidification process of cassava (*Manihot esculenta*). J. Sci. Food Agric. 60 (1990) 457-463.

[20] D. Haab, K. Hagspiel, K. Szakmary, C.P. Kubicek, Formation of the extracellular proteases from *Trichoderam reesei* QM 9414 involved in cellulase degredation, J. Biotechnol. 16 (1990) 187-198.

[21] M.R. Terebiznik, A.M.R. Pilosof, Biomass estimation in solid state fermentation by modeling dry matter weight loss, Biotechnol. Techniq. 13 (1999) 215-219.

Chapter 5

A Simplified Solid-State Fermentation Packed Bed and Intermittently Mixed Packed Bed Bioreactor Model for the Prediction of Temperature and Moisture Gradients

Abstract

A simplified solid-state fermentation bioreactor model was developed to predict temperature gradients, moisture gradients, substrate weight loss, and product formation. The simulated packed bed bioreactor produced cellulase enzymes when *T. reesei* NRRL 11460 was grown on wet distillers grain byproducts from the dry grind corn ethanol production industry. The bioreactor model was solved as a set of ordinary differential equations. Simulations were used to predict operating behavior of packed bed, packed bed with intermittent mixing and moisture addition, and moving bed bioreactors. The effects of water addition, mixing, substrate bed height, and superficial air velocity were evaluated. Results indicate that the maximum bed height may be limited by either the solid phase moisture content or temperature. Water addition incorporated with mixing events can be used in order to change the bioreactor height limiting condition from moisture to temperature. Cocurrent and countercurrent moving bed operations were also investigated. Cocurrent moving bed operations exhibited many advantages including lower maximum temperatures, lower solid phase moisture loss, and higher maximum bed heights when compared to countercurrent moving bed and packed bed bioreactors. The developed bioreactor model is sufficiently simple to solve and is a powerful tool for designing bioreactors and developing operation and control strategies.

5.1. Introduction

Lab scale experimentation has indicated solid-state fermentation (SSF) has several advantages when compared to submerged fermentation [1]. However, the lack of proven industrial scale operations coupled with the complexity of heat and mass transfer phenomena and bioreactor monitoring and control has limited commercial operations [2]. Mitchell et al [3] suggests that three crucial aspects must be addressed when designing a bioreactor: the effects of agitation, the rate of microbial growth as a function of temperature and moisture, and the aeration requirements of the microorganism. Another factor that must be considered is the bioreactor capacity. Durand [4] suggests an intermittently mixed bioreactor with forced aeration may have large capacities in the order of magnitude of several tons for non-sterile processes. Typically bioreactors utilizing forced aeration are not considered limited by oxygen transfer although agglomeration due to mycelial growth can cause channeling and limit oxygen diffusion [5]. By mixing the bed intermittently, channeling can be mitigated and moisture can be added to keep fermentation conditions optimal.

One type of model frequently used to evaluate overheating problems in SSF treats the substrate bed as a homogenous phase that has averaged properties of the solid and gas phases. For the purpose of describing the model, the solid phase includes the substrate particles, microbial biomass, and the liquid water. This assumption allows for simplification of the model by assuming equilibrium between the gas and solid phase at all locations within the bed, eliminating the need for mass and heat transfer coefficients. Typically solid phase water material balances have not been used to predict moisture loss, although evaporative cooling has been accounted for in the energy balance. Sangsurasak

and Mitchell [6] investigated the effects of two dimensional heat transfer in a packed bed SSF bioreactor. The model predicted that convection was the dominant heat transfer mechanism compared to conduction. Overheating problems were observed at the top of the bed, and the most effective method for controlling temperature was maintaining a high superficial air velocity and/or lowering the inlet air temperature. Sangsurasak and Mitchell [7] validated a similar two dimensional model which incorporated evaporative cooling by comparing simulations to experimental data. A sensitivity analysis was also completed comparing different packing densities and substrate thermal properties. The model did not include a water balance on the solid phase even though researchers suggested that the majority of heat removal occurred because of evaporative cooling in most simulations. Mitchell et al [8] used a one-dimensional equilibrium model for heat transfer with the goal of evaluating scale-up strategies and determining the critical bed height when temperature is limiting. Researchers concluded that dimensionless scale-up using a modified Damköhler number yielded similar results as the process model for determining the critical bed height; once again, a water balance on the solid phase was neglected. Ashley et al [9] used the same energy balance model to evaluate strategies to prevent overheating in a packed bed bioreactor. Simulations found that air direction reversal caused an increase in the maximum temperature of the bed when compared to conventional operation and was not an effective temperature control strategy with peak temperatures occurring in the center of the bed. Mixing was found to help control temperature but at perhaps unrealistic frequencies of 10 to 60 times per hour.

Another type of model treats the solid and gas phases separately and requires the use of heat and mass transfer coefficients along with the equilibrium driving forces. One

such model was developed by von Meien and Mitchell [10] to evaluate both water and heat transfer in an intermittently mixed packed bed bioreactor. The model revealed that evaporative cooling causes large moisture gradients in the bed which require mixing events for rehydration. This phenomena occurs even when saturated air is used at the inlet of the bioreactor due to the increased water carrying capacity of air as it absorbs heat. The model also showed that at the base of the bioreactor where air enters, a large temperature difference between the gas phase and the solid phase may exist, especially when a low air temperature is used for cooling purposes. These findings indicate that models based on equilibrium assumptions may not be accurate at the inlet of the bed. However, the remainder of the bed did approach equilibrium. Mixing events were assumed to bring the bed back to an optimum temperature and moisture content, but the model predicted the bed quickly returned to its previous temperature from before mixing due to microbial heat production. Mitchell et al [11] used a similar stage model to evaluate operating strategies for multi-layer packed beds in which layers of the packed bed could be moved at given time intervals. Stages were cycled through the bioreactor in a countercurrent manner relative the air flow rate to simulate a moving packed bed bioreactor. Results showed that the peak temperature was reduced by 4.5°C when compared to traditional packed bed behavior. Brijwani et al [12] used a bioreactor with a complex airflow distribution system to investigate a forcefully aerated packed bed system. A stage model was experimentally validated for the production of cellulolytic enzymes. Sahir et al [13] also used a stage model to investigate temperature gradients in a packed bed for the production of protease. Product formation and denaturation were estimated.

In this study, the behavior of an intermittently mixed, forcefully aerated packed bed bioreactor was modeled and simulated. This type of bioreactor was selected due to their high capacity [4]. The fermentation system modeled used wet corn distillers grain byproduct (WDG) from a dry grind ethanol producing facility as a substrate. The microorganism used was *Trichoderma reesei* NRRL 11460 with the goal of producing an end product of cellulase enzymes. This system has been shown to tolerate mixing at frequencies up to 6 d^{-1} as demonstrated in Chapter 3. The kinetic model developed in Chapter 4 was used as a basis for microbial kinetics. The goal of this study was to evaluate bioreactor behavior for the production of cellulase on WDG by developing a simple model that incorporates both the effects of temperature and moisture and is easily solved as a set ordinary differential equations (ODEs). The model was used to evaluate operating limits to keep the bioreactor at favorable conditions for cellulase production.

5.2. Model Development

A simplified model was developed based on the packed bed bioreactor energy balance used by Sangsurasak and Mitchell [6,7] and Mitchell et al [8]. Several modifications and additions were incorporated into the model including the use of CO_2 production as the basis for measuring microorganism activity and heat evolution. In addition, a water material balance was added to determine the moisture gradient in the packed bed which has the potential to influence the kinetic rate equations. The effects of substrate consumption on the moisture of the solid particles were also taken into account. Product formation was added to the model to estimate the production of cellulase enzymes as a function of axial position and time. The bioreactor model assumes

thermodynamic equilibrium between the solid phase and gas phase; therefore, the air always remains saturated with water vapor. The use of an unsaturated air stream to feed the reactor in order to facilitate evaporative cooling cannot be properly evaluated using the model because of equilibrium assumptions. The model does not take into account changes in porosity or bed density due to mycelial growth and the subsequent changes in pressure drop. The model assumes the bioreactor diameter to be large enough to neglect radial heat transfer and is therefore adiabatic.

Mixing can be incorporated into the model by reinitializing the model with new initial conditions after a mixing event occurs assuming the entire contents of the bioreactor are mixed simultaneously. The effects of superficial velocity, bed depth, and mixing frequency on bed temperature, moisture, and product formation may then be explored. This bioreactor model can be used for various SSF processes with different substrates and microorganisms provided that a kinetic model is available.

5.2.1. Kinetic Model

The kinetic model developed in the previous chapter for the growth of *Trichoderma reesei* on wet corn distillers grain was used as a basis for estimating the CO_2 production, water production, heat evolution, and product formation. Equation 5.1 describes the rate of CO_2 evolution as a function of active fermentation time, temperature, and substrate moisture content.

$$\frac{dG(t,T,\phi)}{dt} = G_{\max}(T,\phi)b(T,\phi)k(T,\phi)\exp(-k(T,\phi)t)\exp(-b(T,\phi)*\exp(-k(T,\phi)t)) \quad (5.1)$$

where G is the quantity of CO_2 produced per unit weight of initial substrate as a function of time (mmol CO_2 / kg initial substrate), G_{max} is the maximum quantity of CO_2 produced (mmol CO_2 / kg initial substrate), k is the production rate constant (hr^{-1}) which

determines the amount of time it takes to reach G_{max}, and b is a unitless factor which determines the shape of the sigmoidal curve. The values of G, G_{max}, b, and k are a function of the local temperature, T (°C), and substrate moisture content, Φ (kg water / kg dry solids). Linear and polynomial expressions developed in the previous chapter were used to the estimate the changes in the Gompertz parameters.

Cooney et al [14] and Lekanda and Perrez-Correa [15] showed the metabolic heat evolution can be estimated by assuming the rate of heat produced is proportional to the rate of CO_2 produced:

$$r_Q(t,T,\phi) = Y_Q \frac{dG(t,T,\phi)}{dt} \tag{5.2}$$

where r_Q is the rate of energy production (J/hr/kg initial substrate) and Y_Q is heat yield coefficient (J/mmol CO_2). Cooney et al [14] calculated a heat yield coefficient from data obtained using multiple microorganisms including bacteria and fungi in a submerged environment. The average yield coefficient was 465 J/mmol CO_2. Lekanda and Perez-Correa [15] calculated a heat yield coefficient of 309 J/mmol CO_2 for SSF for *Gibberella fujikuroi*. Both values have the same order of magnitude indicating that *T. reesei* likely has a similar heat yield coefficient. A value of 309 J/mmol was used in this study.

Similar to Eq. 5.2, the rate of cellulase production was also assumed to be proportional to the rate of CO_2 production by the expression:

$$\frac{dP(t,T,\phi)}{dt} = Y_P(T,\phi)\frac{dG(t,T,\phi)}{dt} \tag{5.3}$$

where P is the cellulase activity produced in FPU per kg of initial substrate and Y_P is the cellulase yield coefficient in FPU per mmol CO_2. The value of Y_P was considered to be a function of temperature and moisture content as described previously.

The quantity of water produced by metabolic activity is estimated based on the rate of CO_2 production:

$$\frac{dW(t,T,\phi)}{dt} = Y_W \frac{dG(t,T,\phi)}{dt} \tag{5.4}$$

where W is the metabolic water production in kg per kg of initial substrate and Y_W is the water yield coefficient in kg water per mmol CO_2. The value of Y_W found in Chapter 4 was considered to be constant with a value of 1.49×10^{-5} kg per mmol CO_2.

The substrate weight loss is incorporated into the model to correct the moisture content of the solid phase due to the production of gaseous products such as CO_2. The substrate weight loss is estimated to be proportional to the CO_2 production:

$$\frac{dS(t,T,\phi)}{dt} = Y_S \frac{dG(t,T,\phi)}{dt} \tag{5.5}$$

where S is the substrate weight loss in kg per kg of initial substrate and Y_S is the substrate weight loss yield coefficient in kg solids lost per mmol CO_2. The value of Y_S was considered to be constant with a value of 2.23×10^{-5} kg per mmol CO_2 as determined in Chapter 4.

The parameters which are considered to vary with temperature and moisture content in Eqs. 5.1-5 can be estimated using the relationship suggested in Chapter 4. For example

$$G_{\max}(T,\phi) = G_{\max}(T,1.00)\frac{G_{\max}(30°C,\phi)}{G_{\max}(30°C,1.00)}. \tag{5.6}$$

Eq. 5.6 is based on the set of experimental data used to formulate the kinetic model expressions. Since data for different temperatures were obtained with an initial moisture content of 1.00 kg water per kg of substrate and data for different moisture contents were

performed at 30°C the expression is used to estimate the kinetic parameters at any temperature and moisture within the range of conditions tested by assuming the interacting effects of temperature and moisture are minimal. This assumption was validated in the previous chapter by experiments.

5.2.2. Energy Balance

An energy balance for a packed bed bioreactor was developed to predict temperature changes as a function of axial position. The model assumes thermodynamic equilibrium indicating the temperature of the substrate is equal to the temperature of the gas phase at any given position in the bioreactor at all times. Another aspect of this assumption is that the air traveling through the reactor remains saturated with water vapor. As the air is heated by absorbing energy from microbial heat production, the fraction of water in the vapor phase must increase to remain saturated. Therefore, water evaporates from the substrate bed to maintain saturation. The latent heat of evaporation is associated with water changing phases from liquid to vapor increasing the effective heat capacity of the cooling air stream. Due to the equilibrium assumption, mass and heat transfer coefficients are not used.

The energy for the system was found by writing a balance around a differential volume element and taking the limit as the volume of element approaches zero. Figure 5.1 shows a diagram of the differential volume element in the reactor. Air enters the bottom of the bioreactor at position 0 and exits the top of the bioreactor bed at position L. The radius of the bioreactor is defined as r. Therefore the total cross sectional area is πr^2. The total volume of the differential element is $\pi r^2 \Delta z$. The volume is occupied by both solid substrate particles and by gas. The void volume is defined as the volume of gas

divided by the total volume and is assigned the variable ε. The void volume was assumed to be 0.35 for the WDG substrate. Therefore the volume of gas in the differential element is $\varepsilon\pi r^2\Delta z$ and the volume of solids is $(1-\varepsilon)\pi r^2\Delta z$. The flow rate of air traveling through the volume element is the velocity multiplied by the gas phase cross sectional area: $v\varepsilon\pi r^2$. It is often more convenient to define the superficial velocity which is the velocity when the bioreactor does not contain solids. The superficial velocity, defined as v_s, is equal to $v\varepsilon$.

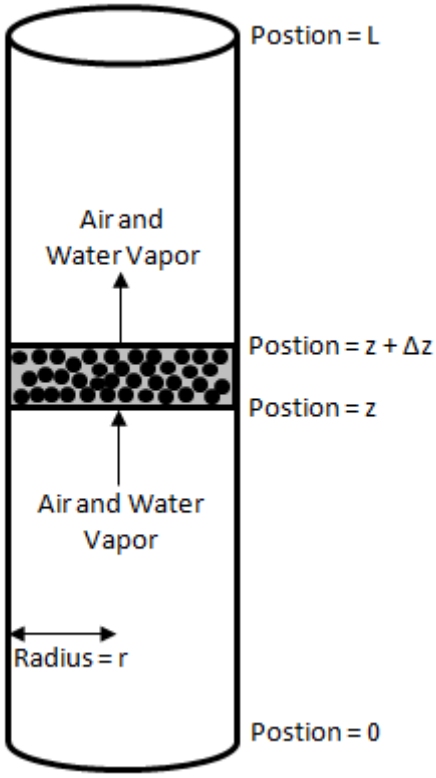

Figure 5.1. Diagram of the packed bed bioreactor with a differential volume element.

The energy balance for the differential element is:

$$\pi r^2 \Delta z \frac{\partial\left(\rho_b C_{Pb} T(z,t)\right)}{\partial t} = \pi r^2 \Delta z \rho_s (1-\varepsilon) Y_Q \frac{\partial G(z,t)}{\partial t} + v_s \pi r^2 \rho_a C_{pa}\left(T(z,t) - T(z+\Delta z,t)\right) +$$
$$\lambda v_s \pi r^2 \rho_a \left(H_{sat}\left(T(z,t)\right) - H_{sat}\left(T(z+\Delta z,t)\right)\right) + \pi r^2 k_b \left[\frac{\partial T(z+\Delta z,t)}{\partial z} - \frac{\partial T(z,t)}{\partial z}\right] \qquad (5.7)$$

where ρ_b is the density of the bed (kg/m^3), C_{Pb} is the heat capacity of the bed (J/kg/°C), ρ_a is the density of gas phase (kg/m^3), v_s is the superficial gas phase velocity (m/hr), C_{Pa} is the heat capacity gas phase (J/kg/°C), H_{sat} is the humidity of the air (kg water / kg air) as a function of temperature, λ is the latent heat of vaporization for water (J/kg), k_b is the thermal conductivity of the bed (J/hr/m/°C), and ρ_s is the density of solid phase (kg/m^3). The term on the left hand side of Eq. 5.7 represents energy accumulation in the volume element. The first term on the right hand side is the heat generated from microbes on the solid particles. The second term on the right hand side represents axial convection due to the cooling capacity of the gas stream. The third term on the right is axial convection due to the vaporization of water from the solid particles which enters the gas phase. The final term accounts for axial conduction in the bed.

The next step is to evaluate which variables in Eq. 5.7 can be considered constants and which vary significantly with temperature. The kinetic model used limits the temperature range in the bioreactor between 22.5°C and 32.5°C. The latent heat of vaporization, λ, can be estimated to change based on Watson's correlation [16]:

$$\lambda(T_2) = \lambda(T_1)\left(\frac{T_c - T_2}{T_c - T_1}\right)^{0.38} \qquad (5.8)$$

where T_c is the critical temperature of water (374.25°C). The enthalpy for vaporization of water at 27°C is 2389.8 kJ/kg [17]. Using Watson's correlation, the heat of vaporization over the valid range for the kinetic sub-model will be 2450 kJ/kg at 22.5°C

and 2424 kJ/kg at 32.5°C, a difference of about 1% which is not expected to have a significant impact. Therefore an average value of 2437 kJ/kg was used for the enthalpy of vaporization.

The saturation humidity (H_{sat}) is expected to be significantly dependent on temperature and can be determined from the Antoine equation and Raoult's law. According to the Antoine equation for water under 60°C [16]:

$$\log_{10}(P_{sat}(mmHg)) = 8.10765 - \frac{1750.286}{T(°C) + 235.0} \tag{5.9}$$

where P_{sat} is the vapor pressure (mm Hg). When only water exists in the liquid state then Raoult's law simplifies to:

$$y = \frac{P_{sat}(T)}{P'} \tag{5.10}$$

where y is the mole fraction of water in the gas phase and P' is the total pressure (mm Hg). Assuming that only water and air are present in the gas phase then the saturation humidity in terms of mass can be written as:

$$H_{sat}(T) = \frac{y(T) * mw_{water}}{(1 - y(T)) * mw_{air}} = \frac{P_{sat}(T) * mw_{water}}{(P' - P_{sat}(T)) * mw_{air}} \tag{5.11}$$

where mw_{water} is the molecular weight of water and mw_{air} is the molecular weight of air. Eq. 5.11 assumes the pressure drop across the reactor bed is negligible, therefore P' is constant. The value of H_{sat} at 22.5°C is 0.01725 kg water per kg air and the value nearly doubles at 32.5°C to 0.03166 kg water per kg air. For simplification, the temperature dependence of H_{sat} was approximated as a linear function as shown in Figure 5.2. Figure 5.2 shows the linear approximation compared to the values calculated using the Antoine equation combined with Raoult's law. The linear approximation is:

$$H_{sat}(T) = n'T + c' . \tag{5.12}$$

The value of n' is the slope and has a value of 1.4346×10^{-3} kg water/kg air/°C and c' is the intercept with a value of -0.01564 kg water/kg air. The linear approximation results in a maximum of 3.5% error which occurs at 22.5°C.

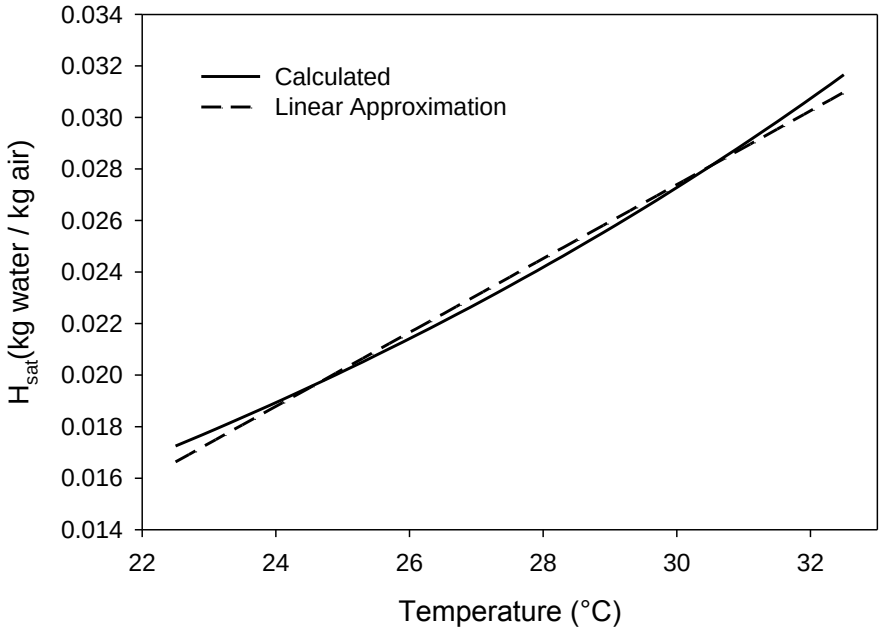

Figure 5.2. Comparison of calculated and approximated saturation humidity as a function of temperature.

The density of the gas phase, ρ_a, varies with temperature according to the ideal gas law. The composition of the gas phase also varies with temperature due to the changing value of H_{sat}. The mole weighted average molecular weight (mw_{avg}) simplifies to:

$$mw_{avg}(T) = \frac{1 + H_{sat}(T)}{\frac{1}{mw_{air}} + \frac{H_{sat}(T)}{mw_{water}}} . \tag{5.13}$$

The ideal gas law then yields:

$$\rho_a(T) = \frac{P'}{R(T + 273.15)} mw_{avg}(T) \tag{5.14}$$

where R is the universal gas constant. The density of the gas varies approximately 4% over the expected temperature range from 1.177 kg/m^3 at 22.5°C to 1.129 kg/m^3 at 32.5°C. The density of the gas phase was considered to be constant with an average value of 1.153 kg/m^3.

One of the remaining terms in Eq. 5.7 is the bed density, ρ_b, which is calculated by:

$$\rho_b = \varepsilon\rho_a + (1-\varepsilon)\rho_s . \tag{5.15}$$

where ρ_s is the particle density of the solid phase. The particle density was assumed to be 700 kg/m^3, similar to that of moist ground corn. Therefore the bed density was calculated to be 455 kg/m^3.

The bed thermal conductivity was calculated using the relationship developed by Chaudhary and Bhandari [18] for two phase unconsolidated materials:

$$n = \frac{0.5(1 - \log(\varepsilon))}{\log\left(\varepsilon(1-\varepsilon)\frac{k_s}{k_a}\right)} \tag{5.16}$$

where k_a is the thermal conductivity of the gas phase (J/hr/m/°C), k_s is the thermal conductivity of solid phase (J/hr/m/°C), and n is the fraction of the whole sample that is regarded as distributed according the model by Chaudhary and Bhandari [18]. The overall bed thermal conductivity can be calculated by:

$$k_b = k_s^{1+n} k_a^{1-n} \frac{\left(\varepsilon(1-\varepsilon)\right)^n}{\varepsilon k_s + (1-\varepsilon)k_a} . \tag{5.17}$$

The value for k_a was assumed to be 74.16 J/hr/m/°C and the value for the solid substrate was assumed to be the same as for moist corn used by Mitchell et al [19], 1080 J/hr/m/°C. The value of the fraction of the whole sample in Eq. 5.16 is n=1.4. The overall bed thermal conductivity, k_b, is 1004 J/hr/m/K.

The heat capacity of the gas phase is expected to change with temperature due to the temperature dependence of heat capacities and also due to the change in water vapor content as the temperature of the gas stream increases. The expression for change in composition of water vapor as a function of temperature is expressed in Eq. 5.11. The average heat capacity of the gas phase can be written as a function of temperature using the mass fraction weighted heat capacities:

$$C_{Pa}(T) = \frac{1}{1+H_{sat}(T)} C_{Pair}(T) + \frac{H_{sat}(T)}{1+H_{sat}(T)} C_{Pv}(T) \tag{5.18}$$

where C_{Pair} is the heat capacity of air (J/kg/°C) and C_{Pv} is the heat capacity of water vapor (J/kg/°C). Correlations for how the heat capacity of air and water vapor change with temperature [16] were used to determine the change in the overall heat capacity of the gas phase. The results of Eq. 5.18 indicate the average heat capacity of the gas phase is 1.021 kJ/kg/°C at 22.5°C and 1.035 kJ/kg/°C at 32.5°C, less than a 2% change. Therefore the heat capacity of the gas phase can be considered a constant for the expected temperature range with an average value of 1.028 kJ/kg/°C.

The overall heat capacity of the bed calculated by weighted mass fractions is:

$$C_{Pb} = \frac{\varepsilon \rho_a C_{Pa} + (1-\varepsilon)\rho_s C_{Ps}}{\rho_b} \tag{5.19}$$

where C_{Ps} is the solid phase heat capacity (J/kg/°C). The heat capacity of the WDG substrate was considered to be similar to corn with a value of 2500 J/kg/°C. The heat capacity of the bed, calculated using Eq. 5.19, is 2499 J/kg/°C.

The only variable in Eq. 5.7 that was significantly dependent on temperature was the saturation humidity which was approximated to have a linear temperature dependence according to Eq. 5.12. After dividing and simplifying, the limit is taken as $\Delta z \rightarrow 0$ in Eq. 5.7 resulting in the partial differential equation:

$$\rho_b C_{Pb} \frac{\partial T(z,t)}{\partial t} = \rho_s (1-\varepsilon) Y_Q \frac{\partial G(z,t)}{\partial t} - v_s \rho_a \left(C_{Pa} + \lambda n'\right) \frac{\partial T(z,t)}{\partial z} + k_b \frac{\partial^2 T(z,t)}{\partial z^2}. \qquad (5.20)$$

This equation differs slightly from the model used by Sangsurasak and Mitchell [6,7] and Mitchell et al [8]. The heat generation from microbial biomass is based on a kinetic model for CO_2 production instead of biomass concentration. The original model only takes into account metabolic heat generation from the growth of biomass, ignoring maintenance metabolism. By basing the heat generation on the rate of CO_2 production, both heat generated from microbial growth and maintenance metabolism are accounted for as well as death since inactive cells no longer produce CO_2. Previous models also did not take into account changes in the solid phase moisture content by incorporating a water material balance for the determination of kinetic rate expressions.

Eq. 5.20 requires an initial condition and two boundary conditions to be solved. The initial condition is the temperature gradient of the bed at time zero as a function of axial position, T(z,0). The first boundary condition specifies the inlet temperature of the saturated air entering the base of the bioreactor as a function of time, T(0,t). The second

boundary condition indicates the temperature of the bed does not change with position at the top of the of the bioreactor bed for all times, $\partial T(L,t)/\partial z = 0$.

5.2.3. Solid Phase Water Material Balance

A solid phase water material balance was performed on the system in order to determine the effects of the changing moisture content on overall bioreactor performance. The water balance on the solid phase was found by writing a water material balance around the differential volume element in Figure 5.1. The material balance yields:

$$\pi r^2 \Delta z(1-\varepsilon)\rho_s \frac{\partial \phi(z,t)}{\partial t} = v_z \pi r^2 \rho_a \left[H_{sat}(T(z,t)) - H_{sat}(T(z+\Delta z,t))\right] + \pi r^2 \Delta z(1-\varepsilon)\rho_s Y_W \frac{\partial G(z,t)}{\partial t} \qquad (5.21)$$

The left hand side of the equation represents the change in the mass of water per unit time. The first term on the right hand side is the loss of water due to evaporation, and the second term on the right hand side is the metabolic water generation from microorganisms. Since it is assumed that the air in the bed remains saturated at all times, the water produced by the biomass is assumed to stay on the solid phase. A factor that is not accounted for in Eq. 5.21 is the apparent increase in water content due to the consumption of solids and production of gaseous products such as CO_2. The consumption of solids will lead to an increase in the mass of water per mass of dry solids. Using the same linear approximation given in Eq. 5.19 and taking the limit as $\Delta z \rightarrow 0$, Eq. 5.21 simplifies to:

$$\rho_s \frac{\partial \phi(z,t)}{\partial t} = -v_z \frac{\rho_a n'}{1-\varepsilon} \frac{\partial T(z,t)}{\partial z} + \rho_s Y_W \frac{\partial G(z,t)}{\partial t}. \qquad (5.22)$$

Since the kinetic equation for substrate weight loss (Eq. 5.5) is based on the mass of dry solids lost per mass of initial dry solids, the substrate weight loss can be incorporated into Eq. 5.22 by multiplying the left hand side of the equation by (1-S(z,t)) to obtain:

$$\rho_s \frac{\partial\left(\phi(z,t)\left(1-S(z,t)\right)\right)}{\partial t} = -v_z \frac{\rho_a n'}{1-\varepsilon} \frac{\partial T(z,t)}{\partial z} + \rho_s Y_W \frac{\partial G(z,t)}{\partial t} \quad . \tag{5.23}$$

The loss of dry solids material is then incorporated into the water material balance, but an additional material balance must be added to the system of partial differential equations. Both Eq. 5.22 and 5.23 require an initial condition to be solved. The initial condition is the moisture content of the bed as function of axial position at time zero, $\Phi(z,0)$.

5.2.4. Dry Solids Weight Loss

The dry solids weight loss for the system becomes important to estimate changes in substrate moisture content as demonstrated in Eq. 5.23. Weight loss is also used to determine the quantity of residual substrate remaining after fermentation. The residual substrate may require disposal or be used as an animal feed product. Solids weight loss has previously been used to estimate microbial biomass concentration by Terebiznik and Pilosof [20]. Using Figure 5.1, a differential material balance leads to the expression:

$$\frac{\partial S(z,t)}{\partial t} = Y_S \frac{\partial G(z,t)}{\partial t} . \tag{5.24}$$

Eq. 5.24 requires the initial condition of substrate weight loss at time zero. The dry solids weight loss at this time is equal to zero since the substrate has not been consumed, $S(z,0) = 0$.

5.2.5. Product Formation

Product formation can be estimated based on the rate of CO_2 production by correcting the yield coefficient for temperature and moisture content as demonstrated in Eq. 5.3.

The goal of the fermentation is to produce the product of interest, in this case cellulase activity. A material balance for product formation results in the partial differential equation:

$$\frac{\partial P(z,t)}{\partial t} = Y_P\big(T(z,t),\phi(z,t)\big)\frac{\partial G(z,t)}{\partial t}. \tag{5.25}$$

Product formation, similar to the energy balance, water balance, and dry solids weight loss depends on the rate of CO_2 production which is calculated using Eq. 5.1. The initial condition for product formation is equal to zero since cellulase activity was not initially present in the bioreactor, P(z,0) = 0.

5.3. Computational Methods

In order to validate numerical solution methods, the model was first simplified and solved using the method of characteristics. The effects of moisture content were considered negligible for the solution validation, therefore only Eq.5.20 was solved. The effect of axial conduction was also neglected due to the relatively small thermal conductivity of the bed. Eq. 5.20 can then be solved by applying the method of characteristics [21]. Eq. 5.20 simplifies to:

$$\frac{\partial T(z,t)}{\partial t} + a\frac{\partial T(z,t)}{\partial z} = \frac{\rho_s(1-\varepsilon)Y_Q}{\rho_b C_{Pb}}\frac{\partial G(z,t)}{\partial t} \tag{5.26}$$

where the constant a is equal to $\frac{v_s\rho_a\left(C_{Pa}+\lambda n'\right)}{\rho_b C_{Pb}}$ with units of m/hr. Applying the method of characteristics to Eq. 5.26 yields ordinary differential equations by transforming from an Eulerian to a Lagrangian point of reference. The exact differential expresses the total derivative in terms of partial derivatives:

$$\frac{dT(z,t)}{d\sigma} = \frac{dt}{d\sigma}\frac{\partial T(z,t)}{\partial t} + \frac{dz}{d\sigma}\frac{\partial T(z,t)}{\partial z} \tag{5.27}$$

where σ is an arbitrary variable. Using Eq. 5.27, a set of ordinary differential equations can written from Eq. 5.26:

$$\frac{dt}{d\sigma} = 1; \qquad \frac{dz}{dt} = a; \qquad \frac{dT(z,t)}{dt} = \frac{\rho_s(1-\varepsilon)Y_Q}{\rho_b C_{Pb}}\frac{dG(z,t)}{\partial t}. \tag{5.28}$$

Eq. 5.28 is then integrated from t* to t, z* to z, and T* to T. For initial conditions, the value of t* is equal to zero and z* is a position between 0 and z at time zero with an initial temperature T*. The initial condition will be valid for positions z* to z for times 0 to [1/a×(z-z*)] until z = H. For the boundary conditions, z* is equal to 0, the inlet position of the bioreactor, and the inlet air temperature has a value of T*. Boundary conditions are valid for positions 0 to z until z = H and times t* to t until t = z/a + t*. The second equation in Eq. 5.28 was integrated by separation of variables. The third equation in Eq. 5.28 was integrated numerically with the ODE solver in Mathcad 13.

Results of Eq. 5.26 solved by the method of characteristics were used to validate a discretized stage model similar to the one used by Flodman and Dvorak [22] for an ion exchange packed bed. The model development is similar to the derivation of Eq. 5.7, with the exception that the contents in the differential volume element are considered to have uniform conditions such as temperature and moisture within the stage. The limit is not taken as $\Delta z \rightarrow 0$ and a series of ordinary differential equations result where the size of the volume element can be specified by Δz. Again neglecting axial conduction, the stage model is:

$$\frac{dT_n(t)}{dt} = \frac{\rho_s(1-\varepsilon)Y_Q}{\rho_b C_{Pb}}\frac{dG_n(t)}{dt} + \frac{v_s\rho_a(C_{pa}+n'\lambda)}{\Delta z\rho_b C_{Pb}}\left(T_{n-1}(t) - T_n(t)\right) \tag{5.29}$$

where n is the stage number starting at the bottom of the bed where air enters. The total number of stages is determined by $H/\Delta z$. Eq. 5.29 was solved sequentially using the stiff ODE solver in Mathcad 13. Solutions obtained using the method of characteristics (symbols) are compared to stage model solutions (lines) in Figure 5.3 for an inlet air temperature of 22.5°C, a superficial velocity of 7.5 cm/s, and a stage size of $\Delta z = 0.05$ m. Temperature profiles at z values of 0.25, 0.5, 0.75, and 1 m are shown in the figure. Stage model errors are expected to accumulate as you move toward the top of the column, whereas errors when solving the equation using the method of characteristics are less dependent on axial position. The figure shows that the stage model solution produces an accurate approximation when compared to the solution by the method of characteristics.

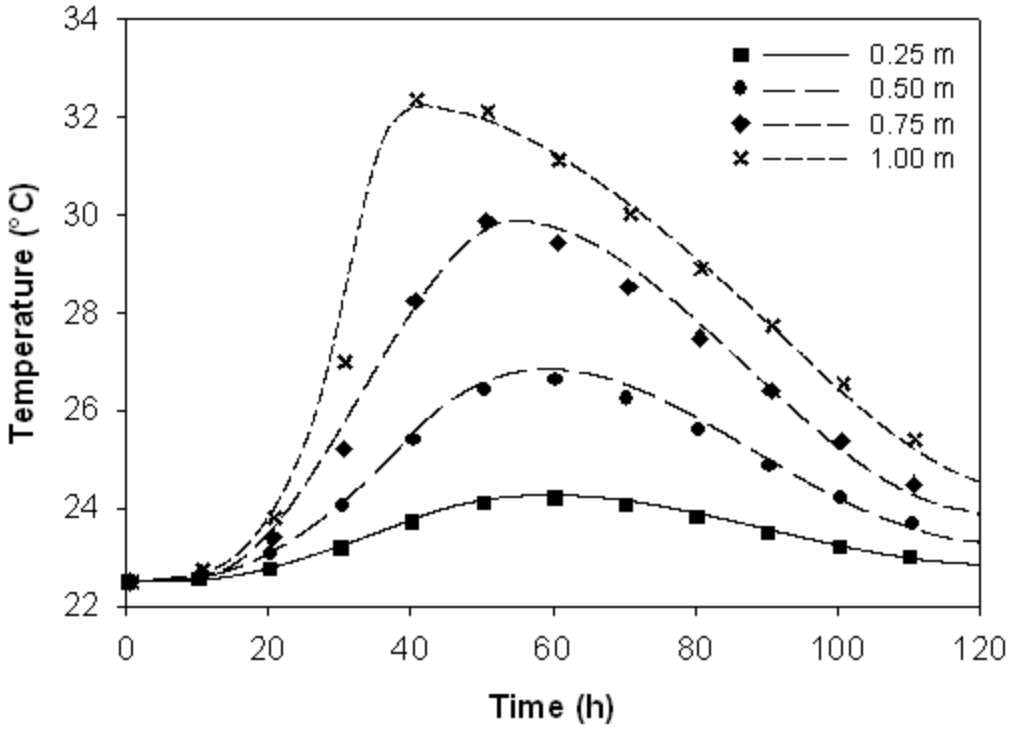

Figure 5.3. Comparison of solutions for temperature profiles by the method of characteristics (symbols) and the discrete stage method (lines) for bioreactor heights of 0.25, 0.5, 0.75, and 1 m.

Similar to the stage model for the energy balance in Eq. 5.29, a solid phase water material balance using the stage methods results in:

$$\left(1-S_n(t)\right)\frac{d\phi_n(t)}{dt}-\phi_n(t)\frac{dS_n(t)}{dt}=v_z\,\frac{\rho_a n'}{\Delta z\rho_s(1-\varepsilon)}\left(T_{n-1}(t)-T_n(t)\right)+Y_W\,\frac{dG_n(t)}{dt}. \qquad (5.30)$$

The substrate weight loss and product formation are found similarly:

$$\frac{dS_n(z,t)}{dt}=Y_S\,\frac{dG_n(z,t)}{dt}, \qquad (5.31)$$

$$\frac{dP_n(z,t)}{dt}=Y_P\left(T_n(z,t),\phi_n(z,t)\right)\frac{dG_n(z,t)}{dt}. \qquad (5.32)$$

Eqs. 5.29-32 were solved as a system of ODEs using the Mathcad ODE solver stiff method. Stages were solved sequentially starting at stage 1. A stage size of $\Delta z = 0.05$ m was used. Mixing events were used to add moisture to the bed and return the bed to a uniform temperature with the assumption of a uniform temperature and moisture in the entire bed after mixing. It was assumed that mixing events took a negligible amount of time when compared to the duration of the fermentation. Due to the limitations of the kinetic model, temperature was limited to a range of 22.5 to 32.5°C and moisture from 0.82 to 1.50 kg water/kg solid.

5.4. Results and Discussion

The bioreactor model was used to evaluate the effects of water addition, mixing, substrate bed height, and superficial air velocity on a packed bed SSF bioreactor. By evaluating different operating strategies using the developed model, many different bioreactor operating strategies were tested in a relatively small amount of time compared to pilot plant studies.

5.4.1. Packed Bed with Mixing and Water Addition

Mixing can be used as a means to uniformly rehydrate the substrate bed when moisture gradients develop which are deemed unacceptable. Research has shown that intermittent mixing is a relatively poor means of controlling bioreactor temperature [10]. Figure 5.3 indicates that it is feasible to maintain a bed temperature within the operating range of the kinetic model for a bioreactor with a bed height of 1 m and inlet temperature of 22.5°C with a superficial air velocity of 7.5 cm/s and an initial moisture content of Φ = 1.00 kg/kg. However, moisture gradients must also be considered due to the impact of evaporative cooling. Using the same conditions as specified in Figure 5.3, but adding the effects of moisture to the kinetic model as well as incorporating the water material balance, reveals the substrate bed rapidly loses moisture at the beginning of the fermentation. Without mixing and moisture addition, the bed would continue to dry rapidly with increasing fermentation time, inhibiting microorganism growth and activity. Therefore a shorter bed height and/or a higher initial moisture content would be required if water addition was not used. Figure 5.4(a) and (b) show the temperature and moisture profile of the bed at axial positions (z) of 0.25, 0.5, 0.75, and 1 m as a function of time for minimum mixing events to keep the moisture content within the acceptable range of the kinetic model.

The first mixing event occurred at 38 h of fermentation due to the top of the bioreactor bed reaching a critical moisture content of 0.82 kg/kg. von Meien and Mitchell [10] predicted the substrate bed will quickly return to its original temperature prior to the mixing event due to metabolic heat production. Figure 5.4(a) shows the bioreactor temperature is actually higher after mixing due to the added water content of

the substrate. This type of behavior is predicted since heat production from maintenance metabolism was accounted for in the kinetic model. Another interesting observation from the model is the critical time for the second mixing event as indicated by Figure 5.4(b). Initially the first mixing event was triggered by the moisture content at the top of the bed reaching the critical value; however, the second mixing event occurred at 60 h due to a position in the middle of the bioreactor (z = 0.75 m) reaching the critical moisture content before the top of the bed. This behavior is non-intuitive indicating care must be taken when determining the frequency of mixing events using online monitoring techniques.

Figure 5.4(c) shows the predicted rate of cellulase production as function of time for minimum mixing frequencies based on moisture content. The figure indicates that the top of the bed is expected to be the least productive due to higher temperatures while productivity increases as z decreases due to the lower temperatures at the air inlet of the bioreactor. Cumulative cellulase product formation is not shown due to the fact that ideal mixing is assumed, redistributing the particles throughout the bed. The simplified product formation model does not take into account the temperature and moisture history of the solids therefore some error is expected as indicated in Chapter 4.

Minimum mixing may be influenced by more than the moisture content of the bed. Another factor that may influence mixing events is agglomeration due to mycelial growth and substrate shrinkage as found by Schutyser et al [5]. Weber et al [23] also observed failure of an unmixed packed bed due to substrate shrinkage combined with a strong hyphal network which caused channeling, overheating, and inhomogeneous fungal growth. In Chapter 3, use of mixing frequencies of 6 d^{-1} were used without causing

significant effects to microorganism activity or product formation for *T. reesei* grown on WDG. Figure 5.4(d), (e), and (f) show the modeling results for the same fermentation conditions as Figure 5.4(a), (b), and (c) at mixing frequencies of 6 d^{-1}. Comparing Figures 5.4(a) and (d) indicate that additional mixing has minimal effects on the temperature profile of the bed. One noticeable difference is the absence of the temperature jump that was observed in Figure 5.4(a) after mixing occurred. Figure 5.4(e) shows that frequent mixing and moisture addition kept the substrate moisture near 1.00 kg/kg and therefore the effects of changing moisture content on maintenance and growth of the microorganism was not apparent and sudden increases in temperature after mixing were not predicted. A comparison of Figures 5.4(c) and (f) shows that the predicted rate of product formation is nearly identical for both cases. However, Chapter 4 showed that the predicted product formation model tended to over-predict the actual product formation rate when frequent changes in temperature occur, similar to the ones caused by mixing, even though mixing alone does not significantly influence product formation.

In conclusion, the maximum bed height should be determined by energy balance restrictions, not water material balance restrictions when mixing and water addition can be incorporated into the process with minimal effects on product formation and microorganism growth. Reducing the temperature of the bioreactor bed during mixing should not be an emphasized design characteristic since the temperature profile in the bed quickly redevelops after mixing events. In fact, rapid changes in temperature may inhibit product formation. By not emphasizing temperature control during mixing, more types of mixing mechanisms can be evaluated during the design phase.

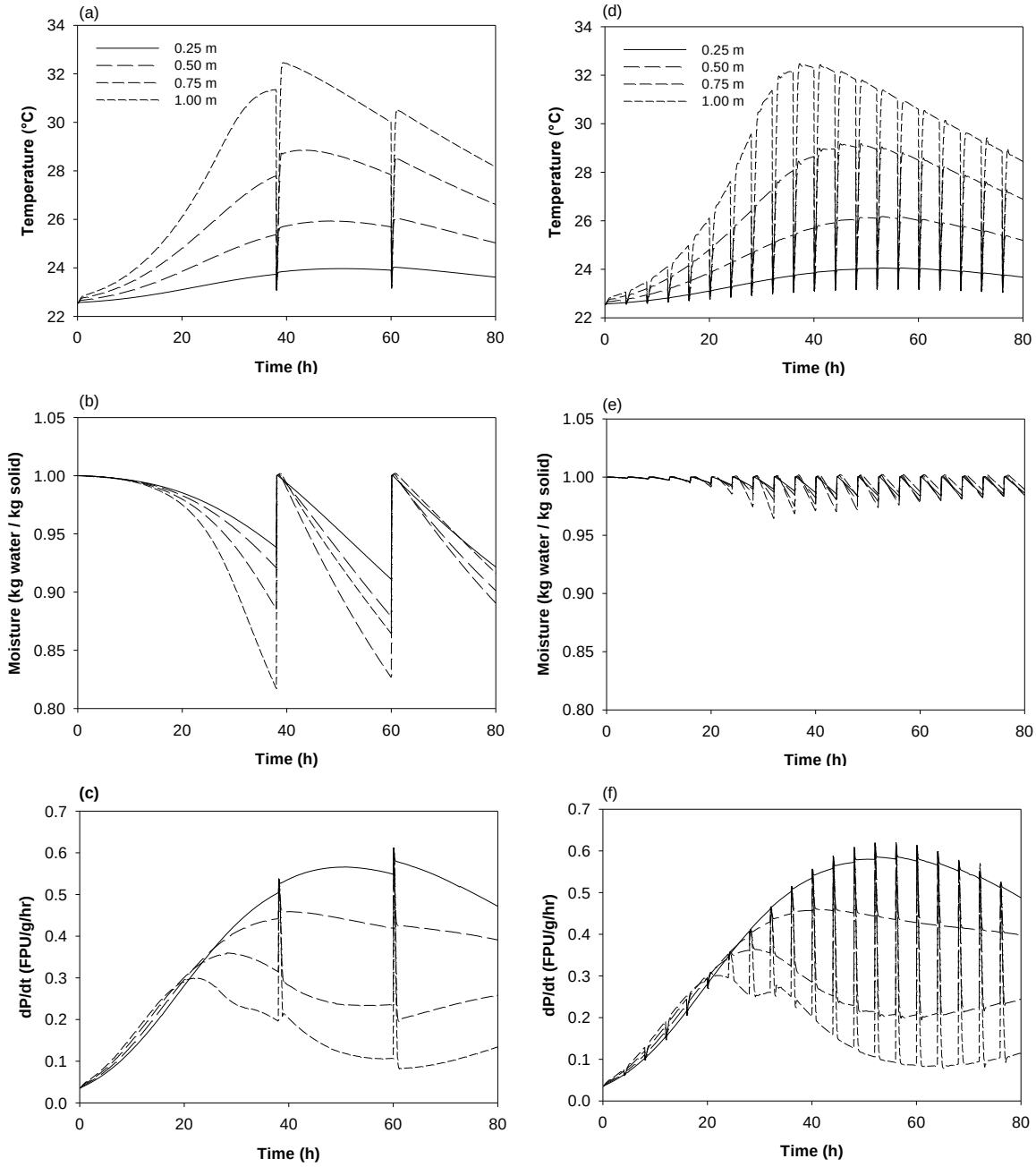

Figure 5.4. Effects of mixing on (a,d) temperature profiles, (b,e) moisture profiles, and (c,f) the rate of cellulase enzyme production at axial positions of z = 0.25, 0.5, 0.75, and 1 m as a function of time. Figures (a), (b), and (c) show predictions from a minimum mixing frequency based on moisture addition. Figures (d), (e), and (f) plot results from a mixing frequency of 6 d^{-1}.

5.4.2. Moving Packed Bed

Mitchell et al [11] investigated the use of a moving packed bed bioreactor for the growth of *A. niger*, and found that the maximum temperature of the bed was reduced compared to traditional packed bed operations. The design of the bioreactor used trays with thin layers of substrate conveyed in countercurrent direction with respect to the inlet air flow. This type of bioreactor was evaluated for the growth of *T. reesei* on WDG. Furthermore, mixing and water addition for individual trays were considered as part of the bioreactor design. A moving packed bed reactor with the substrate bed moving in a cocurrent direction to the inlet air flow was also investigated. Figure 5.5 illustrates the two modes of operation for the moving packed bed bioreactor. For countercurrent operation in Figure 5.5(a), a new substrate layer is added to the top of the bioreactor while the layer at the bottom is removed for product recovery. For cocurrent operation in Figure 5.5(b), a new layer is added to the bottom of the bioreactor while the top layer is removed for product recovery. In both configurations air enters at the bottom of the bioreactor, and each layer has a thickness of 0.05 m. The residence time for a layer to stay at a given position within the bioreactor is calculated by the total residence time (80 h) divided by the total number of layers. This type of bioreactor can be considered continuous even though layers are added discretely in the model. Therefore any given position in the bioreactor will experience the same temperature and moisture profile for each layer residing in that position for the layer residence time.

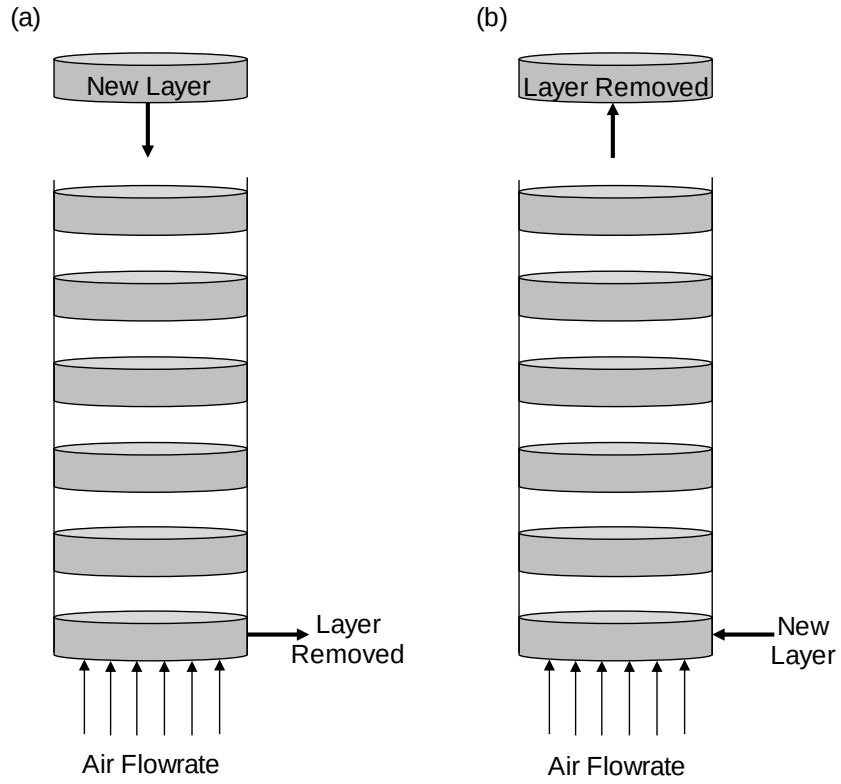

Figure 5.5. Illustration of moving packed bed bioreactors for (a) countercurrent operation and (b) cocurrent operation.

Results of countercurrent and cocurrent moving bed simulations are compared in Figure 5.6 for a bioreactor with 20 layers under the same operating conditions used to produce Figure 5.4. Countercurrent operation results are shown in Figures 6(a), (b), and (c), and cocurrent results are plotted in Figures 5.6(d), (e), and (f). A superficial air velocity of 7.5 cm/s and the initial substrate temperature and moisture was 22.5°C and 1.00 kg/kg for layers entering the bioreactor. Each layer was at a given position within the reactor for 4 h, resulting in a total residence time of 80 h.

The temperature profiles for four positions in the countercurrent and cocurrent moving bed are shown in Figures 5.6(a) and (d), respectively. The figures show that the maximum temperature for both configurations occurred at the top of the bed, but cocurrent operation had a considerably lower maximum temperature. When the

temperature profiles in Figure 5.6 are compared to Figure 5.4, the maximum temperature in the bed was 2.5°C less for countercurrent and 5.0°C less for cocurrent moving bed operations compared to packed bed operation. This indicates that the maximum substrate bed height may be greater for moving bed operations when moisture is not a limiting factor.

For both cocurrent and countercurrent operation, moisture was added at one position within the bioreactor in order to prevent the moisture content from falling below 0.82 kg/kg. This is an improvement compared to packed bed operation in Figure 5.4, where moisture was added twice during the fermentation time to prevent falling below the critical value. For countercurrent operation, moisture was added when each layer reached a position of 0.5 m in the reactor. For cocurrent operation moisture was added when each layer reached a position of 0.8 m from the bottom of the bed. Figures 5.6(b) and (e) show the moisture profiles for various positions within the bioreactor.

The rates of product formation at different positions within the bioreactor are predicted in Figures 5.6(c) and (f). Product formation increased as the position within the bioreactor decreased for countercurrent operation. Cocurrent operation is predicted to have a higher overall average rate of product formation throughout the length of the bioreactor, with the greatest rates occurring in the center of the bioreactor. The difference in the rates of product formation when comparing cocurrent and countercurrent moving bed operations was caused by the temperature and moisture at each stage as well as the overall fermentation time of the layer at that stage. For example, during countercurrent operation the layer at the bottom of the bed has a temperature approaching the air inlet temperature of 22.5°C from 76-80 h of overall

fermentation time. For cocurrent operation, the layer at the bottom of the bed experienced the same conditions from 0-4 h of overall fermentation time. Additional experimentation is required to confirm the product formation predictions in Figure 5.6.

For this system, cocurrent moving bed operation showed several advantages over both countercurrent moving bed and traditional packed bed operations. A lower maximum temperature in the bed along with a uniform rate of product formation along the length of substrate bed make cocurrent moving beds an attractive option for pilot scale investigation.

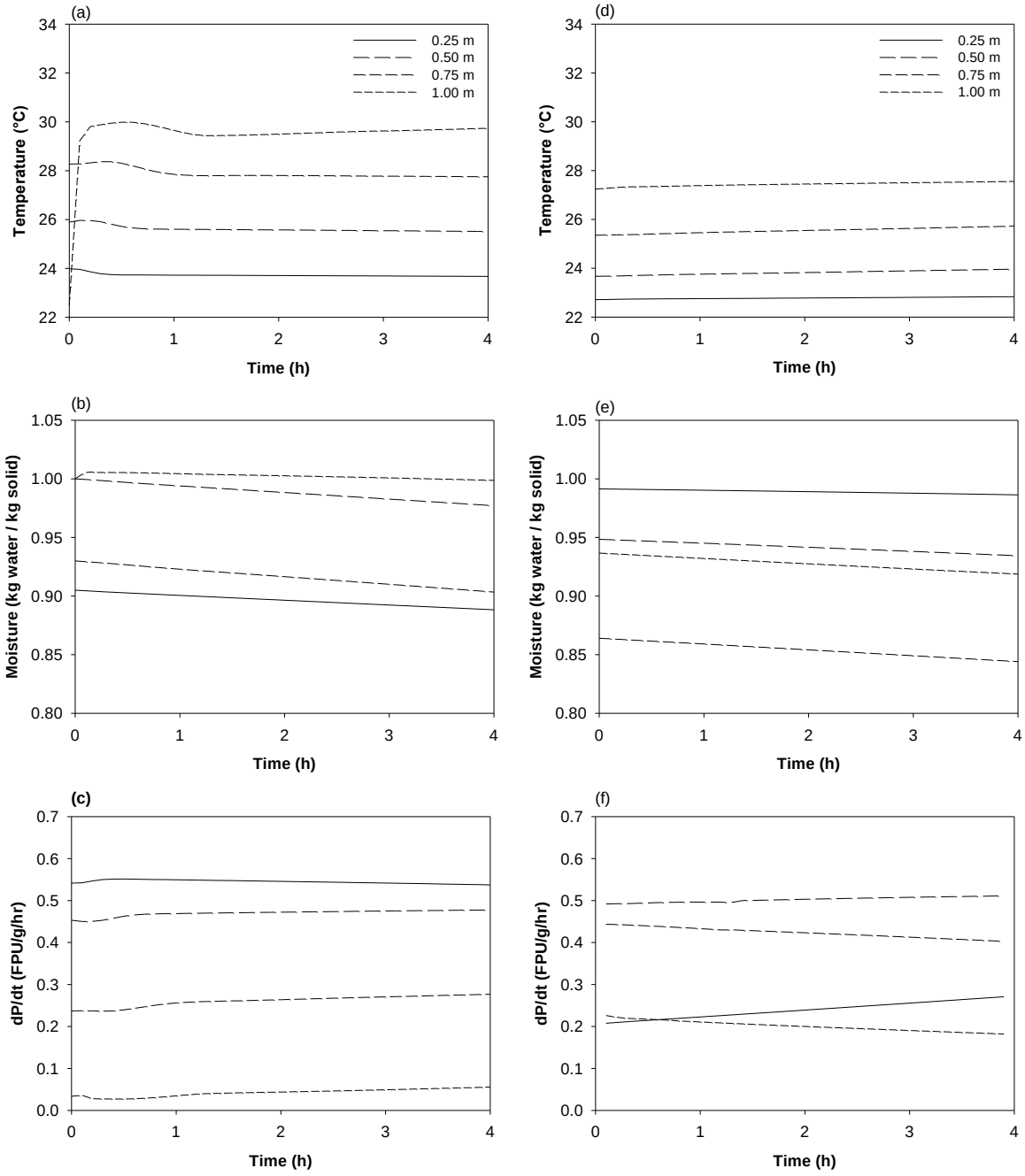

Figure 5.6. Effects of moving bed operation on (a,d) temperature profiles, (b,e) moisture profiles, and (c,f) the rate of cellulase enzyme production at axial positions of z = 0.25, 0.5, 0.75, and 1 m as a function of time. Figures (a), (b), and (c) show predictions from countercurrent moving bed operation. Figures (d), (e), and (f) plot the results of cocurrent moving bed operation.

5.4.3. Bed Height and Superficial Air Velocity

The bed height is a critical factor for determining the dimensions and capacity of bioreactors during the design phase as well as the overall economics of the process. The maximum bed height of the bioreactor is influenced by the superficial velocity of the saturated air stream when overheating is the limiting factor [8]. However, analysis from the previous sections suggests that the limiting factor to maximize bed height may be the moisture content when mixing in conjunction with water addition is not used. When mixing and water addition are used, the bed moisture can be increased and the limiting factor can change from moisture to bed temperature. Both limitations of moisture and temperature were investigated.

When water addition is not incorporated into bioreactor designs either moisture or temperature can limit the maximum bed height. The constraints limiting bed height for this model were that the moisture would stay above 0.82 kg/kg and the temperature would stay below 32.5°C at any position within the bed for a fermentation time of 80 h with an inlet air temperature of 22.5°C. Figure 5.7(a) shows the results of the analysis for a packed bed bioreactor with superficial velocities ranging from 2 to 12 cm/s when moisture was not added to the bed during fermentation. The bed height was limited by moisture content when the initial bed moistures was 1.10 and 1.20 kg/kg indicating water addition would have increased the maximum bed height. For moisture contents of 1.35 and 1.50 kg/kg, the critical bed height was limited by temperature indicating that water addition would likely only have minor effects on the maximum bed height. These minor changes would be caused by the influence of moisture on the kinetics of fungal activity. An initial moisture content of 1.35 kg/kg consistently had a higher maximum bed depth

compared to initial moisture content of 1.50. This is due to the prediction of the kinetic model that less CO_2 and therefore less heat will be produced at lower moisture contents when temperature is limiting.

Figure 5.7(b) shows the model results for maximum bed height when moisture was added to the packed bed during mixing at frequencies 6 d^{-1} in order to return the bed to its original moisture content at the beginning of fermentation. This model differed from the model used to produce the results in Figure 5.4 because it was assumed mixing had negligible effects on the temperature profile of the substrate bed. All of the results in Figure 5.7(b) were limited by the critical temperature of 32.5°C since moisture was frequently added. The figure shows that a low initial moisture content of 0.90 kg/kg consistently produced the highest maximum bed height over the range of superficial velocities examined. This occurred since the kinetic model predicts lower CO_2 and heat production at lower moisture contents. As the moisture content increased, the maximum bed height decreases. Comparing Figure 5.7(a) and (b) indicates that for conditions with initial moisture contents of 1.35 and 1.50 kg/kg, which were limited by temperature in both figures, the lack of water addition produced a slightly higher maximum bed depth at the upper range of air velocities. Therefore, when minimum mixing events are required, it may be advantageous to begin the fermentation at high initial moisture contents and let the bed moisture decrease with fermentation time. When moisture was the limiting factor for initial moistures of 1.10 and 1.20 kg/kg in Figure 5.7(a), moisture addition increased the maximum bed height significantly as shown in Figure 5.7(b) as the limiting factor changed to temperature with frequent moisture additions.

Higher inlet air temperatures would cause the maximum bed height to decrease when temperature is limiting. The use of an unsaturated air stream to enhance evaporative cooling effects could not be investigated due to the nature of the equilibrium model. Operating strategies involving evaporative cooling with an unsaturated air inlet stream would need to be explored using a more advanced model which incorporates heat and mass transfer coefficients.

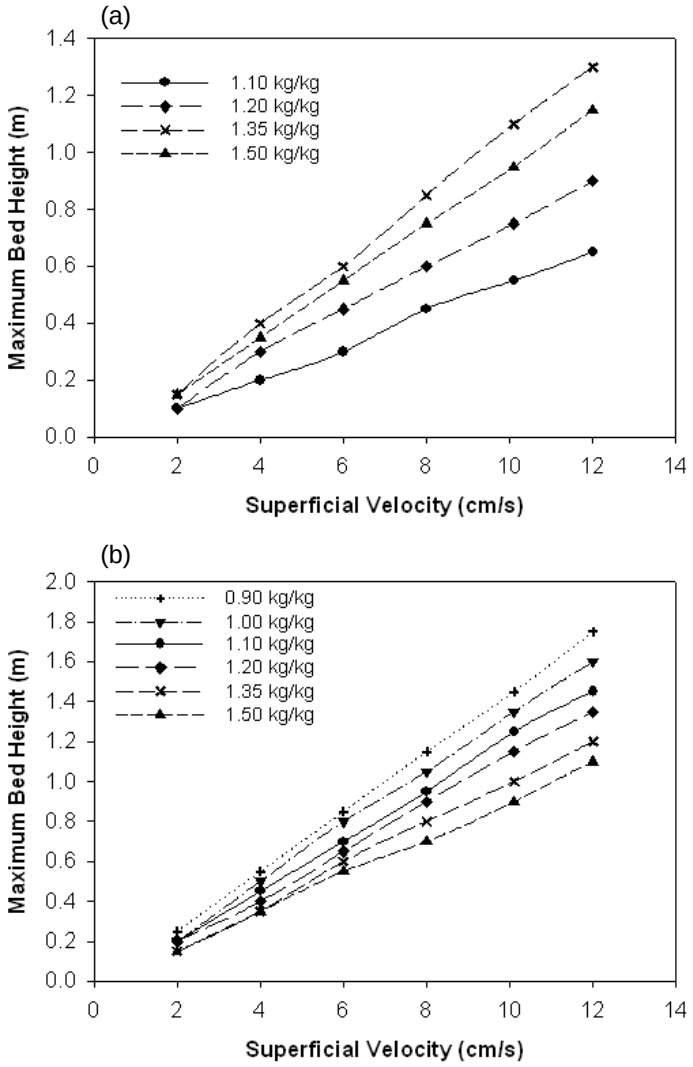

Figure 5.7. Relationship between maximum bed height and superficial air inlet velocity in a packed bed bioreactor for (a) no moisture addition and (b) mixing and moisture addition at a frequency of 6 d^{-1} for various initial moisture contents.

Figure 5.8(a) shows the results of the maximum bed height for cocurrent moving bed operation without moisture addition for layers entering the bioreactor at initial moisture contents of 1.10 and 1.50 kg/kg. Any initial moisture content below 1.10 kg/kg was severely limited by moisture and was not feasible without frequent moisture addition events. Once again the lower initial moisture content has the advantage of having a higher possible bed height since moisture was not limiting. Figure 5.8(b) shows the maximum bed heights when moisture was added at each stage after layers were moved during cocurrent moving bed operation. Comparing Figures 5.7 and 5.8 reveals that cocurrent moving bed operation consistently allows for greater bed heights to be used when compared to packed bed operation indicating that larger volume reactors can be used with lower air flow rate requirements. Figure 5.8(a) also reveals a much smaller difference in maximum bed height when comparing the two initial moisture contents relative to Figure 5.7. Comparing Figures 5.8(a) and (b) reveals that fermentations with and without moisture addition for moving bed operations show a negligible difference in maximum bed height when the initial moisture content is above 1.10 kg/kg and temperature is limiting.

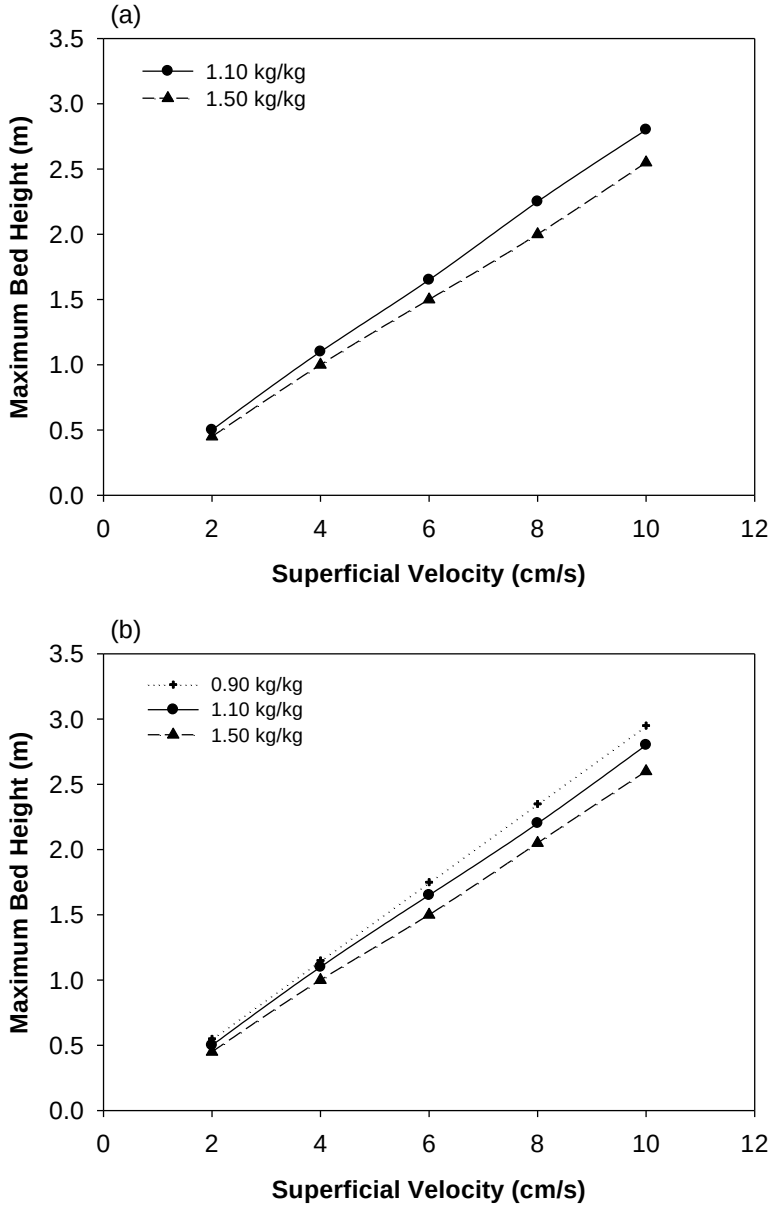

Figure 5.8. Relationship between maximum bed height and superficial air inlet velocity in a cocurrent moving bed bioreactor (a) without moisture addition and (b) with moisture addition when layers are moved.

5.5. Conclusions

A simple SSF equilibrium bioreactor model was developed and solved sequentially as a set of ODEs for the growth of *T. reesei* on WDG substrate in a packed bed bioreactor with mixing. The bioreactor model predicts temperature gradients, solid phase moisture

gradients, substrate weight loss, and cellulase product formation. The developed bioreactor model was used to predict the effects of mixing for moisture addition at specific fermentation conditions. In addition, a cocurrent and countercurrent moving bed bioreactor was also investigated. It was determined that cocurrent moving bed operation was advantageous, having a lower predicted maximum temperature with less solid phase moisture loss and higher predicted product formation when compared to countercurrent moving bed and packed bed operations.

The maximum bed height for packed beds, intermittently mixed packed beds, and cocurrent moving beds with and without moisture addition were determined. Simulations were used to determine whether temperature or solid phase moisture content was the limiting factor to maximize the bioreactor height. As the saturated inlet air velocity increased, the maximum bed height increased. When moisture was limiting, moisture addition could be incorporated into bioreactor design in order to make temperature limiting. Cocurrent moving bed operations had a significantly higher maximum bed height when compared to packed bed operation.

References

[1] U. Holker, M. Hofer, J. Lenz, Biotechnological advantages of laboratory-scale solid-state fermentation with fungi. Appl. Microbiol. Biotechnol. 64 (2004) 175-186.

[2] R.R. Singhania, A.K. Patel, C.R. Soccol, A. Pandey, Recent advances in solid-state fermentation, Biochem. Eng. J. 44 (2009) 13-18.

[3] D.A. Mitchell, M. Berovic, N. Krieger, Introduction to Solid-State Fermentation Bioreactors, in: D.A. Mitchell, N. Krieger, M. Berovič (Eds.), Solid-State Fermention Bioreactors Fundamentals of Design and Operation, Springer, Berlin, 2006, pp. 33-44.

[4] A. Durand, Bioreactor designs for solid state fermentation, Biochem. Eng. J. 13 (2003) 113-125.

[5] M.A.I. Schutyser, P. de Pagter, F.J. Weber, W.J. Briels, R.M. Boom, A. Rinzema, Substrate aggregation due to aerial hyphae during discontinuously mixed solid-state fermentation with *Aspergillus oryzae*: Experiments and modeling, Biotechnol. Bioeng. 83 (2003) 503-513.

[6] P. Sangsurasak, D.A. Mitchell, Incorporation of death kinetics into a 2-dimensional dynamic heat transfer model for solid state fermentation, J. Chem. Tech. Biotechnol. 64 (1995) 253-260.

[7] P. Sangsurasak, D.A. Mitchell, Validation of a model describing two-dimensional heat transfer during solid-state fermentation in packed bed bioreactors, Biotechnol. Bioeng. 60 (1998) 739-749.

[8] D.A. Mitchell, A. Pandey, P. Sangsurasak, N. Krieger, Scale-up strategies for packed-bed bioreactors for solid-state fermentation, Proc. Biochem. 35 (1999) 167-178.

[9] V.M. Ashley, D.A. Mitchell, T. Howes, Evaluating strategies for overcoming overheating problems during solid-state fermentation in packed bed bioreactors, Biochem. Eng. J. 3 (1999) 141-150.

[10] O.F. von Meien, D.A. Mitchell, A two-phase model for water and heat transfer within an intermittently-mixed solid-state fermentation bioreactor with forced aeration, Biotechnol. Bioeng. 79 (2002) 416-428.

[11] D.A. Mitchell, L.E.N. Cunha, A.V.L. Machado, L.F.L. Luz Jr., N. Krieger, A model-based investigation of the potential advantages of multi-layered packed beds in solid-state fermentation, Biochem. Eng. J. 48 (2010) 195-203.

[12] K. Brijwani, P.V. Vadlani, K.L. Hohn, D.E. Maier, Experimental and theoretical analysis of a novel deep-bed solid-state bioreactor for cellulolytic enzymes production, Biochem. Eng. J. 58-59 (2011) 110-123.

[13] A.H. Sahir, S. Kumar, S. Kumar, Modelling of a packed bed solid-state fermentation bioreactor using the N-tanks in series approach, Biochem. Eng. J. 35 (2007) 20-28.

[14] C.L. Cooney, D.I.C. Wang, R.I. Mateles, Measurement of heat evolution and correlation with oxygen consumption during microbial growth, Biotechnol. Bioeng. 11 (1968) 269-281.

[15] J.S. Lekanda, J.R. Perez-Correa, Energy and water balances using kinetic modeling in a pilot-scale SSF bioreactor, Process Biochem. 39 (2004) 1793-1802.

[16] R.M. Felder, R.W. Rousseau, Elementary Principles of Chemical Processes 3rd Ed, Wiley, 2000.

[17] D.M. Himmelblau, J.B. Riggs, Basic Principles and Calculation in Chemical Engineering 7th Ed, Prentice Hall, Upper Saddle River, NJ, 2004.

[18] D.R. Chaudhary, R.C. Bhandari, Thermal conductivity of two-phase porous materials: dry soils, Brit. J. Appl. Phys. Ser. 2 2 (1969) 609-610.

[19] D.A. Mitchell, P. Srinophakun, O.F. von Meien, L.F.L. Luz Jr, N. Krieger, Models of Packed-Bed Bioreactors, in: D.A. Mitchell, N. Krieger, M. Berovič (Eds.), Solid-State Fermention Bioreactors Fundamentals of Design and Operation, Springer, Berlin, 2006, pp. 331-348.

[20] M.R. Terebiznik, A.M.R. Pilosof, Biomass estimation in solid state fermentation by modeling dry matter weight loss, Biotechnol. Techniq. 13 (1999) 215-219.

[21] T.W. Navrkal, H.R. Flodman, D.C. Timm, A water-water preheater and a steam-water heater network: Temperature dynamics, Int. J. Heat Mass Transfer 55 (2012) 166-178.

[22] H.R. Flodman and B.I. Dvorak, Brine reuse in ion-exchange softening: Salt discharge, hardness leakage, and capacity tradeoffs, Water Environ. Res. 84 (2012) 535-543.

[23] F.J. Weber, J. Oostra, J. Tramper, A. Rinzema, Validation of a model for process development and scale-up of packed-bed solid-state bioreactors, Biotechnol. Bioeng. 77 (2002) 381-393.

Chapter 6

Extraction of Soluble Fiber from Distillers Grain

Abstract

The feasibility of using coproducts from dry grind corn ethanol production as a substrate for the production of soluble fiber was examined. Acid- and base-catalyzed hydrolysis experiments were performed using sulfuric acid and sodium hydroxide to partially hydrolyze the hemicellulose content of whole stillage, a precursor to distillers grain, to soluble fiber. The influences of temperature, reaction time, and hydrolyzing agent concentration on the formation of soluble fiber were studied. Soluble fiber was recovered by precipitation in a 95% ethanol solution. Results indicate that appreciable quantities of soluble fiber may be extracted using either acid- or base-catalyzed reactions. The highest yield of soluble fibers was 13.2 g per 100 g-db of treated whole stillage using one weight percent sodium hydroxide at 80ºC for 1 h. HPLC analysis was used to quantify the amount of monomeric sugars which were formed during the hydrolysis procedures.

6.1. Introduction

Distillers grain (DG) is the major coproduct of beverage alcohol production and dry grind corn ethanol production for fuel. For every bushel of corn processed, up to 2.8 gallons of ethanol and 16-18 pounds of DG are produced. In 2010, the dry grind industry produced 27 million metric tons of DG [1]. DG is predominantly used as animal feed in various forms. With an increasing demand for the production of ethanol, there is a

growing interest in producing value-added products from DG including cellulosic ethanol. The production of value added products from DG could contribute significantly to the overall economy of the grain ethanol production.

In the dry grind process, ethanol is removed from residual non-fermentable fractions, known as whole stillage (WS), by distillation. WS is then dried to various degrees to form wet DG or dry DG. WS and DG contain primarily protein, oil, and carbohydrates consisting of lignocellulose along with small quantities of a variety of other compounds. As presented in this study, WS contains 23.9 ± 0.9 wt.% db hemicelluloses, making it an ideal substrate for the production of soluble fibers. Hemicelluloses are made up of random, amorphous structures comprised of branched chains of sugars including aldopentoses and aldohexoses; sugars include xylose, arabinose, glucose, mannose, and galactose [2]. Hemicelluloses are noncovalently cross-linked to cellulose via hydrogen bonds [3]. Hemicelluloses have a complex structure leading to a variety of different conformational possibilities. Because of variability, many different reaction mechanisms exist when hydrolyzing hemicelluloses [2].

Jacobsen and Wyman [2] proposed a kinetic model for dilute acid hydrolysis of hemicelluloses which consisted of an initial fast or slow hydrolysis step, depending on the structural characteristics of the hemicellulose structure, resulting in the formation of oligomeric fractions. The formed oligomers of certain size are classified as soluble dietary fiber (SDF). It is generally assumed that oligomers are broken down further to monomeric sugars such as xylose, quickly after formation. Monomers undergo degradation to form products such as furfural. WS is made up of a variety of compounds

other than lignocellulose, adding further complexity because of the potential for competing reactions and mass transfer restrictions.

Dietary fibers are described as the edible parts of plants, or carbohydrates that are resistant to digestion and absorption by the human digestive system [4]. Dietary fibers are further classified into two groups according to solubility in water: SDF or insoluble dietary fibers (IDF). Research has shown that SDF can be extracted from corn, wheat, and rice through chemical and biological treatment of the hemicellulosic fractions [5-7]. Potential products derived from SDF extracted from hemicelluse include emulsifiers, adhesives, thickeners, and stablizers [8,9]. Yadav et al [10] identified extracted corn fiber gum to be a potential replacement for acacia gum.

Multiple studies have indicated pH to be one of the most important factors for the extraction of soluble fiber from hemicellulose. Aoe et al. [7] examined the effect of pH on the extraction of soluble fibers from defatted rice bran. Extraction reagents used for pH adjustments were: sodium hydroxide at pH 14, calcium hydroxide at pH 12, sodium carbonate at pH 11, acetic acid at pH 3, and hydrochloric acid at pH 0.5. The highest extraction yield of SDF from a starch-free rice bran samples was 8.0 % using sodium hydroxide. In another study, Doner and Hicks [5] used an alkaline hydrogen peroxide extraction method to isolate water soluble and insoluble hemicellulose from starch free corn fiber. The highest yield of soluble hemicellulose was 51%. The optimum yield occurred when the extraction was carried out for 2 h at 60 ºC with the pH adjusted to 12.5. In the absence of hydrogen peroxide, yields were lowered by more than 30%. Yapo et al [11] used sulfuric acid to extract pectin, a soluble fiber used extensively in the food industry, from sugar beet pulp and found pH to be the main parameter influencing the

yield of soluble fibers, mainly pectin. The pectin extraction yield ranged from 4.1 to 16.2 wt.%. The highest yield was obtained when the substrate was treated at pH 1.5, for 4 h, and at 90 ^{o}C. A modest change in the pH from 1.5 to 2 resulted in about a one-third decrease in the yield of the extracted pectin. Rouse and Crandall [12] used nitric acid to extract pectin from lime and lemon peels. The results showed the highest yield at pH 1.6 and 95ºC. Renard and co-workers [13] used apple pomace from cider and juice manufacturers as the source of xyloglucan. Researchers found the alkaline concentration to be the most important factor in the extraction of xyloglucan. A comparison of previous studies [5-7,12,13] indicates optimum hydrolysis conditions for the formation of soluble fiber to be also impacted by the hydrolyzing agent used.

Other studies have shown reaction time and temperature to be key factors in the formation and extraction of soluble fiber from hemicellulosic sources using chemical and enzymatic treatments [2,6]. Oh et al [6] used a technical grade hemicellulase to enzymatically modify the soluble fiber content of a purified wheat fiber substrate. The yield was found to be considerably dependent on enzyme concentration and time. The treatment of wheat fiber resulted in an increase from 16% soluble fiber in the substrate to 30% in the enzymatically modified sample.

In this study, the feasibility of SDF formation and extraction from WS was investigated. WS was treated with sulfuric acid and sodium hydroxide to partially hydrolyze the hemicellulose fraction to oligosaccharides classified as SDF. Effects of concentration, time, and temperature were examined. Experiments were carried out at 40, 60, 80, 100, and 110ºC, with 0.4, 1.0, 1.5, 2.0 wt.% sodium hydroxide or 0.5,1.0 wt.% sulfuric acid for reaction times of 30, 60, 90, and 120 min. HPLC analysis was performed

to determine the concentration of monomeric sugars which were formed during the hydrolysis procedure.

6.2. Materials and Methods

6.2.1. Materials

WS was provided by Abengoa Bioenergy, a dry grind corn ethanol facility in York, Nebraska. Defatted WS was produced following procedures outlined by Noureddini et al [14]. Acid-washed Celite, hydrogen peroxide (30 wt.%), hexanes, sulfuric acid (98 wt.%) and sodium hydroxide (10N) were purchased from Sigma Chemical Company (St. Louis, MO). HPLC mobile phase was purified deionized water. Purification was performed with a Simplicity™ 185 purification system (Millipore Inc., Burlington, MA).

6.2.2. Compositional Analysis of Whole Stillage

Composition of the WS substrate was determined by analytical procedures based on the Laboratory Analytical Procedures (LAPs) documented by NREL [15]. The procedures used were for moisture [16], starch [17], carbohydrates and lignin [18], protein [19], ash [20], and extractives [21].

6.2.3. Equipment

The apparatus for acid and base catalyzed reactions at 40, 60, and 80ºC was a temperature controlled water bath. Water was circulated by a VWR scientific model 1157 Bath/Circulator (Bristol, CT) which controlled the temperature of the bath to within ± 0.1ºC. A Thermolyne Mirak model S73135 magnetic stirrer (Dubuque, IA) was used to agitate the reaction mixture. The reaction was completed in 250 mL Erlenmeyer flasks with rubber stoppers.

Reactions at temperatures of 100 and 110 ºC were performed in a 450 mL Parr 4562 bench-top high pressure reactor with a detachable head (Parr Instrument Company, Moline, IL). The reactor assembly was constructed of type 316 stainless steel. A 2.5" ID Parr 762HC2 glass liner was used. The reactor was equipped with a turbine impeller powered by a 1/12 hp variable speed motor. An electric heating mantle and an internal water cooling loop maintained the desired temperature, measured by a type K thermocouple, using a Parr 4843 PID controller. The hydrolyzing agent was added via a catalyst basket once the substrate reached the desired temperature. The basket was opened using air pressure.

6.2.4. Acid and Base Catalyzed Reaction Procedures

Experiments were carried out by varying conditions for temperature (40, 60, 80, 100, and 110ºC), hydrolyzing agent concentration (sodium hydroxide of 0.4, 1.0, 1.5, 2.0 wt.% and sulfuric acid of 0.5 and 1.0 wt.% all based on the total amount of substrate), and reaction time (30, 60, 90, and 120 min). The particle size of WS was reduced by mixing in a Waring laboratory blender (Torrington, CT) for 2 min at 22,000 rpm. Additional experiments used defatted WS and alkaline hydrogen peroxide hydrolysis at 1.0 and 2.0 wt.% NaOH with 1.0 and 2.0 wt.% hydrogen peroxide.

For temperatures of 40, 60, and 80°C, 70g of WS was placed in 250 mL Erlenmeyer flasks and heated in a water bath. After reaching the desired temperature, a specific amount of the hydrolyzing agent (sodium hydroxide for alkaline treatment or sulfuric acid for acid treatment) was added to the flask. For alkaline treatment, 0.4, 1.0, 1.5, and 2.0 wt.% amounted to 0.95, 2.4, 3.7, and 5.0 g of 10N sodium hydroxide. For acid

treatment, 0.5 and 1.0 wt.% amounted to 0.36 and 0.72 g of 98 wt.% sulfuric acid. The reaction time started immediately after the addition.

For reaction temperatures of 100 and 110 ºC, the Parr reactor was first charged with 70 g of the blended WS. The specified quantity of hydrolyzing agent was placed in the catalyst basket, a cylindrical stainless steel vessel with an O-ring sealed cap on the bottom. The top of the catalyst basket was attached to an air pressure valve on the outside of the Parr reactor. Once the reaction mixture reached the desired temperature, the air valve was opened and the hydrolyzing agent was released, starting the reaction time. All the reactions were carried out batch wise, sacrificing the entire sample once the desired reaction time was reached. The reaction mixture was immediately cooled in an ice bath; recovery and quantification of the SDF followed. All experiments were performed in duplicates.

6.2.5. Soluble Fiber Recovery Procedure

Experiments were carried out to recover the SDF from the liquid phase according to the AOAC 991.43 [22]. The liquid phase was first removed from residual solids after the reaction by centrifugation at 6500 g for 10 min. The liquid phase was then vacuum filtered through a Pyrex 60 mL Büchner funnel fritted crucible (Corning No. 36060, ASTM 40-60). One gram of Celite was wetted with distilled water and distributed onto the frit as an even mat. The Celite acted as the filter media. Approximately 2 mL of the vacuum filtrate was passed through a 0.2 µm cellulose acetate syringe filter (Toyo Roshi Kaisha, Japan) and into a vial for the HPLC analysis of monomeric sugars. Thirty mL of the remaining filtrate was placed into a 250 mL flask and mixed with 120 mL of 95 vol.% ethanol which was preheated to 60 ^{o}C. The SDF was allowed to precipitate at room

temperature for 1 h. The precipitate was vacuum filtered through a separate funnel fritted crucible with a bed of 1 g Celite that had been distributed with 75 volume percent ethanol. The precipitate was washed with 75 vol.% ethanol and dried overnight at 103 ºC. Quantification of the SDF product followed.

6.2.6. Quantification of SDF

The amount of SDF was determined using duplicate samples from the procedures outlined above. The precipitated samples were used to determine the total protein content and the ash content of the product. The fraction of SDF in the precipitate was calculated assuming only protein, ash, and SDF were present. Protein content was determined by combustion analysis (LECO FP-528, St. Joseph, MI). Ash content was determined by the method recommended by NREL [20].

6.2.7. Quantification of Monomeric Sugars

A HPLC analysis was performed to quantify the concentration of monomeric sugars in the liquid fraction of the treated WS. Monomeric sugars were determined according the method documented by NREL [23]. A Waters 2695 HPLC Alliance system (Waters Corporation, Milford, MA) was used for the chromatography work, and Waters Empower software was used for the analysis of data. The HPLC was equipped with an ion-exchange Aminex® HPX-87P 300 x 8.7 mm column (Bio-Rad Laboratories, Hercules, CA), a Bio-Rad micro-guard de-ashing 30 x 4.6 mm guard column, and a Waters 2414 RI detector. Sugars analyzed included glucose, xylose, galactose, and arabinose. Sugars were quantified based on calibration curves which were prepared using standard solutions.

6.3. Results and Discussion

In the base and acid treatment of WS, the hemicellulose fraction is hydrolyzed, resulting in oligomers, monomers, and degradation products. Jacobsen and Wyman [2] proposed a simplified reaction mechanism, shown in Figure 1, to analyze the kinetics of hemicellulose hydrolysis. The rate constants k_f and k_s represent the conversion of fast hydrolyzing and slow hydrolyzing hemicellulose, respectively, to oligomers. Some of the oligomers formed are classified as soluble fiber. Soluble fiber molecules with less than 10-12 degrees of polymerization (DP) cannot be separated by precipitation in 95% ethanol [24]. The AOAC method for the analysis of SDF used in this study determines soluble fiber components with a DP of 12 or higher [25]. Oligomers are broken down to monomeric sugars represented by the rate constant k_1 in Figure 1. Monomeric sugars undergo further degradation described by rate k_2 to form degradation products.

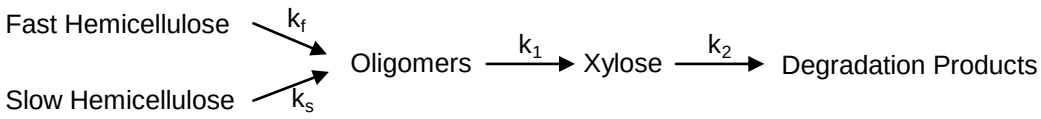

Figure 6.1. Proposed kinetic model for dilute acid hydrolysis of hemicellulose by Jacobsen and Wyman [2].

6.3.1. WS Composition

The composition of the WS substrate was determined using standard procedures described above. The results of the compositional analysis are presented in Table 6.1. The moisture content of the substrate was 84.2 ± 0.1 wt.%. The WS contained 23.9 ± 0.9 wt.%-db hemicellulose and 14.5 ± 0.3 wt.%-db cellulose. Extractives made up 10.9 ±

0.4wt.%-db, which included fats and oils. The yield of SDF extracted was calculated based on the mass of SDF recovered from the hemicellulose content of the sample.

Experiments were performed to determine the amount of SDF in untreated WS which resulted in the recovery of 3.4 g of SDF per 100 g-db of WS. The presence of SDF in the untreated WS suggests the partial hydrolysis of hemicellulose content of corn during the dry grind ethanol production process. Partial hydrolysis of the hemicellulose fraction in corn is likely to occur during the cooking process when starch is gelatinized and also during the distillation process. Both processes involve heating the substrate to high temperatures at around 5.5 pH due to the presence of added sulfuric acid and other reagents.

Table 6.1. Composition of WS in weight percent on a dry basis except for moisture.

Components	Weight Percent
Moisture	84.2 ± 0.1
Extractives	10.9 ± 0.4
Starch[a]	13.2 ± 0.3
Cellulose[b]	14.5 ± 0.3
Hemicellulose[c]	23.9 ± 0.9
Lignin	7.7 ± 0.4
Protein	24.0 ± 0.6
Ash	4.5 ± 0.2
Unknown	1.3

[a] as a source of glucose from residual starch and glucose
[b] as a source of glucose from cellulosic part
[c] as a source of xylose, galactose, and arabinose

6.3.2. Effects of Hydrolyzing Agent

Previous studies have indicated that reagent concentration has significant effects on soluble fiber yield [5-7,12,13]. Experiments were carried out to investigate the effect of sodium hydroxide and sulfuric acid concentration on the formation of SDF from WS. Sodium hydroxide concentrations of 0.4, 1.0, 1.5, 2.0, and 2.5 wt.% were examined at

100 ºC for 1 h. Sulfuric acid concentrations of 0.5 and 1.0 wt.% were examined at 110 ºC for 1 h. Experimental results are presented in Table 6.2. Values in the table are based on g recovered per 100 g-db of treated WS. Data in Table 6.2 shows the quantity of the hydrolyzed supernatant recovered by precipitation in 95% ethanol and the amount of SDF, protein, and ash in the precipitated fraction. Examination of the results for the base catalyzed reactions reveals that the amount of SDF in the supernatant of the hydrolysis product increased as sodium hydroxide concentration increased up to 2.0 wt.%. The highest amount of SDF was 11.4 g/100g-db WS at 2.0 wt.% sodium hydroxide which corresponded to 47% yield. A further increase in the concentration of sodium hydroxide to 2.5 wt.% resulted in a similar yield of the SDF.

Table 6.2. SDF extraction from WS at various chemical concentrations for 1 h at 100ºC for sodium hydroxide treatment and 110ºC for sulfuric acid treatment.

Chemical Concentration	Precipitated Extract	SDF	Ash	Protein
(wt.%)	(g/100g-db WS)			
Sodium Hydroxide				
0.4%	14.5	7.0	4.7	2.8
1.0%	15.9	7.0	5.4	3.5
1.5%	13.3	9.3	2.4	1.7
2.0%	16.5	11.4	4.0	1.1
2.5%	15.8	10.5	4.5	0.8
Sulfuric Acid				
0.5%	17.0	8.9	4.2	3.9
1.0%	19.0	9.6	4.4	5.0

The effect of sulfuric acid on the formation of SDF was similar to hydrolysis with sodium hydroxide. The two concentrations of sulfuric acid tested, 0.5 and 1.0 wt.%, yielded similar quantities of SDF, 8.9 to 9.6 g/100 g-db WS, respectively. On the whole, the base and acid catalyzed hydrolysis results confirmed that significant quantities of SDF are produced from WS using either base or acid treatment.

6.3.3. Effects of Reaction Temperature

Previous studies have indicated reaction temperature to be an important variable for soluble fiber extraction [2]. Experiments examining the effects of temperature on the extraction of soluble fiber from WS were completed for both acid and base catalyzed reactions. Experimental results are shown in Table 6.3.

Table 6.3. SDF extraction from WS at various reaction temperatures for 1 h using 1.0 wt.% sodium hydroxide and 0.5 wt.% sulfuric acid.

Reaction Temperature	Precipitated Extract	SDF	Ash	Protein
(ºC)	(g/100g-db WS)			
Sodium Hydroxide				
40	13.4	5.3	5.5	2.6
60	20.9	11.6	5.1	4.2
80	23.7	13.2	5.6	4.9
100	15.9	7.0	5.4	3.5
110	13.4	7.7	3.3	2.4
Sulfuric Acid				
40	10.8	4.2	4.3	2.4
60	11.8	5.0	4.1	2.7
80	13.7	6.1	4.7	2.9
100	16.4	8.3	4.7	3.4
110	17.1	8.9	4.3	3.9

Base catalyzed reactions covered temperatures ranging from 40 to 110 °C. Sodium hydroxide concentration was 1.0 %, and the reaction time was 1 h. Results reveal that the recovery of SDF was increased as temperature was increased up to 80°C resulting in 13.2 g SDF per 100 g WS, yielding 55 g of SDF per 100g hemicellulose, based on the composition of WS. Further increases in the reaction temperature resulted in a considerable decrease in the SDF recovery. The decrease in the production of SDF at 100°C and 110ºC may be due to an increase in competing reactions such as saponification of triglycerides. Saponification occurs when fats and oils, classified as extractives, react with sodium hydroxide to form glycerol and fatty acid salts.

Saponification reactions are accelerated at higher temperatures [26] indicating that excess sodium hydroxide may be needed for the degradation of hemicellulose to SDF. Results shown in Table 6.2 support this theory as higher sodium hydroxide concentrations up to 2.0 % produced higher recoveries of SDF.

Temperature effects for acid catalyzed reactions were explored at 40, 60, 80, 100, and 110 ºC using 0.5% sulfuric acid for a reaction time of 1 h. Results in Table 6.3 show that the formation of SDF was increased as the reaction temperature was increased. According to the reaction mechanism proposed by Jacobsen and Wyman [2] shown in Figure 1, oligomers are formed at greater rates (k_f, k_s) than they are being consumed (k_1).

6.3.4. Effects of Reaction Time

In general, reaction time is important because the diffusion of the chemical reactants into the fiber matrix and the dissolution of SDF progress in time and are not instantaneous [13]. Sufficient time is required for dissolution and diffusion, but excessively long reaction times may hydrolyze the SDF formed into lower DP molecules, monomeric sugars, or degradation products.

Experiments were performed to examine the effect of reaction time on the production of SDF from WS using 1.0 wt.% sodium hydroxide at 100 ºC for 30, 60, 90, and 120 min. Experimental results are presented in Table 6.4. Examination of the results reveals that the highest amount of SDF was 7.3 g/100 g-db WS which was produced after 30 min of reaction. Further increases in the reaction time resulted in decreases in the total amount of the formed SDF. After 120 min of reaction time, the total amount of the produced SDF reached a minimum of 3.0 g/100 g-db which was lower than the initial amount of SDF in the untreated WS suggesting significant degradation of the produced oligomeric SDF.

The effect of reaction time on the treatment of WS at 110 ºC with 0.5% sulfuric acid is also presented in Table 6.4. As is shown in this table, the production of SDF was increased as the reaction time was increased to 60 min. Further increases in the reaction time to 90 min did not have a significant effect on the proudction of SDF.

Table 6.4. SDF extraction from WS at various reaction times using 1.0 wt.% sodium hydroxide at 100ºC and 0.5 wt.% sulfuric acid at 110ºC.

Reaction Time	Precipitated Extract	SDF	Ash	Protein
(min)	(g/100g-db WS)			
Sodium Hydroxide				
30	14.3	7.3	3.5	3.6
60	15.9	7.0	5.4	3.5
90	6.5	3.4	1.9	1.3
120	5.3	3.0	1.3	0.9
Sulfuric Acid				
15	14.4	6.4	4.5	3.5
30	15.0	7.7	3.7	3.6
60	17.0	8.9	4.2	3.9
90	16.6	8.6	4.2	3.9

6.3.5. Effect of Alkaline Hydrogen Peroxide Treatment on Defatted Whole Stillage

Significant increases in hemicellulose extraction have been shown by adding hydrogen peroxide to extraction [5]. The presence of oil and protein in WS have also been linked to slower hydrolysis rates [14]. Alkaline hydrogen peroxide hydrolysis of defatted WS was investigated to determine potential SDF yield increases with additional pretreatment and hydrolysis procedures.

Table 6.5 shows results of the SDF extractions using 1.0 and 2.0 wt.% sodium hydroxide with 1.0 and 2.0 wt.% hydrogen peroxide for 1 h at 100ºC. Results indicate a trend of incremental increases in SDF recovery as hydrogen peroxide concentration increases using the defatted WS. There was also a significant improvement in the color of the alkaline peroxide treated SDF product (results not shown). The improved color

associated with SDF is believed to be due to the oxidative destruction of phenolic acids by hydrogen peroxide [5].

Table 6.5. SDF extraction from defatted WS at various alkaline hydrogen peroxide concentrations for 1 h at 100ºC.

Sodium Hydroxide Concentration	Hydrogen Peroxide Concentration	Precipitated Extract	SDF	Ash	Protein
(wt.%)	(wt.%)	(g/100g-db WS)			
1.0%	1.0%	12.6	8.6	2.8	1.2
1.0%	2.0%	16.8	11.0	4.0	1.8
2.0%	1.0%	14.6	11.1	3.0	0.5
2.0%	2.0%	18.9	13.2	3.9	1.8

6.3.6. Monomeric Sugar Concentrations

The HPLC analysis was used to determine the quantities of monomeric sugars present in the liquid fraction of the WS after hydrolysis. Monomeric sugar content reveals information on the formation and degradation of monomeric sugars. This information is useful, especially when the residual WS substrate is processed further into value added products, such as bioethanol, after the recovery of SDF.

The formation of monomeric sugars from DG using sulfuric acid has been documented by Noureddini and Byun [27] and by Noureddini et al [14]. Experimental results in these studies indicated that the presence of protein and oil in WS caused lower yields of monomeric sugars when compared to similar treatment with corn fiber and defatted DG [14]. Researchers have postulated that mass transfer restrictions caused by protein and oil molecules are responsible for the slower rate of hydrolysis [14].

The results of the monomeric sugar analysis in mg/mL of the supernatant fraction after sulfuric acid hydrolysis are presented in Table 6.6. As is shown in this table the individual and the total amount of monomeric sugars was increased as the concentration

of sulfuric acid was increased from 0.5 to 1.0% and as the reaction time was increased from 30 to 60 min. This is consistent with previous research which targeted the hydrolysis of WS for the purpose of transforming the hydrocarbon fractions to monomeric sugars [27].

Table 6.6. Monomeric sugar concentration after sulfuric acid treatment at 110ºC.

Sulfuric Acid Concentration (wt.%)	Reaction Time (minutes)	Monomeric Sugar (mg/mL)				
		Glucose	Xylose	Galactose	Arabinose	Total
0.5%	30	1.19	0.36	0.00	1.38	2.93
0.5%	60	1.08	0.41	0.00	3.96	5.46
1.0%	30	1.58	0.66	0.25	5.46	7.95
1.0%	60	2.12	0.97	0.22	5.95	9.26

Monomeric sugar analysis for base catalyzed hydrolysis of WS was investigated at sodium hydroxide concentrations of 0.4, 1.0, 2.0, and 2.5 wt.%. The results of the analysis, shown in Table 6.7, indicate the monomeric sugar content was decreased as sodium hydroxide concentration was increased. This decrease may be due to the degradation of glucose resulting in the formation of lactic, formic, glycolic, and acetic acids [28,29]. Xylose has also been shown to degrade into cyclic enols and phenolic compounds under high temperatures in the presence of sodium hydroxide [30].

Table 6.7. Monomeric sugar concentration at various sodium hydroxide concentrations for 1 h at 100ºC.

Sodium Hydroxide Concentration (wt.%)	Monomeric Sugar (mg/mL)				
	Glucose	Xylose	Galactose	Arabinose	Total
0.4%	5.60	0.76	0.42	0.45	7.23
1.0%	1.28	0.14	0.00	0.11	1.53
2.0%	0.84	0.07	0.00	0.19	1.10
2.5%	0.19	0.14	0.00	0.00	0.33

The effects of reaction temperature on the formation of monomeric sugar using 1.0 wt.% sodium hydroxide for 1 h were also investigated at 40, 80, and 100ºC. The results presented in Table 6.8 reveal that as the reaction temperature was increased the amount of monomeric sugar was decreased. The degradation of monosaccharides in the presence of sodium hydroxide and the formation of organic acids and aromatic compounds [29] are likely to be responsible for this decrease. The degradation reactions are further accelerated as the temperature is increased resulting in lower total amount of monomeric sugars.

Table 6.8. Monomeric sugar concentration at various reaction temperatures for 1 h using 1.0 wt.% sodium hydroxide.

Reaction Temperature (ºC)	Monomeric Sugar (mg/mL)				
	Glucose	Xylose	Galactose	Arabinose	Total
40	7.25	1.22	0.61	1.19	10.27
80	2.15	0.42	0.00	0.00	2.57
100	1.28	0.14	0.00	0.11	1.53

6.4. Conclusions

Acid and base catalyzed hydrolysis experiments were performed using sulfuric acid and sodium hydroxide to partially hydrolyze hemicellulose content of WS, a precursor to DG, to SDF. The influence of reaction time, hydrolyzing agent concentration, and temperature on the conversion of hemicellulose fraction of WS to SDF was investigated. The highest recovery of SDF was 13.2 g/100 g-db WS which occurred using 1.0 wt.% sodium hydroxide at 80 ºC for 1 h and the associated total monomeric sugar formation was 2.57 mg/mL. The highest recovery of SDF for acid hydrolysis was 9.6 g/100 g-db WS which occurred at 1.0 wt.% sulfuric acid at 110ºC for 1 h and the associated total monomeric sugar formation was 9.26 mg/mL. Strategies for processing WS and DG into

higher value products favored acid catalyzed hydrolysis for several reasons. While SDF yields were higher with base catalyzed hydrolysis, acid hydrolysis typically promoted the highest combined yield of SDF and monomeric sugars. Also, base catalyzed hydrolysis likely produced more degradation products which may act as inhibitors to the enzymatic degradation of cellulose and to the fermentation of sugars. Competing reactions, such as the saponification of extractives, likely played a role when sodium hydroxide was used as the hydrolyzing agent. Increasing hydrogen peroxide concentration for alkaline extractions using defatted WS resulted in incremental increases in SDF recovery and improvements in the color of the extracted SDF.

The high concentration of hemicellulose in WS suggests a substantial potential for the production of SDF from dry grind ethanol production facilities. Experimental results presented in this study suggest that an appreciable quantity of SDF could be produced from this byproduct. For example, a 50 million gallon per year fuel ethanol plant will produce approximately 400 tons-db of DG per day. Even modest yields will result in significant quantities of SDF. Potential products derived from SDF include adhesives, thickeners, and stabilizers.

References

[1] Renewable Fuels Association, 2011. 2011 Ethanol Industry Outlook. Available from http://www.ethanolrfa.org/page/-/2011%20RFA%20Ethanol%20Industry%20Outlook.pdf?nocdn=1. Accessed August 2, 2011.

[2] Jacobsen, S.E. & Wyman, C.E. (2000), Cellulose and hemicellulose hydrolysis models for application to current and novel pretreatment processes. *Applied Biochemistry and Biotechnology*, **84-86**, 81-96.

[3] Alberseim, P., Darvill, A., Roberts, K., Sederoff, R., & Staehelin A. (2011) Plant Cell Walls, Garland Science, New York.

[4] DeVries, J. W. (2003), On defining dietary fiber. *Proceeding of the Nutrition Society*, **62**, 37-43.

[5] Doner, L.W. & Hicks, K.B. (1997), Isolation of hemicellulose from corn fiber by alkaline hydrogen peroxide extraction. *Cereal Chem.*, **74**, 176-181.
[6] Oh, Y.N., & Grundleger, M.L. (1990), Improvement in soluble fiber content of wheat fiber through enzymatic modification. *J. Agric. Food Chem.*, **38**, 1142-1145.

[7] Aoe, S., Oda, T., Tatsumi, K., Yamauchi, M., & Ayano, Y. (1998), Extraction of soluble fiber from defatted rice bran. *Cereal Chem.*, **70**, 423-425.

[8] Whistler, R.L. (1993), in Industrial Gums: Hemicelluloses. (R.L. Whistler & J.N. BeMiller, eds.) Academic Press: New York, pp. 295-308.

[9] Wolf, M.J., MacMasters, M.M., Cannon, J.A., Rosewell, E.C., & Rist, C.E. (1953), Preparation and some properties of hemicellulose from corn hulls. *Cereal Chem*., **30**, 451-470.

[10] Yadav, M.P., Johnston, D.B., Hotchkiss Jr., A.T., & Hicks, K.B. (2007) Corn fiber gum: A potential gum arabic replacer for beverage flavor emulsification. *Food Hydrocolloids*, **21**, 1022-1030.

[11] Yapo, B.M., Robert, C., Etienne, I., Wathelet, B., & Paquot, M. (2005), Effect of extraction conditions on the yield, purity and surface properties of sugar beet pulp pectin extracts. *Food Chemistry*, **100**, 1356-1364.

[12] Rouse, A.H. & Crandall, P.G. (1978), Pectin content of lime and lemon peel as extracted by nitric acid. *Journal of Food Science*, **43**, 72-73.

[13] Renard, C.M.G., Lemeunier, C., & Thibault, J. F. (1995), Alkaline extraction of xyloglucan from depectinised apple pomace: optimisation and characterisation. *Carbohydrate Polymers*, **28**, 209-216.

[14] Noureddini H., Byun J., & Yu TJ. (2009) Stagewise Dilute-Acid Pretreatment and Enzyme Hydrolysis of Distillers' Grains and Corn Fiber. Applied Biochemistry and Biotechnology 159:553-567.

[15] National Renewable Energy Laboratory (2011), Standard Biomass Analytical Procedures. Available from http://www.nrel.gov/biomass/analytical_procedures.html. Accessed January 15, 2011.

[16] Sluiter, A., Hames, B., Hyman, D., Payne, C., Ruiz R., Scarlata, C., Sluiter, J., Templeton, D., & Wolfe, J. (2008) in NREL laboratory analytical procedure. Determination of total solids in biomass and total dissolved solids in liquid process

samples. Available from http://www.nrel.gov/biomass/pdfs/42621.pdf. Accessed January 15, 2011.

[17] Sluiter, A. (2005) in NREL laboratory analytical procedure. Determination of starch in solids biomass samples by HPLC. Available from http://www.nrel.gov/biomass/ pdfs/ 9360.pdf. Accessed December 27, 2007.

[18] Sluiter, A., Hames, B., Ruiz R., Scarlata, C., Sluiter, J., Templeton, D., & Crocker, D. (2008) in NREL laboratory analytical procedure. Determination of structural carbohydrates and lignin in biomass. Available from http://www.nrel.gov/biomass/pdfs/42618.pdf. Accessed January 15, 2011.

[19] Hames, B., Scarlata, C., & Sluiter, A. (2008) in NREL laboratory analytical procedure. Determination of protein content in biomass. Available from http://www.nrel.gov/biomass/pdfs/42625.pdf. Accessed January 15, 2011.

[20] Sluiter, A., Hames, B., Ruiz, R., Scarlata, C., Sluiter, J., & Templeton, D. (2005) in NREL laboratory analytical procedure. Determination of ash in biomass. Available from http://www.nrel.gov/biomass/pdfs/42622.pdf. Accessed January 15, 2011.

[21] Sluiter, A., Ruiz, R., Scarlata, C., Sluiter, J., & Templeton, D. (2005) in NREL laboratory analytical procedure. Determination of extractives in biomass. Available from http://www.nrel.gov/biomass/pdfs/42619.pdf. Accessed January 15, 2011.

[22] AOAC official Method of Analysis 991.43 Total, Soluble, and Insoluble Dietary Fiber in Foods - Enzymatic–Gravimetric Method.

[23] Ruiz, R., & Ehrman, T. (1996) in NREL laboratory analytical procedure. HPLC Analysis of Liquid Fractions of Process Samples for Monomeric Sugars and Cellobiose. Available from http://www.nrel.gov/biomass/pdfs/4696.pdf. Accessed December 27, 2007.

[24] Ku, Y., Jansen, O., Oles, C.J., Lazzr, E.Z., & Rader, J.I. (2003), Precipitation of inulins and oligoglucoses by ethanol and other solvents. *Food Chemistry*, **81**, 125-132.

[25] Ohkuma, K., Matsuda, I., Katta, Y., & Tsuji, K. (2000), New method for determining total dietary fiber by liquid chromatography. *JAOAC International*, **83**, 1013-1019.

[26] Das, K., Sahoo, P., Sai Baba, M., Murali, N., & Swaminathan, P. (2011), Kinetic studies on saponification of ethyl acetate using an innovative conductivity-monitoring instrument with a pulsating sensor. *Int. J. Chemical Kinetics*, **43**, 648-656.

[27] Noureddini H. & Byun J. (2010) Dilute-acid pretreatment of distillers' grain and corn fiber. Bioresource Technology 101:1060-1067

[28] Ellis, A.V, & Wilson, M.A. (2002). Carbon exchange in hot alkaline degradation of glucose. *Journal of Organic Chemestry*, **67**, 8469-8474.

[29] Yang, B.Y. & Montgomery, R. (1996) Alkaline degredation of glucose: effect of initial concentration of reactants. *Carbohydrate Research*, **280**, 27-45.

[30] Forsskahl, I., Popoff, T., & Theander, O. (1976), Reactions of D-xylose and D-glucose in alkaline aqueous solutions. *Carbohydrate Research*, **48**, 13-21.

Chapter 7

Recommendations for Future Work

Future work is required in order to confirm assumptions made particularly in Chapter 5 of this dissertation. In order to validate the simplified bioreactor model, it is recommended a pilot scale bioreactor be tested. A fully automated bioreactor has been designed and built for this purpose as shown in Figure 7.1. Temperature, moisture, CO_2 production, substrate weight loss, and cellulase production will need to be monitored and compared to simulation results. At this time a more advanced model which includes heat and mass transfer coefficients should be developed and validated. The complex model will allow additional operating strategies to be evaluated including the use of evaporative cooling by introducing an unsaturated air stream.

Process control strategies can be developed and evaluated based on the validated models. The models can then be used for process scale-up and optimization. It is then recommended that the overall economics of the process be evaluated along with a life cycle analysis. These results will determine the feasibility of the production of cellulase from wet corn distillers grain using solid-state fermentation.

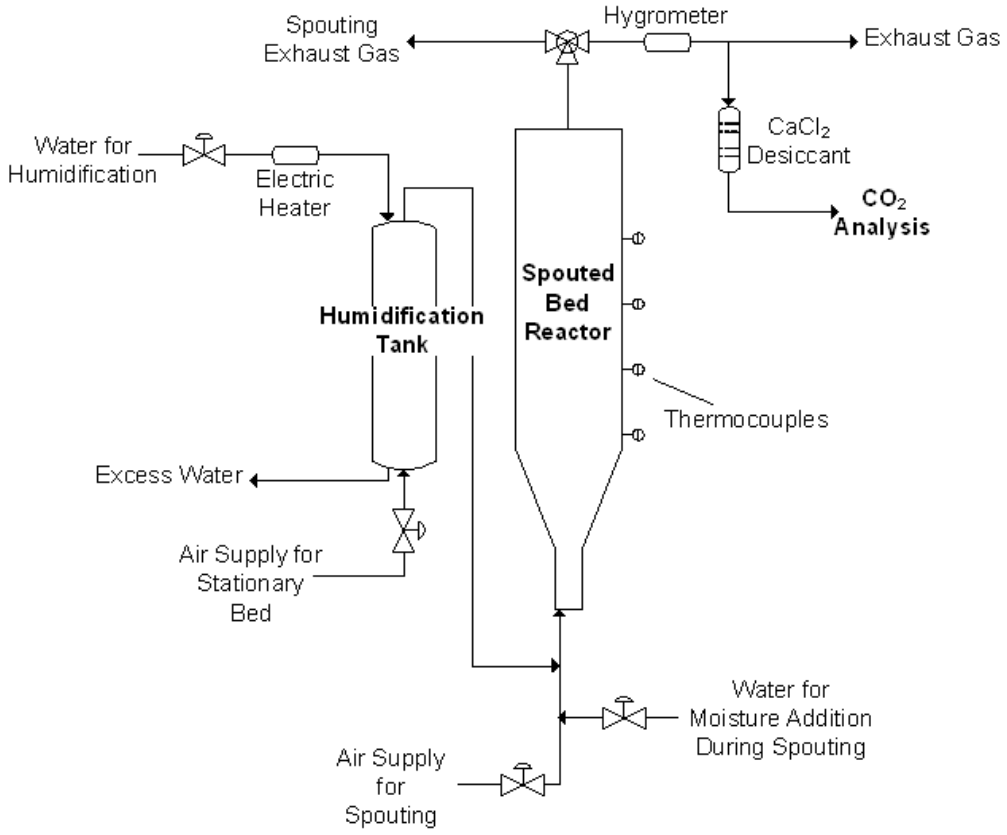

Figure 7.1. Process flow diagram of the pilot scale bioreactor.

Chapter 8

Nomenclature and Abbreviations

8.1. Nomenclature

b – dimensionless factor for CO_2 production
c' – intercept for the linear approximation of H_{sat} as a function of T
C_{Pa} – heat capacity of the gas phase
C_{Pair} – heat capacity of dry air
C_{Pb} – heat capacity of the packed bed
C_{Pv} – heat capacity of water vapor
G – quantity of CO_2 produced per unit weight of substrate as a function of time
G_{max} – maximum quantity of CO_2 produced
H – total height of the bioreactor
H_{sat} – humidity of the air
k - production rate constant of CO_2 produced
k_a – thermal conductivity of the gas phase
k_b – thermal conductivity of the packed bed
k_s – thermal conductivity of the solid phase
m_P – coefficient for product formation related to maintenance metabolism
mw_i – molecular weight of compound "i"
n – fraction of sample considered distributed for thermal conductivity calculations
n' – slope for the linear approximation of H_{sat} as a function of T
P – cellulase activity produced
P' – total pressure
P_{sat} – vapor pressure of water
r – radius
r_Q – rate of energy production
S – substrate weight loss
t – time
T – temperature
T_c – critical temperature of water
v – air velocity
v_S – superficial air velocity
W – metabolic water production
X – microbial biomass concentration
X_m – maximum microbial biomass concentration
y – mole fraction of water in the gas phase
Y_P – cellulase yield coefficient with respect to CO_2
Y_{PX} – product yield coefficient with respect to microbial growth
Y_Q – metabolic heat yield coefficient with respect to CO_2
Y_S – substrate weight loss yield coefficient with respect to CO_2
Y_W – metabolic water yield coefficient with respect to CO_2

z – axial position
ε – void volume
λ – latent heat of vaporization for water
μ - specific growth rate
μ_T – specific growth rate as a function of temperature
μ_W – specific growth rate as a function of moisture content
ρ_b – density of the packed bed
ρ_a – density of the gas phase
ρ_s – density of the solid phase (particle density)
Φ – moisture content in mass of water per mass of dry solids
Φ_0 - initial moisture content of the substrate

8.2. Abbreviations

ADF – acid detergent fiber (cellulose and lignin)
CBU – cellobiase units for cellulase activity
CDS – condensed distillers solubles
db – dry basis
DG – distillers grain
DGS – distillers grain with solubles
DP – degrees of polymerization
FPU – filter pater units for cellulase activity
IDF – insoluble dietary fiber
LAPs – Laboratory Analytical Procedures
NDF – neutral detergent fiber (cellulose, lignin, and hemicellulose)
NREL – National Renewable Energy Laboratory
NRRL – Northern Regional Research Laboratory
SDF – soluble dietary fiber
SmF – submerged fermentation
SSF – solid-state fermentation
WDG – wet corn distillers grain
WDGS – wet corn distillers grain with solubles
WS – whole stillage